# Using micropatterned substrates to study the spatial organization of dorso-ventral identities within an in vitro model of spinal cord

Gabriel Thon

Université de Paris
**Ecole Doctorale** 564 - Physique en Ile-de-France

**Laboratoire Matières et Systèmes Complexes (UMR 7057)**
**Laboratoire Physico-Chimie Curie (UMR 168)**

# Using micropatterned substrates to study the spatial organization of dorso-ventral identities within an *in vitro* model of spinal cord

Par Gabriel Thon

Thèse de Doctorat de Physique

Dirigée par Jean-Marc Di Meglio
Et par Benoit Sorre

Soutenue publiquement le 16 Février 2022

Devant le jury composé de :

| | |
|---|---|
| **Sylvie Hénon**<br>Professeur des Universités, Université de Paris | **Présidente** |
| **Fabienne Pituello**<br>DR, Centre de Biologie Intégrative, Toulouse | **Rapporteur** |
| **Guillaume Blin**<br>Lecturer, The University of Edinburgh | **Rapporteur** |
| **Elisa Marti**<br>Professor, Institut de Biologia Molecular de Barcelona | **Examinatrice** |
| **Jean-Marc Di Meglio**<br>Professeur des Universités, Université de Paris | **Directeur de thèse** |
| **Benoit Sorre**<br>CR, Laboratoire Physico-Chimie Curie | **Invité** |

**Titre : Utilisation de substrats micropatternés pour l'étude de l'organisation spatiale des identités dorso-ventrales dans un modèle *in vitro* de tube neural**

**Résumé :**

Au cours du développement embryonnaire, les progéniteurs neuraux acquièrent des identités dorso-ventrales spécifiques en réponse à des gradients antiparallèles de BMP, Wnt et SHH au sein du tube neural. Si les modèles classiques d'étude de ce patterning dorso-ventral ont permis de mettre en évidence l'implication de ces morphogènes, ils ne permettent pas d'étudier la réponse cellulaire de manière quantitative et de suivre son évolution temporelle de manière optimale.

Dans cette thèse, j'ai utilisé un procédé de microfabrication pour obtenir des micropatterns d'adhérence cellulaire permettant de différencier des cellules en 2D de manière spatialement contrôlée, ce qui permet de surmonter les limites présentées précédemment. Les substrats micropatternés ont déjà été utilisés pour étudier les voies de signalisation impliquées au cours de la gastrulation ou lors du patterning du neuroectoderme, et ont permis de préciser les mécanismes gouvernant la spécification cellulaire.

J'ai donc adapté des protocoles de différenciation de cellules souches embryonnaires humaines (hESCs) en progéniteurs neuraux à la culture sur micropatterns, et j'ai identifié des conditions permettant d'obtenir des populations pures de progéniteurs spinaux caudaux à partir d'hESCs. J'ai également étudié la réponse des cellules en l'absence de stimulation exogène et en présence de signaux de dorsalisation (BMP) ou de ventralisation, en utilisant un agoniste de la voie SHH (SAG). Cette étude a permis de montrer l'implication de voies de signalisation endogènes qui tendent à dorsaliser les identités cellulaires en l'absence de stimulation exogène, ainsi que d'observer l'organisation spatiale de colonies soumises à différentes concentrations de BMP ou de SAG.

Je me suis également intéressé aux mécanismes moléculaires pouvant expliquer l'émergence d'une organisation spatiale dans les différentes conditions étudiées. Les résultats suggèrent notamment un rôle de la voie de signalisation Activin/Nodal dans l'établissement d'un patterning ventral, qu'il reste encore à élucider.

Finalement, j'ai commencé à étudier la différenciation de progéniteurs neuraux sur d'autres dispositifs pour pallier les limites liées aux substrats micropatternés, dans l'optique d'appliquer une stimulation basale, voire en forme de gradient. J'ai également tenté de générer des lignées cellulaires rapportrices propices à l'imagerie en temps réel de progéniteurs neuraux.

Dans son ensemble, cette thèse a constitué un travail exploratoire autour de l'utilisation de nouvelles techniques de culture cellulaire pour l'étude du patterning dorso-ventral du tube neural, qui pourrait permettre de sonder les mécanismes impliqués de manière plus contrôlée.

**Mots clefs :** patterning dorso-ventral, tube neural, micropatterns, hESC, voies de signalisation, signaux endogènes, suivi temporel, modulation spatiale de la stimulation

**Title: Using micropatterned substrates to study the spatial organization of dorso-ventral identities within an *in vitro* model of spinal cord**

**Abstract:**

During embryonic development, neural progenitors acquire distinct dorso-ventral identities in response to antiparallel gradients of BMP, Wnt and SHH along the neural tube. If classical models of this dorso-ventral patterning have provided clear evidence of the role of these morphogens, they are not suited for quantitative and time-trackable analysis of the cell response to those signals.

In this thesis, we used a microfabrication technique to generate micropatterns of cell adherence that enabled us to differentiate cells in a spatially-controlled manner on a 2D plane, which allows us to overcome the issues presented previously. Micropatterned substrates have already been used to study signaling pathways involved in gastrulation or neuroectoderm patterning and to refine mechanisms that rule cell specification.

We adapted protocols to differentiate human embryonic stem cells (hESCs) into neural progenitors for cell culture on micropatterns, and identified conditions to generate pure spinal neural progenitor populations from hESCs. We also studied the cell response in absence of exogenous stimulation and in presence of dorsalizing (BMP) or ventralizing signals (using an agonist of the SHH pathway, SAG). This study enabled us to show the implication of endogenous signaling pathways that tend to dorsalize cell identities in absence of exogenous stimulation, as well as to monitor the spatial organization of colonies submitted to different concentrations of BMP or SAG.

We also investigated the molecular mechanisms that could explain how spatial organization emerges in the different conditions. For instance, our results suggest a role of the Activin/Nodal signalization pathway in ventral patterning, which remains to be fully understood.

Finally, we began to study the differentiation of neural progenitors on other experimental devices that overcome some limits linked to micropatterned substrates and apply a basal stimulation, with the ultimate goal to apply a graded basal stimulation. We also tried to generate reporter cell lines that could be used for live imaging of neural progenitors. As a whole, this thesis is an exploratory work on how new cell culture techniques can be used to study dorso-ventral patterning of the neural tube, which could help decipher the involved mechanisms in a more controlled way.

**Keywords:** dorso-ventral patterning, neural tube, micropatterns, hESC, signaling pathways, endogenous signaling, time tracking, spatial modulation of the stimulation

# Remerciements

Je voudrais tout d'abord remercier Fabienne Pituello et Guillaume Blin d'avoir accepté d'être les rapporteurs de ma thèse, ainsi qu'Elisa Marti et Sylvie Hénon pour leur rôles d'examinatrices. Merci d'avoir pris le temps de lire mes travaux de thèse.

Je voudrais ensuite remercier mon directeur de thèse officiel, Jean-Marc, d'avoir accepté de porter cette casquette et de m'avoir ainsi permis d'entreprendre cette thèse. Merci également d'avoir pris part à mon comité de thèse et d'avoir su apporter un regard extérieur toujours pertinent sur l'avancée du projet. J'en profite pour remercier par la même occasion Mathieu Coppey et Pascale Gilardi-Hebenstreit d'avoir été les membres de mon comité de thèse et de s'être assurés que ma thèse avançait dans les meilleures conditions possibles.

Je tiens à remercier tout particulièrement Benoit, mon directeur de thèse officieux. C'est un projet ambitieux et passionnant que tu m'as permis de porter ces dernières années, et j'aurais pu m'y perdre ou me décourager bien souvent si tu n'avais pas su m'encadrer comme tu l'as fait. Même si nous n'avons que défriché cette problématique interdisciplinaire, j'espère sincèrement que le travail que nous avons accompli te sera utile par la suite.

Je voudrais aussi remercier Vanessa Ribes et Stéphane Nédélec d'avoir supervisé l'aspect neuro de la thèse, en prenant notamment part à de longues réunions qui permettait toujours de clarifier dans mon esprit ce qui avait été accompli et ce qui restait à faire. Merci à Vanessa de ta bonne humeur

communicative et de constamment booster le moral des troupes : je pense que le projet d'article ne serait pas si proche de l'aboutissement sans l'énergie que tu y as consacrée et que tu nous as transmise.

Merci à tous les membres de l'équipe restreinte : Sara, Fabien, Jean-Louis, Geoffray, et une mention particulière à Tom qui m'a appris tout ce que je sais faire en terme de culture cellulaire et de microfluidique, et m'a accompagné jusqu'au bout et à la relecture du manuscrit !

J'aimerais remercier Pascal Hersen de m'avoir intégré au sein de son équipe. Merci plus généralement aux membres de l'équipe élargie : Sylvain, Matthias, Dimitrije, Alvaro, Lionel, Simon, Karine et Maud. Merci à Céline d'avoir toujours été une force motrice dans l'organisation d'activités pour l'équipe, même si je n'étais pas aussi motivé par la course que d'autres !

Je remercie les membres, passés et présents, du MSC, mon laboratoire de cœur. Merci à mes amis de la 777 : Mathieu, Gabriel (Homonyme, juste pour cette fois ?), Aina, Amandine, Johann, Alice et Alice (Alices ?), sans oublier Jules, Darius et David bien qu'ils ne soient pas vraiment en 777. Sans vous, la thèse n'aurait pas laissé autant de bons souvenirs. Merci aussi à Carine, pour m'avoir non seulement aidé dans le projet de lignées rapportrices mais surtout pour les nombreuses discussions informelles. Et merci bien évidemment au bureau d'étude, Arnaud et Mathieu, de m'avoir accueilli et fait profiter de la convivialité de leur salle.

Je tiens également à remercier les membres de mon nouveau laboratoire de PCC de m'avoir aidé à m'adapter à un nouvel environnement. Merci à celles que je connaissais déjà, Mathilde et Nastassia, et à ceux que j'ai rencontrés dans mon nouveau bureau, Romain, Ander et Sam. J'ai également trouvé une ambiance chaleureuse dans la salle de culture de Curie, et j'en tiens pour responsable Fanny et Aude : il y a des fois où un sourire peut illuminer une journée !

Si la thèse m'a permis de rencontrer de nouvelles personnes merveilleuses, j'aimerais tout de même remercier mes amis de longue date. A Martin, qui

occupera toujours une place particulière à mes yeux. A mes amis de prépa, Aurélien, Clémentine, Loïc, Oksana, Théo, Pierre, Mathilde, Romain, Michel, Bastien, Tiphaine et Hugo, décidément trop nombreux pour être remerciés un à un : bientôt dix années et encore tant que j'espère passer à vos côtés. A Laetitia, Maud, Yu Jia, Pierre, Thibaut, Thibault, Thomas, Jean-Côme, Louise, Malo, Gautier, et aux souvenirs de Polytechnique et d'après. A François-Pierre, et à notre colocation confinée qui nous aura permis de parler de tout et de rien. A Jean et Cécile, et à notre amitié indescriptible qui me rend fort chaque jour.

Et enfin, je remercie ma famille d'être si merveilleux. A mes grands-parents et à mes cousins, qui comptent beaucoup pour moi. A Aurélien, Héloïse et Emmanuel, que j'aime plus qu'ils ne peuvent l'imaginer. Et à Maman et Papa pour tout ce que vous avez fait pour moi et de moi. Vous êtes ma source d'inspiration et je n'aurais pu rêver mieux.

# Contents

# List of Figures

# List of Tables

# List of abbreviations

| | |
|---|---|
| **bHLH** | basic helix-loop-helix |
| **BMP** | Bone morphogenetic protein |
| **Bra** | Brachyury |
| **BRE** | BMP Responsive Element |
| **Bsd** | Blasticidin |
| **CHIR** | CHIR99021, Wnt agonist |
| **DAPI** | 4',6-diamidino-2-phénylindole, a DNA intercalating agent |
| **DAPT** | N-[N-(3,5-difluorophenacetyl)-l-alanyl]-s-phenylglycine t-butyl ester, Notch inhibitor |
| **DNA** | Deoxyribonucleic acid |
| **EB** | Embryoid bodies |
| **ESC** | Embryonic stem cell |
| **hESC** | Human embryonic stem cell |
| **mESC** | Mouse embryonic stem cell |
| **FACS** | Fluorescence-activated cell sorting |
| **FGF** | Fibroblast growth factor |
| **FP** | Floor plate |
| **GBS** | Gli binding site |
| **GDF11** | Growth differentiation factor 11 |
| **GRN** | Gene regulatory network |
| **iWP2** | Inhibitor of Wnt Production-2, Wnt inhibitor |
| **LDN** | LDN-193189, BMP inhibitor |

| | |
|---|---|
| **MLE** | Maximum likelihood estimation |
| **MN** | Motoneuron |
| **pMN** | Motoneuron progenitor |
| **NCC** | Neural crest cell |
| **NMP** | Neuromesodermal progenitor |
| **NP** | Neural progenitor |
| **PBS** | Phosphate-buffered saline |
| **PDMS** | Polydiméthylsiloxane |
| **PSC** | Pluripotent stem cell |
| **PNP** | Preneural progenitor |
| **Puro** | Puromycin |
| **RA** | Retinoic acid |
| **RI** | Y-27632, Rock inhibitor |
| **RNA** | Ribonucleic acid |
| **sh-RNA** | short hairpin ribonucleic acid |
| **RP** | Roof plate |
| **RT-qPCR** | Reverse transcription quantitative polymerase chain reaction |
| **SAG** | Smoothened Agonist, SHH agonist |
| **SB** | SB-431542, TGF-$\beta$ (Activin/Nodal) inhibitor |
| **SHH** | Sonic hedgehog |
| **TF** | Transcription factor |
| **TGF-$\beta$** | Tranforming growth factor $\beta$ |
| **WNT** | Wingless type |

# Chapter 1

# Introduction

Among the fascinating mysteries of life, how an embryo can develop from one cell and initiate such complex differentiation programs, yet manage to generate individuals in a highly reproducible way, is certainly one that is impassioning. The three developmental axes appear sequentially and in a conserved way in the animal reign: embryonic tissues are patterned along the antero-posterior axis, then along the dorso-ventral axis, and finally the left-right asymmetry arises. To get a grasp of what ensures that common features are preserved across a species, it seems all the more relevant to look at the moment in embryonic development when these features appear and to monitor how they are gradually refined into well-organized structures. In order to do so, we need every tool available to capture these features. The project at the origin of this thesis aimed at evaluating how a new cell culture setup, namely the use of micropatterned substrates, could be integrated into the armada of the neurobiologist.

Of all the structures generated throughout embryonic development, the present thesis focuses on the dorso-ventral specification of neural progenitors within the neural tube, the embryonic structure that will form the nervous system. In the first two parts of this introduction, we will give an overview of why the neural tube is a rich example in terms of patterning and has

drawn the attention of many scientists interested in how cell fates are specified at early developmental stages. We will follow a chronological timeline and present patterning models that have been used to describe neural tube patterning. We will start from the well-known "French Flag" model, which applies to many types of tissues, then dive deeper into the specificity of the neural tube and explore a more refined model, often referred to as Gene Regulatory Network (GRN), that has been used to understand ventral neural patterning.

To complement embryological studies, *in vitro* systems can be used to investigate developmental questions: explants, embryonic stem cells (ESCs) monolayer cultures, and more recently a variety of sophisticated systems to generate spatial organization. In an attempt to reproduce neural differentiation *in vitro* and characterize it, many studies during the last decades have focused on identifying the signals involved in neural specification. In the third part, we will briefly present some of the main signaling pathways that should be considered in neural differentiation protocols.

Last but not least, we will give an overview of why micropatterned substrates are a promising tool to probe signaling pathways involved in self-organization. Before proceeding to the core of the thesis, we will present some of the work that has already been done in transposing neural differentiation protocols to micropatterns.

## 1.1 Patterning of the neural tube relies on gradients of morphogens

### 1.1.1 Patterning along developmental axis: The "French Flag" model

There are several ways to induce patterning of a tissue from a uniform state. Among the earliest and simplest models, Turing proposed a reaction-diffusion

model, in which Turing patterns emerge as a result of diffusion and interaction of two diffusible factors [Turing, 1952]. This model is sufficient to account for several biological observations: how stripes of zebras or spots in the fur of leopards are formed, how the left-right asymmetry arises in bilaterian embryos as a consequence of interactions between Nodal and Lefty, how hair cells appear locally and regularly on the skin... A review of how Turing patterns is widely found in development of the embryo has been published by [Marcon and Sharpe, 2012].

The main drawback of Turing patterns lie in the lack of robustness – parameters of the model have to be tuned over a narrow range for patterns to be generated. Thus, Turing patterns cannot fully explain how regionalization within embryos occurs in a highly reproducible way. This leads us to introduce another historical and relevant patterning model, which was formulated by [Wolpert, 1969] and is often referred to as the "French Flag" model. (Fig. 1.1). Wolpert introduced the notion of positional information – where a cell lies within a tissue – and suggested that the ability of cells to sense this positional information and initiate the appropriate program of differentiation accordingly could lead to tissue patterning.

In this model, the only requirement to induce patterning is the existence of a gradient of concentration of a "morphogen", a molecule capable of diffusion in the tissue that can dictate cell identity in a concentration-dependent manner. In practice, such a gradient of concentration is achieved whenever there is a source and a sink of morphogen: the source is the secretion of the morphogen by a surrounding tissue located at a specific side from the tissue to be patterned; the sink is the degradation of the morphogen, that can be passive because of protein instability or actively performed by other proteins present in the extracellular matrix. Let's note that the sink could also be localized inhibition of the activity of the morphogen by another protein, *e.g.* a protein competing for the same receptors. Solving the diffusion equation of this source/sink mechanism leads to a graded concentration profile. In 1D,

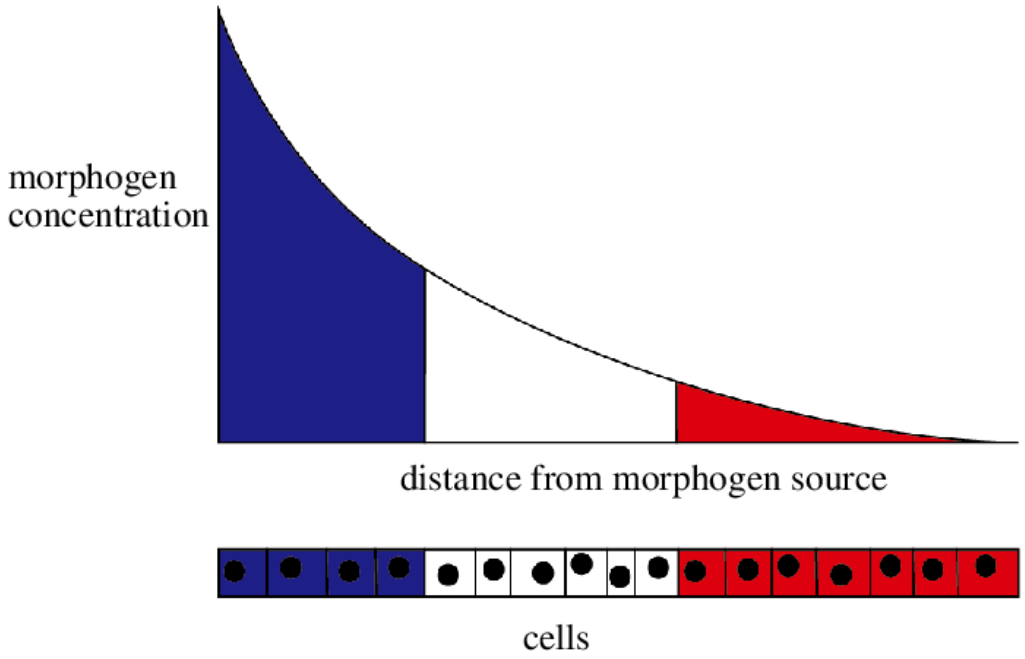


Figure 1.1: **The "French Flag" model.** A profile of concentration of morphogen is interpreted by cells as cell fate depending on thresholds of concentration. Credits to [Multerer et al., 2018].

we typically observe an exponentially decaying concentration.

The "French Flag" model relies on the assumption that a cell can interpret thresholds of concentration of the morphogen of interest and directly convert those into cell fate predictions. Once this hypothesis is formulated, the correspondence between the graded concentration profile and bands of cells is straightforward. One can either be satisfied with this model where cells are considered as some kind of "black box" or try to explain cellular mechanisms leading to this threshold sensing. Minimal kinetic scheme – consisting in the activation of two downstream effectors of the morphogen at different rates and mutual repression between them – have proven sufficient to trigger a bistable switch at a critical concentration. [Saka and Smith, 2007]. Gradient interpretation, as well as how it scales with an expanding

tissue, has been the subject of intense investigations [Ashe and Briscoe, 2006; Ben-Zvi et al., 2011; Bier and De Robertis, 2015; Li and Elowitz, 2019].

Gradients of morphogen are ubiquitous in development. The transcription factor Bicoid dictates the specification of anterior structures (head and thorax) in the *Drosophila* embryo while Nanos specifies posterior structures (abdomen) [Driever and Nüsslein-Volhard, 1988; Lehmann and Nusslein-Volhard, 1991]. The gastrulating mouse embryo is submitted to gradients of BMP4, Wnt3 and Nodal that determine the establishment of the antero-posterior axis and the location of the primitive streak [Bardot and Hadjantonakis, 2020]. And, as we will detail later, the neural tube of the chick or the mouse is submitted to both antero-posterior gradients of Wnt, FGF and GDF11 and dorso-ventral gradients of BMP, Wnt and SHH, that help define neural identities along two axes.

### 1.1.2 The neural tube, a textbook case of "French Flag" patterning?

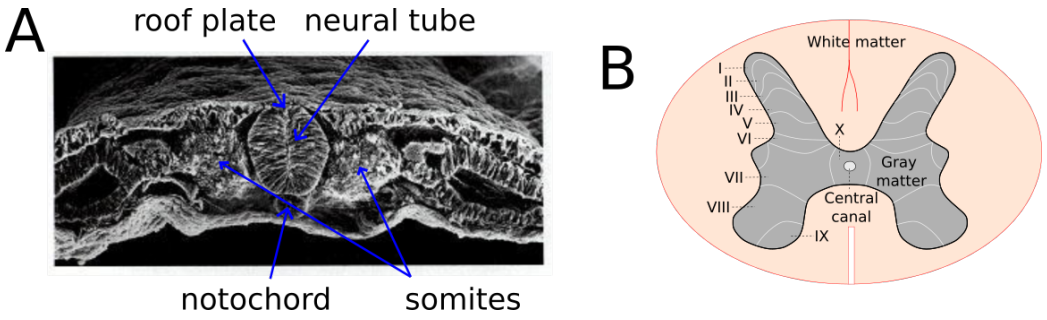


Figure 1.2: **The stratified organization of the neural tube. A** Closure of the neural tube leads to an early stratified structure. Adapted from [Gilbert, 2000]. **B** Scheme of the organization of neurons of the adult spinal cord according to Rexed Laminae based on historical cytological data. Different somatosensory stimuli are processed within different subsets of laminae. Adapted from `https://en.wikipedia.org/wiki/Rexed_laminae`.

The neural tube emerges as a result of the thickening, folding and closure of the ectoderm adjacent to the notochord concomitant to antero-posterior elongation. The neural tube is the precursor to the brain and the spinal cord, and neural crest cells that undergo epithelial-mesenchymal transition at the location where the closure occurs will colonize diverse tissues and give rise to neurons and glial cells of the peripheral nervous system, melanocytes, smooth muscle cells, craniofacial bones and cartilage, and connective tissue [Dupin et al., 2018; Shakhova et al., 2010].

If the dorso-ventral organization of the neural tube has become such a paradigm of tissue patterning, it is mostly due to how well-stratified it is and to how important its layered organization is in conveying information through the circuitry of the central nervous system. This stratified organization stems from early development and is reflected in the adult spinal cord (Fig. 1.2). While dorsally-located neurons are involved in the response to somatic sensory stimuli – pain, temperature, itch, mechanosensation and body equilibrium — which has been reviewed in detail by [Lai et al., 2016] –, ventrally-located neurons control locomotion and reflex response, with both excitatory and inhibitory neurons innervating motor neurons to generate repetitive patterns of motor activity as shown in [Goulding and Pfaff, 2005]. This stratification of anatomical functions originates in early development when 11 stripes of neural progenitors are specified along the dorso-ventral axis (Fig. 1.3). Therefore, it is essential that the establishment of this layered organization during development be robust and scientists have been looking for patterning mechanisms of the neural tube since the 1950s.

The role of peripheral structures in the ventral patterning of the neural tube was first suggested by *in vivo* observations such as those in mutant chick embryos [Watterson et al., 1955]. Mutants growing two notochords showed thickenings of the neural tube – characteristic of floor plate tissues – whose position faces that of the notochord. (see Fig. 1.4)

This observation was supported by graft and deletion experiments [Van Straaten

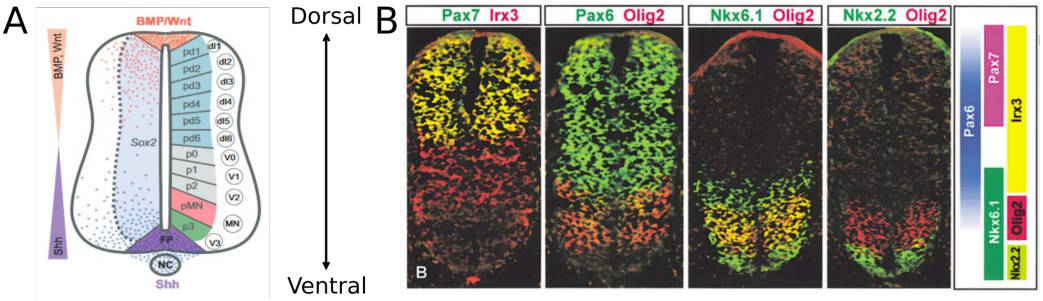


Figure 1.3: **Patterning of the developing neural tube. A** The neural tube is patterned by antiparallel gradients of BMP/Wnt secreted by the roof plate (red triangular structure) and Shh secreted by the floor plate (purple triangular structure). This leads to the specification of 11 domains of neural progenitors (dorsal progenitors pd1-6, ventral progenitors p0-3 and motoneuron progenitors pMN) and their corresponding differentiated neurons (dI1-6, V0-3 and MN). Credits to [Briscoe and Small, 2015]. **B** Expression of several transcription factors showing stratification in the developing neural tube. Credits to [Wichterle et al., 2002].

et al., 1985; Placzek et al., 1990]. For instance, an additional floor plate when grafting a notochord fragment on a chick embryo [Van Straaten et al., 1985]. Further grafts of notochord – this time on chick neural explants – were sufficient to generate $Isl1^+$ motoneurons within the explants [Yamada et al., 1993], hinting that a signal secreted by the notochord was responsible for ventral patterning. Indeed, the notochord induces the floor plate which becomes a signaling centre in the neural tube. The diffusible signal, an N-terminal peptide resulting from the cleavage of Sonic Hedgehog (Shh) was identified and demonstrated to be able to induce ventral fates in chick explants by [Marti et al., 1995].

On the dorsal part of the embryo, the role of the adjacent epidermal ectoderm in inducing dorsal neural structures in lateral regions of the closing neural plate was similarly unveiled by [Liem Jr et al., 1997], who showed that only neural explants grown in the presence of adjacent epidermal ectoderm gave rise to the prospective roof plate. Bone Morphogenetic Proteins

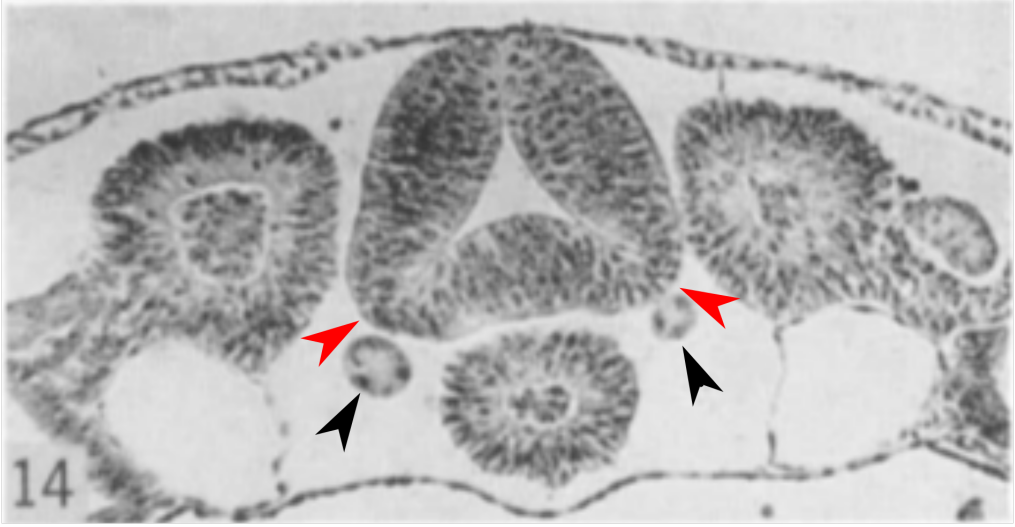


Figure 1.4: **Mutant chick growing two notochords.** Transverse section of mutants growing two notochords. In these mutants, floor plate induction (red arrows) matches the position of the notochords (black arrows). Adapted from [Watterson et al., 1955].

(BMPs) that are transiently expressed in the epidermal ectoderm have been considered as great candidates for roof plate specification, since stimulating naïve caudal neural explants with BMP4 and BMP7 induced roof plate formation, while blocking their action in vivo led to defects in roof plate formation [Liem Jr et al., 1997]. Yet, it remains complicated to provide clear *in vivo* evidence to uncouple the role of BMP in roof plate specification from its earlier role in gastrulation. Apart from BMPs, members of the Wnt family are also secreted by the epidermal ectoderm and have drawn the attention of scientists. Their implication in the proliferation of dorsal cell types [Chesnutt et al., 2004] and in the induction of neural crest cells [Garcia-Castro et al., 2002] has been characterized.

After neural tube closure, the organizing role of the roof plate itself was later demonstrated by [Lee et al., 2000]. Targeted genetic ablation of the roof

plate resulted in a loss of dorsal-most dp1 to dp3 progenitors to the benefit of dp4 to dp6 progenitors. Interestingly, the roof plate also secrets BMP and Wnt once induced [Lee and Jessell, 1999].

### 1.1.3 The "French Flag" model does not account for the dynamics of response to morphogens

Although the "French Flag" model enables us to understand how a spatially organized tissue can emerge from an initially homogeneous population, it presents too simplistic a vision of signal transduction. Its only parameter being a spatial concentration of morphogen, it does not incorporate dynamics of early development signaling, where cells have so-called "windows of opportunity" during which they can generate different cell types and are then drawn towards specific subsets of cell fates. The importance of dynamics had already been pointed out as of 1957 in *The Strategy of the Genes* [Waddington, 1957] with the description of "Waddington landscapes" along which cells evolve and acquire specific identities.

The number of families of morphogens identified throughout embryonic development is rather low compared to the number of tissues they help specify, and the same pathway can be involved at different stages of development to pattern different tissues. To give an example, BMP is involved in the specification of germ layers during gastrulation before it is involved in the patterning of the dorsal neural tube. This hints at the importance of time as a key parameter in cell fate specification.

Last but not least, duration of morphogen signaling should be considered as a parameter to be able to account for experimental observations. For example, the exposition of neural explants to different BMP4 concentrations and with different exposure times can generate either dp1 progenitors for high doses/long exposure or dp2 progenitors for low doses/short exposure [Tozer et al., 2013].

## 1.2 The Gene Regulatory Network: a means to capture cell specification dynamics

Since the embryo undergoes a lot of cell movement and tissue growth during development, profiles of morphogen concentration are noisy and variable in time [Zagorski et al., 2017]. In some species such as the zebrafish, specification of ventral neural fates even seem to occur when the gradient of Shh signaling is not well established [Xiong et al., 2013]. This raises the question of how an analog, noisy signal is converted into discrete cell identities and forms domains with sharp boundaries despite the positional information conveyed by the morphogen gradient decaying in time.

### 1.2.1 Morphogenetic pathways signal to the cells

To answer this question in the context of neural tube specification, it is important to investigate how morphogen signaling is integrated by the cell. When a morphogen binds to a cell receptor, it triggers a cascade of reactions within the cell that usually ends up in translocation or accumulation of a protein downstream in the nucleus. This protein has the ability to recognize specific sequences of bases on DNA, bind to these sequences thanks to its 3D organization that can involve the formation of a complex with other proteins or specific motifs within the amino-acid sequence (e.g. homeodomains, basic helix-loop-helix), and modulate transcription of genes in the vicinity of the binding site. Because of this characteristic behavior, they are called transcription factors (TFs). For BMP, phosphorylation of the Smad1/5/8 proteins enables them to form a complex with Smad4 that translocates into the nucleus and binds to DNA. (Fig. 1.5)

The case of Shh is a bit more complex but we will focus on it in the next paragraphs since there has been a lot of research undertaken to understand how boundaries are refined for ventral neural specification. The membrane receptor Patched1 (Ptch1) is inactivated upon Shh binding and cannot in-

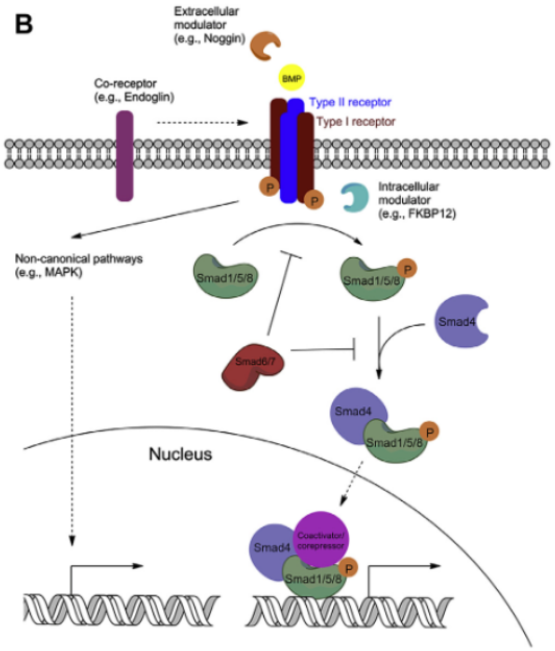


Figure 1.5: **The BMP pathway.** The binding of BMP to a receptor leads to phosphorylation of Smad1/5/8 proteins that can subsequently form a complex with Smad4, transverse the nuclear membrane and regulate transcription. Adapted from [Wang et al., 2014].

hibit another transmembrane protein called Smoothened (Smo). Smo is able to relieve the sequestration that the Suppressor of fused homolog protein (SUFU) exerts on three Gli proteins: Gli1, Gli2 and Gli3. As the result of this complex network of inhibitions, Gli proteins undergo posttranslational modifications and can translocate into the nucleus and bind to DNA. While Gli1 mostly activates transcription of genes, Gli2 and Gli3 activate some genes and repress some others. [Niewiadomski et al., 2019] (Fig. 1.6)

While signaling pathways are the first step of the response to morphogens and can transduce changes in morphogen concentration as well as integrate a temporal profile of the external output – as has been described in the case

of TGF-$\beta$ [Sorre et al., 2014] –, they cannot account for a binarisation of the signal that is necessary to encode for sharp domain boundaries.

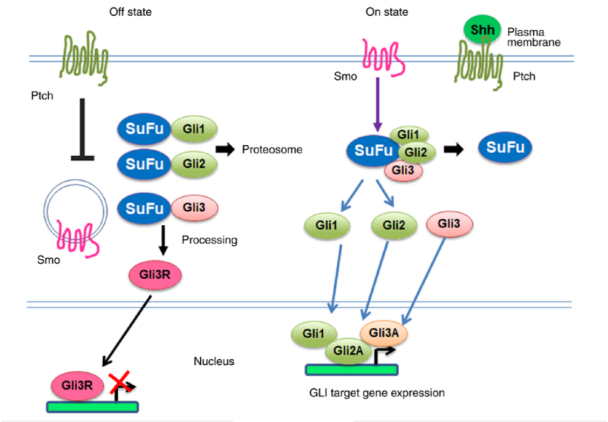


Figure 1.6: **The Shh pathway.** The binding of Shh to the membrane results in the activation of transcription by Gli factors as the result of sequential inhibitions. Adapted from [Jeng et al., 2019].

### 1.2.2 Transcription factors take over the response to morphogenetic cues

Among the genes regulated by Gli, several TFs have been identified that regulate the expression of a large number of genes that will enable cell subtypes to depict different proteomes – all the proteins expressed by a cell – and serve different functions. These TFs have been classified depending on whether their expression is repressed (class I) or activated by Shh signaling (class II) [Briscoe et al., 2000], and the combinatorial expression of a subset of these TFs gives predictive information of the type of neuron a progenitor will generate (see Fig. 1.7). Repressive interactions between TFs have been suggested from experiments in mutant mice. For example, upon mutation of the sequence of the class I protein Pax6, the domain of expression of the

class II protein Nkx2.2 is larger, which suggests that Pax6 inhibits Nkx2.2 independently from Shh signaling. [Ericson et al., 1997]

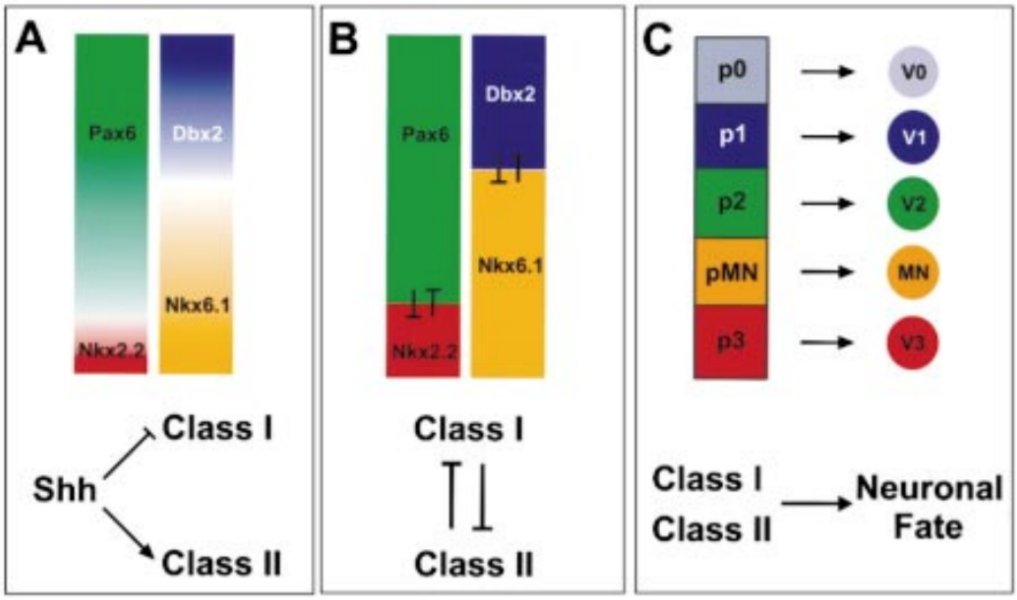


Figure 1.7: **Mutual repression between TFs. A** Shh signaling results in the expression of class I and II TFs. **B** Mutual repression between TFs results in sharpened boundaries. **C** Combinatorial expression of TFs is translated into neuronal fate. Credits to [Briscoe et al., 2000].

Not only do these TFs enable us to identify which class of neurons neural progenitors will differentiate towards, but the mutual repression that they exert on each other is a key element in refining boundaries between domains of progenitors beyond morphogen signaling. All the interactions between TFs build a complex kinetic graph that is referred to as the Gene Regulatory Network (GRN). [Balaskas et al., 2012] showed how this GRN can be modeled with linked ordinary differential equations (ODEs) that can capture the *in vivo* dynamics of expression of these TFs. The mutual repressions between TFs that build the GRN create bistable states – only one or the other of the TFs can be expressed – and enable sharp shifts between discrete cell

identities. Simulations carried out within a certain range of parameters could recapitulate how the ventral-most cells had successive expression of Pax6, Olig2 and Nkx2.2 as well as infer how domains of expression of Olig2 and Nkx2.2 would be shifted in $Pax6^{-/-}$ mutants. ODEs also predicted hysteretic behavior of Nkx2.2 expression that could be reproduced in cultured explants.

In kinetic terms, the GRN can be broken down into simple elements like positive feedback loops – which promote amplification of the expression of a TF –, and incoherent feed-forward loops – that enable a given TF to be induced at a slower rate but take over other TFs upon reaching a given concentration. Although kinetic constants are hard to measure experimentally, it seems that the architecture of the GRN promotes robustness in the sense that it is the relative strength between these kinetic constants that matters. Robustness also ensures that cells be less sensitive to fluctuations of the input morphogen signal.

To account for the "window of opportunity" that cells exhibit, one could infer that kinetic constants depend on developmental time and the current state of the cell. After some time, cells would become less sensitive to the induction of transcription factors by the morphogen of interest.

All in all, the existence of a GRN downstream of morphogen pathways provides cells with a precise and robust way to interpret noisy and varying morphogen gradient profiles. The GRN constitutes a general framework to understand how cells make fate decisions following inputs of morphogens.

## 1.3 ESCs to recapitulate neural differentiation *in vitro*

So far, we have presented experiments where *in vivo* observations and *in vitro* explants have been used to address developmental questions and identify morphogenetic cues involved in neural differentiation. While these have proven very effective in identifying critical morphogenetic pathways that structure the embryo, the groundbreaking discovery of stem cells and conditions to cultivate and even induce them [Martin, 1981; Thomson et al., 1998; Takahashi and Yamanaka, 2006] has paved the way to another experimental approach of studying development. Rather than perturbing an *in vivo* system, could one disentangle involved mechanisms more efficiently by deriving neural progenitors in defined culture media? Not mentioning the fact that human stem cells can also be derived and therefore human development studied, when human embryos cannot.

In this section, we do not intend to review the actions of how every morphogenetic pathway is currently thought to be involved in neural differentiation. Instead, we propose to identify common features among the numerous neural protocols. Following differentiation from one stem cell to a differentiated neuron, three milestones have to be encountered: first, stem cells are differentiated into neural progenitors (NPs); then, these neural progenitors acquire a dorso-ventral identity; finally, dorso-ventrally primed neural progenitors mature into functional neurons.

We want to insist on the fact that these steps are overlapping in time when not considering a single cell but the embryo as a whole: some rostral neural progenitors are specified dorso-ventrally while the neural tube is still extending; similarly, a pool of dorso-ventral progenitors is maintained in the ventricular zone while progenitors that migrated towards the marginal zone start differentiating into mature neurons.

### 1.3.1 From ESCs to NPs

#### The default model: sequential neuralization and posterization signals

Neural induction was first studied in the amphibian embryo *Xenopus laevis* and led to the default model, according to which neural fates are generated in the absence of the instructive signals secreted by adjacent cells, and has been reviewed by [Muñoz-Sanjuán and Brivanlou, 2002]. Protocols were derived from this default model and refined so as to grow undissociated cells.

The main recurring features that these protocols share consist in the inhibition of BMP signaling with natural inhibitors like Noggin or chemical inhibitors like LDN-193189 (LDN), and the inhibition of TGF-$\beta$ (Activin/Nodal) signaling with SB-431542 (SB). This dual inhibition greatly enhances the yield at which neural progenitors are produced, as has been detailed by [Chambers et al., 2009], and fosters the development of anterior neuroectodermal structures.

To derive more posterior neurons within this model, dual inhibition has to be coupled with the addition of caudalizing signals. Several pathways have been shown to play a role in this caudalization step: Wnt [Kiecker and Niehrs, 2001; Maury et al., 2015], FGF [Cox and Hemmati-Brivanlou, 1995], retinoic acid (RA) [Maden, 2006; Maury et al., 2015] and GDF11, a member of the TGF-$\beta$ family, for caudalmost structures [Liu, 2006]. There appears to be a synergetic action of these pathways to control the HOX clock and generate the most posterior region of the spinal cord, which has been documented by [Mouilleau et al., 2021].

Apart from its caudalizing role, RA also plays a significant role in neural differentiation since it is required for the expression of proneural genes Neurog2 and Pax6 as well as ventral patterning genes such Nkx6.1, Nkx6.2 and Olig2 [Gajović et al., 1998; del Corral and Storey, 2004].

### Deriving NPs from neuromesodermal progenitors (NMPs)

Contrasting with the default model of neural induction presented in the former subsection, a pool of progenitors located in the caudal lateral epiblast of the mouse embryo – the region at the end of the expanding neural tube next to the tail bud – has been characterized by its simultaneous expression of the neural marker Sox2 (and concomitant downregulation of Oct4) and the mesodermal marker Brachyury (Bra), and its potency to generate caudal neural progenitors as well as paraxial mesoderm, *ie* the prospective somites [Cambray and Wilson, 2007]. (see Fig. 1.8)

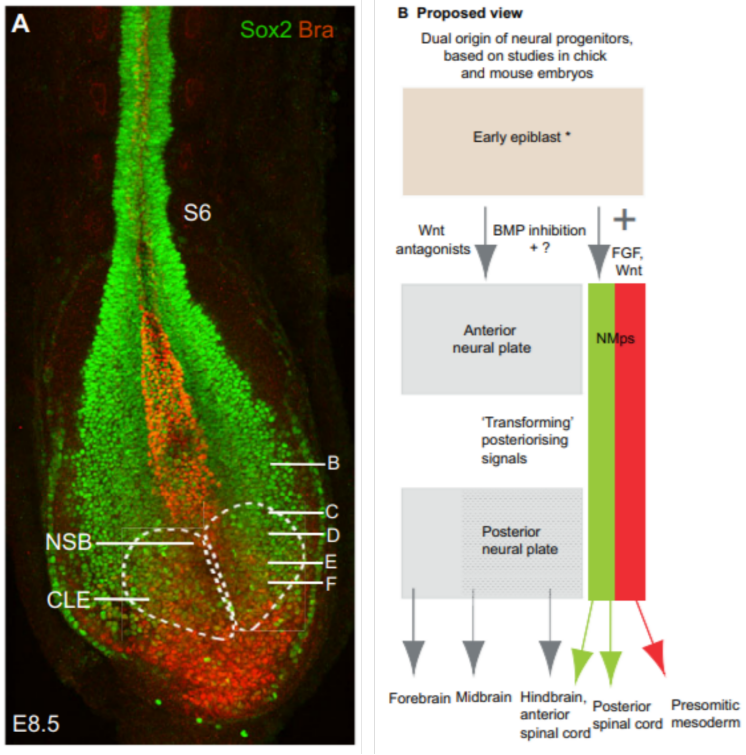


Figure 1.8: **From hESCs to NPs. A** *In vivo* stainings of Sox2 and Bra on a E8.5 mouse embryo highlights presence of double-positive cells in the CLE. **B** Proposed view on the dual origin of neural progenitors to take both models into account. Credits to [Henrique et al., 2015].

Derivation of NMPs *in vitro* relies on transient Wnt and FGF signaling, and these two signals are sufficient to generate $Sox2^+/Bra^+$ cells in mESCs and hESCs *in vitro* [Gouti et al., 2014]. Interestingly, relative levels of expression of Sox2 and Bra are indicative of whether NMPs will follow a neural or mesodermal differentiation path [Wymeersch et al., 2016]. The exit of this NMP state towards posterior neuroectodermal fates depends on subsequent RA signaling, while prolonged exposure to Wnt and FGF signaling induces paraxial mesoderm [Frith et al., 2018; Romanos et al., 2021].

**Two distinct pools of progenitors give rise to distinct rostro-caudal neural progenitors**

It is complicated to give prevalence to either of the two models presented above. It seems even more ambitious to give a definitive answer in the context of human neural tube formation because of interspecies differences: differences in the location of the pools of NMPs between the chick and the mouse embryos have been noticed [Shaker et al., 2021].

However, a consensus seems to emerge that both models apply to different regions of the embryo: while the dual inhibition protocol corresponds to the generation of more anterior neural progenitors – ranging from the brain up to the cervical spinal cord –, NMPs are involved in the generation of posterior neural progenitors – brachial, thoracic and lumbar spinal cord. This consensus is in line with the view that has been proposed by [Henrique et al., 2015] – a dual origin of neural progenitors either from anterior plate caudalization or NMP derivation – and seems to be corroborated by ulterior articles that were presented in this section. (see Fig. 1.8)

### 1.3.2 Dorso-ventral specification of NPs

We already presented the main actors involved in the dorso-ventral specification of NPs in the first two parts: SHH for the ventral part and BMP/Wnt

for the dorsal part. In this section, we will summarize how these signaling pathways act to pattern the neural tube dorso-ventrally.

### SHH

Generation of the five categories of ventral neural progenitors (p0, p1, pMN, p2 and p3) (see Fig. 1.3) is mediated by SHH signaling in a dose-dependent manner, with a  2-fold increase in SHH concentration needed to switch from one of these domains to a more ventral one [Ericson et al., 1997]. *In vivo*, the SHH gradient initially spans a large portion of the neural tube before getting restricted to the most ventral region, at which point the boundaries are not encoded anymore by the SHH profile but by the downstream GRN [Zagorski et al., 2017]. Floor plate cannot be generated from NPs but requires earlier exposure to SHH [Fasano et al., 2010].

### BMP

The dorsal neural tube is composed of six domains of NPs (dp1 to dp6), with dp1-3 NPs giving rise to relay interneurons and dp4-6 NPs to associating interneurons. In addition to these six domains, roof plate (RP) and neural crest cells (NCCs) can also be derived from neural progenitors [Duval et al., 2019]. Varying the concentration and duration of BMP stimulation, proportions of cells within each progenitor domain can be tuned [Tozer et al., 2013].

BMP is a family of molecules and several BMPs display different profiles of expression. The most studied one being BMP4. Yet, different BMPs might play different roles. For example, in the chick embryo, targeted shRNA-mediated inactivation of BMP4 drastically lowers the number of dI1 neurons and that of BMP7 of dI1, dI3 and dI5 neurons. (see Fig. 1.9)

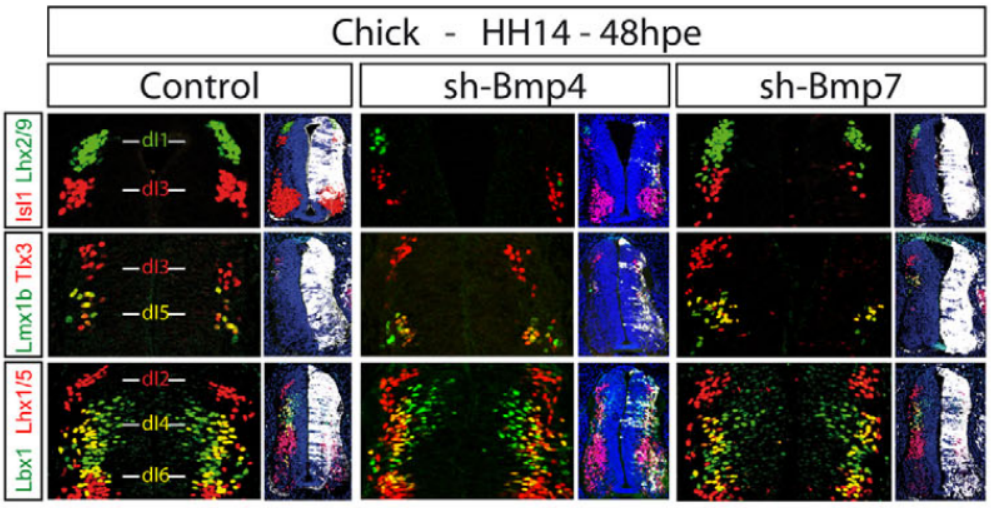


Figure 1.9: **Different BMPs induce different dorsal neural identities.** Identities of interneurons generated in control and sh-BMP4 and sh-BMP7 mutants at HH14 (chick embryo). Credits to [Le Dréau et al., 2012].

### BMP and SHH provide more information when interpreted simultaneously

SHH and BMP are often considered separately when envisioning patterning of the neural tube. In extremal regions where one is at a high concentration and the other at a low concentration, they appear sufficient to explain patterning on their own. This becomes a bit more tricky when considering the intermediate region of the neural tube, where both pathways display low activity.

Following the idea developed by [Zagorski et al., 2017], if we take into account how noisy signals can be *in vivo* and restrict cell fate to a maximum likelihood estimation (MLE) of the morphogen profile at a given time (forgetting in doing so that integration of signal is primordial), it appears that more information can be found in the case where both SHH and BMP profiles are interpreted simultaneously, and cells can infer their position with

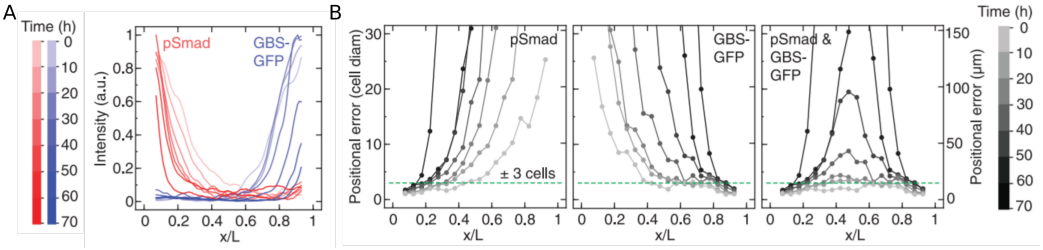


Figure 1.10: **BMP and SHH provide more information together. A** Experimental mean signals of activity reporter of the BMP (pSmad) and SHH (GBS-GFP) pathways at different developmental times of mouse neural tube formation. **B** Positional error and joint positional error inferred from the MLE theoretical model. Credits to [Zagorski et al., 2017].

a precision of less than 3 cell diameters prior to 30 hours of development. (see Fig. 1.10)

#### Wnt

Wnt role in dorsal neural tube specification remains unclear and Wnt is often relegated as a secondary signal that promotes a mitogenic activity of neural progenitors – therefore regulating the proportion of each domain of neural progenitors rather than specifying them –, and antagonizes SHH signaling [Chesnutt et al., 2004; Le Dréau and Martí, 2012]. Yet, as we will see in 1.4.3, BMP and Wnt display complementary roles in the context of neuroectoderm specification, and future research should try to disentangle BMP and Wnt respective roles in neural tube dorso-ventral patterning.

### 1.3.3 Maturation of dorso-ventrally primed NPs

In the present thesis, we did not continue culture of progenitors until maturation of neural progenitors. Still, we performed some stainings for mature neurons at early stages when the first mature neurons start to appear.

### Notch inhibition

Notch inhibition, usually performed with the small molecule DAPT, has been described as a useful way to enhance neuronal differentiation independently of dorso-ventral position by [Crawford and Roelink, 2007]. The putative mechanisms have been reviewed by [Louvi and Artavanis-Tsakonas, 2006] and [Lai et al., 2016]. In a very simplified version, Notch activation in one cell is mediated via interactions with neighboring cells and results in transcription of HES1 which represses the expression of proneural factors (ASCL1, NEUROG2, MASH1). These proneural factors present a basic loop-helix-loop (bHLH) domain that allows them to bind to DNA as heterodimeric complexes and activate neural differentiation genes [Bertrand et al., 2002]. Feedback from bHLH factors expressed by mature neurons on Notch signaling in neighboring cells is thought of as a means to keep a balance between numbers of progenitors and mature neurons *in vivo*.

In an attempt to produce mature neurons with high efficiency in *in vitro* cultures, the last step of neuronal differentiation usually consists in inhibiting the Notch pathway with DAPT. Before this step is achieved, we can expect to see a few isolated mature neurons surrounded by progenitors, reminiscent of how hair cells and supporting cells are distributed in the mammalian cochlea as a result of Notch signaling [Lanford et al., 1999].

### TGF-$\beta$ (ACTIVIN/NODAL)

More recently, TGF-$\beta$ signaling was reported to display a dynamic expression profile in p3 progenitors that correlates with the extinction of the early neural identity gene Phox2b, and activation of the TGF-$\beta$ pathway at earlier stages could trigger premature downregulation of Phox2b [Dias et al., 2014]. Analysis of single-cell RNA data in the mouse embryo highlights that the role of TGF-$\beta$ in regulating the pace of progenitor maturation does not appear to be restricted to precise domains of progenitors, but maintained in all dorsal and ventral progenitors [Sagner et al., 2020]. (see Fig. 1.11)

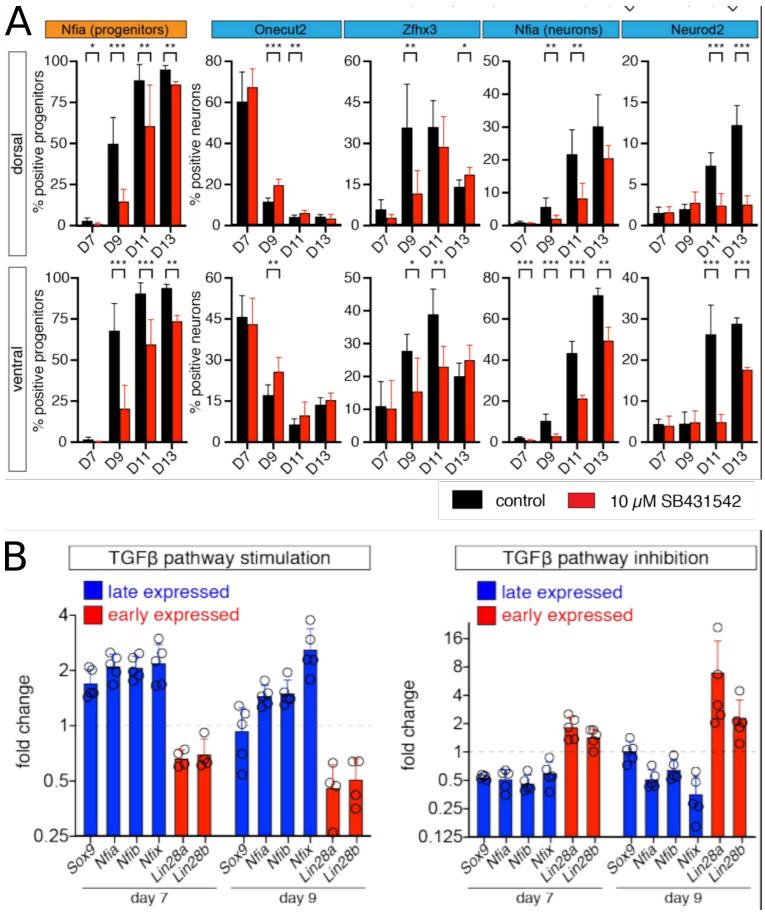


Figure 1.11: **TGF-$\beta$ regulates the pace of neural differentiation. A** Flow cytometry classification of progenitors in control condition and under TGF-$\beta$ inhibition. The early marker Onecut2 is maintained longer, while late markers Zfhx3, Nfia and Neurod2 are significantly lowered under TGF-$\beta$ inhibition. **B** RT-qPCR of early and late expressed neural markers under TGF-$\beta$ stimulation or inhibition confirms the role of TGF-$\beta$ in maturation of neural progenitors (the ratio is computed with a control sample). Credits to [Sagner et al., 2020].

In this section, we saw that many signals have been identified that generate the diversity of neural identities. Sequential exposure to the right combination of morphogens, making sure at each checkpoint that the identity

of intermediates correspond to what is observed *in vivo*, allows us to differentiate PSCs or ESCs into pure populations of specific types of neurons, *e.g.* motoneurons [Chambers et al., 2009]. It is important to mention that these protocol optimization studies generally do not aim at reconstructing the diversity of the neural tube. However, circuit formation between different types of progenitors can define emergent properties such as periodicity of the electric signal [Magown et al., 2017]. Recently, scientists have been trying to change protocols to generate diversity in embryoid bodies (EBs) and organoids as a whole. In the next section, we will present another approach to this question and compare it to existing systems that generate spatial organization of neural progenitors.

## 1.4 Using micropatterned substrates to investigate developmental questions

In this section, we would like to present a rather recent technique that has been described in an attempt to study tissue patterning. It is often referred to as "micropatterning" and relies on microfabrication steps which aim at controlling where cells can grow and where they cannot. In this project, we used photolithography and microprinting to alternate between regions of adherence and regions of non-adherence on a polydimethylsiloxane (PDMS) coated coverslip. The full details of this protocol are described in the Materials and Methods section.

There are other ways to achieve similar organization, either through spatially-controlled chemical treatments or physical shaping of the mold, that we will not describe here and have been reviewed by [D'Arcangelo and McGuigan, 2015]. Instead, we will explain why micropatterns are an interesting framework to investigate cell specification, and focus on a few examples where they were used to decipher to what extent morphogen pathways are involved in the specification process.

### 1.4.1 2D confinement on micropatterned substrates can induce self-organization of differentiating hESC colonies

#### Germ-layer specification can be observed on micropatterns

The first attempt to study the differentiation of ESCs on micropatterns was described by [Warmflash et al., 2014]. It was initially thought of as a means to get rid of uncontrolled heterogeneous differentiation that was observed in standard culture. The underlying reasoning was that having a hold on the colony size, the spacing between colonies and the boundary conditions would lead to more reproducible results.

A result reported in this article and not to be overlooked consisted in noticing that there are already spatial differences of levels of expression of pluripotency markers in stem cell culture media. Indeed, cells at the periphery of colonies exhibit higher levels of OCT4, NANOG and SOX2 than cells located at a distance higher than 150µm to the border (see Fig. 1.12). This explains that boundary conditions – such as the shape and the size of colonies – are key in regulating cell response, even in standard culture. And that is probably why micropatterns are so efficient at controlling and revealing those edge effects.

Even more strikingly, colonies respond to a morphogenetic signal provided in bulk in a heterogeneous but highly reproducible way. When stimulated with BMP for 2 days, concentric rings of fate arise, and their relative position is reminiscent of germ layer specification: from the periphery to the center, one successively observe trophectoderm-like ($CDX2^+$), endoderm ($SOX17^+$), mesoderm ($BRA^+$) and ectoderm ($SOX2^+$) markers.

**Symmetry-breaking mechanisms account for self-organization**

How can a supposedly constant concentration of morphogen provided in bulk lead to spatial patterning? Elements of answer were given by [Warmflash et al., 2014] and characterized in a later paper by [Etoc et al., 2016]. The idea is that while the signal is provided in a homogeneous way, its interpretation is tied to local characteristics. In this study, two factors were identified, namely receptor accessibility and levels of secreted inhibitors.

In the instance of BMP stimulation described earlier, receptor accessibility is highly dependent on cell density. To prove that, the phosphorylation of the downstream effector SMAD1 was monitored in low (3000 $cells/mm^2$), intermediate (7500 $cells/mm^2$) and high (9600 $cells/mm^2$) seeding densities (see Fig. 1.13). Only the high-seeding condition – which is the one for which circular rings had been observed – lead to localization of the pSMAD1 signal at the periphery of the colony. This is in line with transwell experiments on

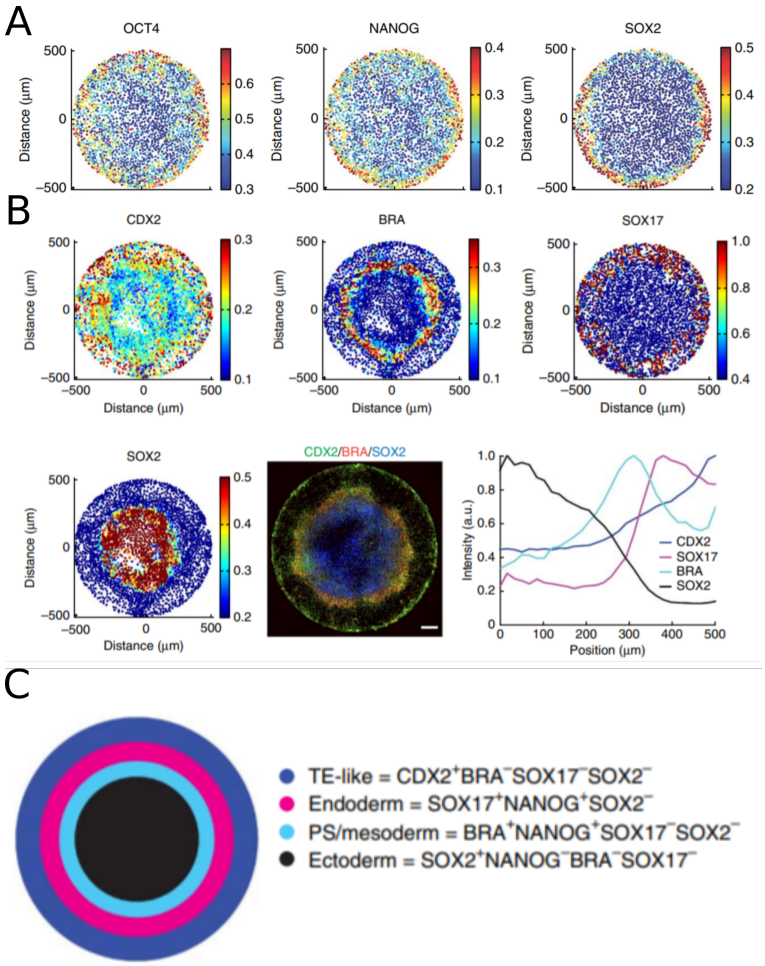


Figure 1.12: **Germ-layer specification on micropatterns.** **A** Pre-patterning of ESCs highlights higher levels of OCT4, NANOG and SOX2 at the border of the colony. **B** Upon 48h of BMP stimulation, germ layer specification is reproduced on micropatterns. **C** Scheme of cell fates induced corresponding to stainings. Adapted from [Warmflash et al., 2014].

monolayers, where cells at low density exhibit pSMAD1 signals independent of apical or basal stimulation whereas cells at a high density only respond to

BMP provided basally. In dense conditions, cells at the center of the colony are highly-packed and the BMP provided in bulk cannot reach BMP receptors that are located laterally on the basal side. Mature tight junctions form an impermeable barrier that can be measured experimentally by electrical resistivity.

Another factor to account for a spatially patterned response despite bulk stimulation relies on a negative retroaction loop exerted by a secreted inhibitor. In the case of BMP, NOGGIN plays such a role. Its production rate follows the pSMAD profile, as evidenced by stainings 1 hour after stimulation. However, it is secreted and diffuses within the colony (in 2D) or in the media (in 3D), in which case it is highly unlikely to return to the colony. To account for this, one can assume NOGGIN is lost at the edge and be left with a diffusion equation where boundary conditions are that the concentration of NOGGIN is zero at the periphery and where production is proportional to the pSMAD signaling profile. Solving this diffusion equation, [Etoc et al., 2016] showed that at steady state, NOGGIN establishes a dome-shaped profile. Inhibition at the center of the colony amplifies the differential response between the center and the border of the colony.

### 1.4.2 Micropatterns avoid drawbacks of other culture conditions

Why did we first consider using micropatterns to study neural tube specification? All the results that were presented in the third part have been possible thanks to one of the following techniques: *in vivo* observations, explants culture, adherent monolayer culture or EBs. We will give a few elements that prompted us to consider micropatterns as an attractive option in the experimental field.

- *in vivo* observations and explants culture do not allow a precise control on the studied cells, be it from a biophysical perspective (*e.g.* if one

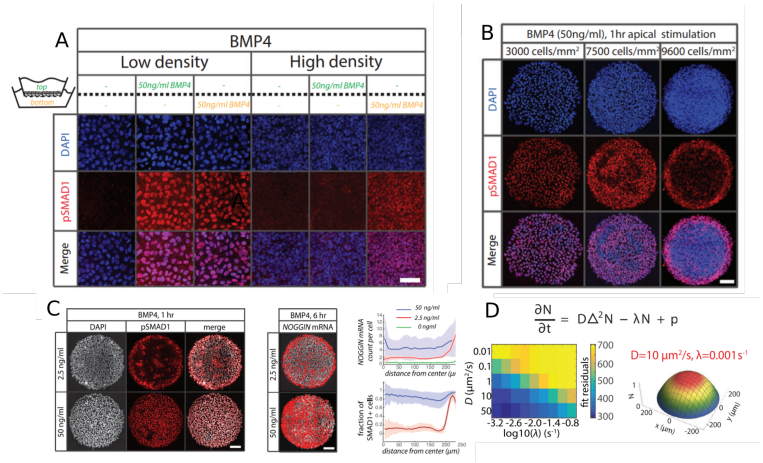


Figure 1.13: **Mechanisms that regulate self-organization on micropatterns.** **A** Apical BMP stimulation is hindered at high density on transwells. **B** pSMAD1 signal gets restricted to the periphery at high density on micropatterns. **C** Soon after stimulation, NOGGIN expression profile follows that of pSMAD1. **D** At steady state, modeled diffusion of NOGGIN account for a dome-like profile. Adapted from [Etoc et al., 2016].

wishes to impose a given concentration on a tissue, have a tissue of a precise shape and size) or from a biological perspective (*e.g.* cells within a sample are heterogeneous and may be at different developmental stages).

- Culture of adherent monolayers has been optimized to yield one specific type of cell, which prevents the study of spatial patterning. In some experimental conditions where cells are not forced towards a unique cell fate, several cell fates can be generated, but that occurs in an anarchic and uncontrollable way.

- EBs have been the most convincing tool to study spatial organization *in vitro* as shown in recent publications [Duval et al., 2019; Zheng et al., 2019]. Yet, they require non-adherent conditions, which hinders our capability to perform live microscopy or tracking. Even if we do

not present live imaging results in the present thesis, micropatterned substrates can be a good alternative to investigate more dynamical processes.

### 1.4.3 Moving from gastrulation towards neural tube specification: neuroectoderm patterning

In this section, we would like to present two examples of how micropatterns have been used in recent years to carry out developmental studies on neuroectoderm patterning.

#### Mechanics-guided embryonic patterning of neuroectoderm tissue from human pluripotent stem cells

[Xue et al., 2018] seeded hESCs on vitronectin-coated micropatterns of different sizes at low density compared to what was described in the former section (200 $cells/mm^2$) and waited 2 days for cells to cover the micropattern before stimulation. They then induced neural plate border formation with a dual SMAD inhibition and brief CHIR stimulation protocol, and stained colonies after 7 days of differentiation. At that point, they observed spatial patterning, with cells near the center of the colony exhibiting neuroepithelial characteristics ($PAX6^+$) and cells at the periphery leaning towards neural plate border fates ($PAX3^+$, $ZIC1^+$, $MSX1^+$). (see Fig. 1.14)

The authors attributed the pattern to basal BMP activity and mechanical forces exerted within the colony. Indeed, the KSR media used to cultivate cells displayed basal BMP activity, since switching to a less rich E6 media lowered pSMAD1/5 signal. Non-YAP/TAZ-dependent mechanical forces were also responsible for patterning the colony: stretching of colonies led to a homogenization of pSMAD1/5 signal, but YAP inhibition did not. Receptor accessibility presented in Fig. 1.13 was dismissed since tight-junction disruption with Y-27632 (Rock Inhibitor, RI) did not affect the pattern.

While this article presents interesting observations, characterization of intermediate fates was not carried out, and it is hard to understand whether neuroectoderm patterning occurs from a homogeneous ectoderm.

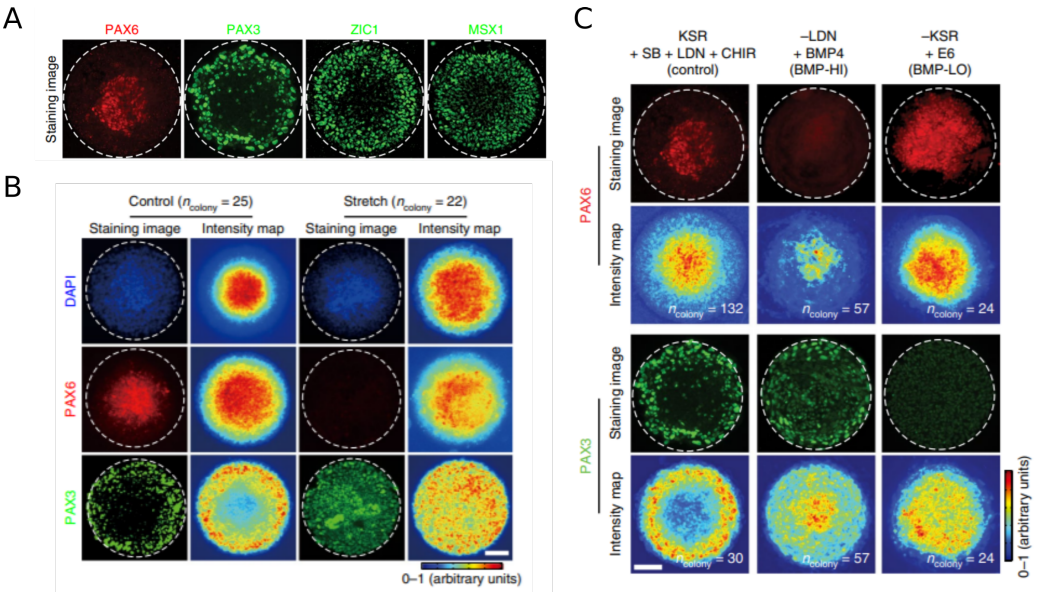


Figure 1.14: **Neuroectoderm patterning and the role of mechanical forces. A** Immunostainings 7 days after differentiation, showing neural PAX6 fates at the center and neural plate border PAX3, ZIC1 and MSX1 fates at the periphery of the colony. **B** Stretching of colonies promotes neural plate border specification. **C** Media without BMP basal activity promotes neural fate specification. KSR and E6 are culture media. LDN is a BMP inhibitor, SB a TGF-$\beta$ inhibitor and CHIR a Wnt agonist. Adapted from [Xue et al., 2018].

### A novel self-organizing embryonic stem cell system reveals signaling logic underlying the patterning of human ectoderm

[Britton et al., 2019] insisted on finding the right temporal window for neuroectoderm patterning. They noticed that hESCs cultivated for 2 days in N2B27 media supplemented with SB displayed a loss of OCT4 and NANOG

and that PAX6 only appeared at a significant level on day 4. Thus, to study neuroectoderm patterning rigorously, one has to stimulate cells between day 2 and day 4: stimulating before can lead to non-ectodermal fates, and stimulating afterward leads to consider ectoderm that is committed to neural fates.

The authors then studied the influence of BMP and WNT pathways on neuroectoderm patterning. We will focus on the main findings of this paper: (see Fig. 1.15)

- Pre-stimulation, endogenous BMP signaling is necessary to derive surface ectoderm.
- Exogenous BMP stimulation leads to patterns displaying concentric rings of surface ectoderm, placode, neural crest and neural progenitors, demonstrating *in vitro* a clear role for BMP in neuroectoderm spatial patterning.
- From 24 hours post-stimulation onwards, endogenous WNT signaling plays an important role in neural crest differentiation at the expanse of placodal cells.
- BMP specifically induces AP2$\alpha$ and WNT specifically induces PAX3 (although BMP might enhance its expression), and both are necessary to induce SOX9, therefore suggesting different and complementary modes of action of both pathways.

In this section, we showed the ability of micropatterns to induce spatial organization in developing tissues. Although it occurs in 2D and not in 3D, this spatial organization can be used as a proxy to correlate signaling pathways and cell identities while having experimental control on some of the parameters, be it geometrical or chemical.

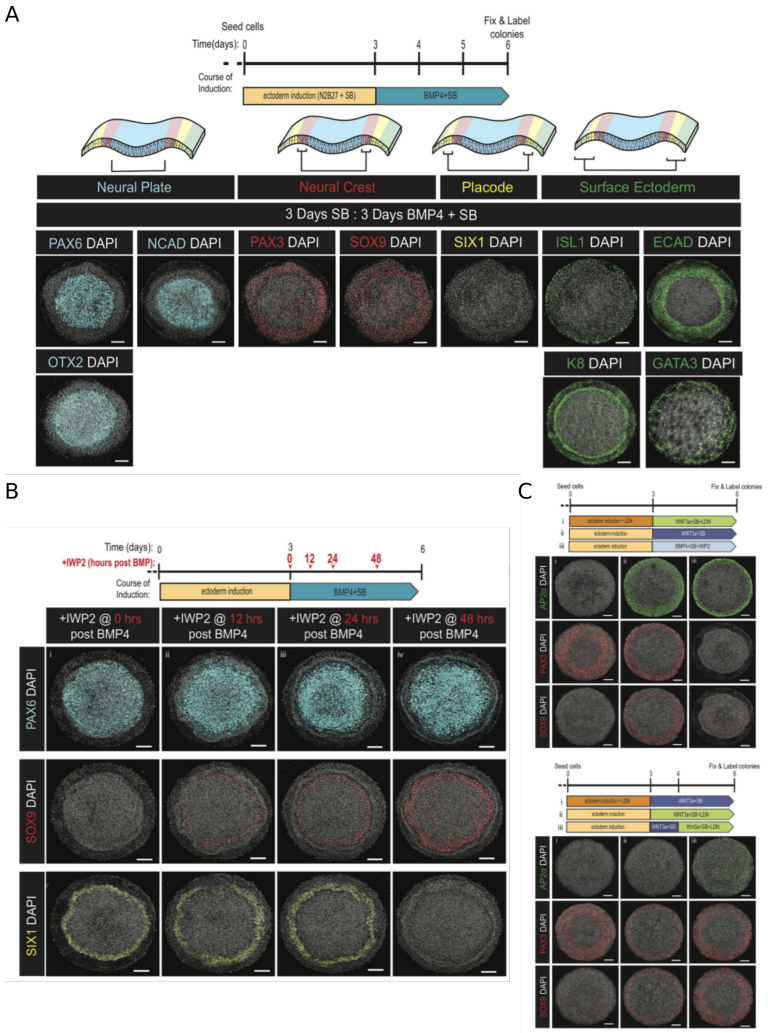


Figure 1.15: **Disentangling BMP and WNT roles in neuroectoderm patterning.** **A** Neuroectoderm patterning under exogenous BMP stimulation. **B** Endogenous WNT promotes neural crest differentiation at the expanse of placodal cells. **C** Varying BMP and WNT signaling to investigate AP2$\alpha$ and PAX3 and SOX9 induction. Adapted from [Britton et al., 2019].

## 1.5 Thesis project

From the biophysicist point of view, being able to control the spatial organization of neural progenitors *in vitro* and vary experimental parameters is the best way to build and test models of patterning. During my thesis, I worked on a few experimental setups that have proven efficient in inducing and monitoring self-organization of hESCs.

Before diving into experimental work, we will present the methods we used for cell culture, microscopy and image analysis

Then, we will focus on the core of my thesis project, which consisted in studying dorso-ventral identities acquired by neural progenitors when cultivated on micropatterns.

Finally, we will give an overview of what we think needs to be done to complement my work on micropatterns. We will also try to point out some limitations of micropatterns and propose alternative setups to study the dorso-ventral specification of neural progenitors.

# Chapter 2

# Material and Methods

## 2.1 Cell culture

Unless specified otherwise in the manuscript, experiments were conducted using the Wild Type human Embryonic Stem Cell (WT hESC) line RUES2 generated by The Rockefeller University.

### 2.1.1 Matrigel coating

hESCs were cultivated on Matrigel-coated 35mm Petri dishes. Coating of Petri dishes was conducted on ice, and all equipment used in the coating process was kept at -20°C for at least 30 minutes. 30 minutes before coating, a Matrigel aliquot was moved from -20°C to -4°C to allow thawing. Matrigel was diluted at a 1:50 ratio in cold DMEM-F12 and added on a cold Petri dish (typically 1mL in a 35mm Petri dish). Petri dishes were kept overnight at -4°C and used within 2 weeks.

### 2.1.2 Cell maintenance and passaging

hESCs were cultivated in mTESR or mTESR-Plus media with the addition of Penicillin-Streptomycin (PS) at 50µg/mL. When cells reached confluency

(typically every 6-7 days), cell density was estimated and cells were passaged as clumps at a 1:60 to 1:30 ratio using ReLeSR – an enzyme-free reagent for dissociation and passaging of ESCs – and the following protocol:

1. A Matrigel-coated 35mm Petri dish was placed at 37°C for about 30 minutes.

2. mTESR was aspirated and cells were washed once with PBS.

3. Cells were incubated in ReLeSR (1mL for a 35mm Petri dish) at 37°C for 2 minutes, and ReLeSR was then aspirated.

4. 1mL of room temperature DMEM-F12 was gently pipetted in and out of the Petri dish until clumps of cells were detached, and transferred into a 15mL Falcon tube containing an extra 9mL of DMEM-F12.

5. Cells were centrifugated at 300g for 4 minutes. Supernatant was aspirated and cells were resuspended in 1mL mTESR.

6. Dilution in mTESR to obtain the desired passaging ratio was carried out so that the appropriate number of cells was found in a 500mL volume.

7. The Matrigel-coated 35mm Petri dish was taken out of the incubator and media was aspirated and replaced by 1mL mTESR without cells.

8. The 500mL volume containing the cells was added into the Petri dish, making sure they were spread evenly, and the Petri dish was placed at 37°C in the incubator.

9. Media was replaced every day with mTESR, every other day with mTESR-Plus.

### 2.1.3 Culture media

mTESR and mTESR-Plus were purchased from StemCell Technologies and used to cultivate hESCs.

N2B27 was made using the following recipe (volumes for 400mL of total media):

- 192 mL of DMEM/F12 (Lifetech #21331-020)
- 192 mL of Neurobasal medium (Lifetech #21103-049)
- 2ml of N2 (Lifetech #17502-048)
- 4ml of B27 (Lifetech #17504-044)
- 4ml of Penstrep (Lifetech #15140-122)
- 4ml of L-Glutamin (Lifetech #25030-024)
- 2.6ml BSA 7,5% (Lifetech #15260-037)
- $\beta$-mercaptoethanol was added at a concentration of 0.1mM simultaneously to signaling molecules.

We aliquoted N2B27 in 50mL Falcon tubes and kept them at -20°C for a few months.

## 2.2 Making of micropatterned substrates

The different steps we used to make micropatterned substrates are detailed in the following section and illustrated in Fig. 2.1

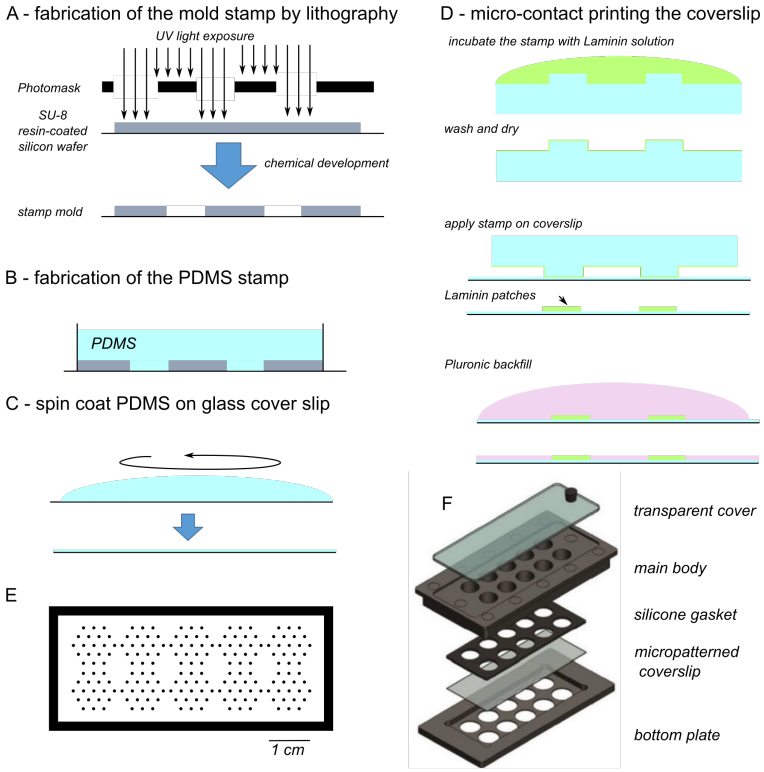


Figure 2.1: **Making of micropatterns.** **A** Spatially-controlled exposure of a silicon wafer coated with SU-8 resin to UV followed by chemical development leads to patterned wafers. **B** A negative PDMS stamp is made out of the wafer. **C** Glass coverslips are coated with a thin layer of PDMS thanks to spin-coating. **D** Laminin is deposited on the PDMS stamp and spatially transferred onto the glass coverslip. **E** Typical photomask used in our experimental setup. **F** The Chamlide 10-well chamber device used for hESCs culture on micropatterns.

### 2.2.1 Making of wafers

To make micropatterned wafers, we resorted to photolithography.

1. A photomask of the desired image was first designed using Inkscape, black color corresponding to the area we want the cells to attach to.

2. The photomask was printed at a 10k dpi resolution on polyester films by a mask supplier such as `https://www.jd-photodata.co.uk/`.

3. In a clean room, a silicon wafer was cleaned by successive washes with acetone and isopropanol and dried by gently blowing nitrogen, then leaving it on a hot plate at 150°C for 10 minutes.

4. The wafer was placed on a spin-coater and SU8-2100 resin was poured at the center of the wafer to cover half of its surface. Spin coating was typically done in 2 steps to achieve a 50-100µm thick resin: 10 seconds at 500 rpm, then 40 seconds at 4000 rpm.

5. Soft baking was carried out by slowly transferring the wafer on a hot plate at 65°C for 10 minutes then on another hot plate at 95°C for 30 minutes.

6. In a mask aligner, the photomask was taped onto the mask holder and the wafer was positioned. The resin was exposed to 365nm UV light at 12mW for 60 seconds.

7. Post-exposure bake was carried out by transferring the wafer on a hot plate at 65°C for 5 minutes then on another hot plate at 95°C for 10 minutes.

8. The wafer was developed in SU8 developer in a beaker on a rotary shaker for 2 minutes, then washed with isopropanol and dried with nitrogen.

9. Quality of the development was monitored with a reflected light upright microscope, and thickness of the layer was measured using a profiler.

10. The wafer was silanized in a vacuum desiccator next to a beaker containing one drop of 1H,1H,2H,2Hperfluorooctyl-trichlorosilane. After establishing vacuum, the pump was turned off and left for at least 2 hours before breaking vacuum.

### 2.2.2 Making of PDMS stamps

1. The appropriate amount of PDMS (20-25g per wafer) was carefully mixed from Sylgard 184 using a 1:10 ratio between crosslinker and base.

2. The PDMS mix was degassed in a desiccator under vacuum.

3. Photoprinted wafers were transferred in a 100mm Petri dish and the PDMS mix was poured onto the wafer.

4. The Petri dish was degassed once more in the desiccator until all bubbles disappeared.

5. The Petri dish was cured at 65°C overnight, then stored indefinitely.

### 2.2.3 Making of PDMS coverslips

1. The same degassed PDMS mix as described in 2.2.2 was prepared (smaller amounts are needed, typically 5g for 20 coverslips).

2. We made sure to use clean $24 * 60$ mm coverslips. If coverslips were not clean enough, they were successive washed with acetone and isopropanol and left to dry.

3. Coverslips were centered on the chuck of a spin-coater and vacuum was established to immobilize it.

4. A drop of PDMS was poured at the center of the coverslip and spread manually using a P1000 tip to cover the rectangular surface

5. The coverslip was spin-coated using a 2-step protocol: 15 seconds at 500 rpm, then 45 seconds at 3000 rpm. This resulted in a $\sim$ 30µm thick layer of PDMS.

6. The coverslips were cured at 65°C overnight, then stored indefinitely and hermetically to protect them from dust.

### 2.2.4 Microprinting of Laminin521 on coverslips

1. A 10 well Chamlide magnetic chamber (see model WL-2460-10 on `https://www.gataca-systems.com/wp-content/uploads/Brochure-Chamlide-Magnetic-Chambers.pdf`) was carefully washed with water and dish soap, then rinsed abundantly with hot water, then with distilled water, and finally sterilized with 70% ethanol.

2. The chamlide was left to dry under a sterile hood.

3. The PDMS stamp made in 2.2.2 was cut out of the mold with a sterile sharp scalpel and transferred into a 100mm Petri dish, motifs facing upwards.

4. Laminin521 purchased at `https://biolamina.com/products/laminin-ln-521-stem-cell-matrix/` was diluted 5 times in PBS with Ca and Mg ions (PBS++) to achieve a 20µg/mL concentration. We prepared 100µL of diluted laminin per well, then added it to the appropriate location on the stamp, judging from the motifs. Incubate for 1 hour after closing the lid to prevent drying.

5. Laminin521 was aspirated, then the stamps were washed once with PBS++, then distilled water. Stamps were then left to dry under the hood during the following step.

6. A coverslip made in 2.2.3 was marked with a slight cross on one corner (to give an orientation indication) and exposed to deep UV in a UV-ozone cleaner for 5 minutes.

7. The dried stamp was put on top of the coverslip, and gentle pressure was applied, by using the bottom end of a tweezer, to ensure contact on all the motifs.

8. The coverslip was then released from the stamp and transferred into the bottom part of the Chamlide. The silicone gasket was inserted into the top part, and the Chamlide was closed carefully.

9. 100µL of a solution of 1% Pluronic F-127 in PBS++ was added to each well to prevent adhesion outside the motives.

10. After 3 washes with PBS++, the Chamlide is ready for cell seeding.

## 2.3 Neural differentiation on micropatterned substrates

### 2.3.1 D0 seeding

1. Three falcons were prepared: one with Accutase+RI (1mL per 35mm Petri Dish), one with DMEM+RI (9mL per 35mm Petri Dish) and one with N2B27+RI+signaling molecules indicated in the protocols such as CHIR, LDN, SB or FGF (N2B27+RI++, 300µL per well to be seeded, we usually prepare it in excess).

2. hESCs from a confluent 35mm Petri Dish were washed in PBS and incubated in 1mL Accutase+RI at 37°C for 6-7 minutes.

3. Cells were detached and dissociated by gently pipetting in and out of the Petri Dish, then transferred into a 15mL falcon containing 9mL

DMEM-F12+RI to prevent further action from the Accutase. The number of cells was determined using a Malassez counting chamber.

4. Cells were centrifugated at 300g for 4 minutes. Supernatant was aspirated and cells were resuspended in the appropriate volume of N2B27+RI++ to get a concentration of 3M cells/mL.

5. PBS from Chamlides prepared in 2.2.4 was aspirated and replaced with 200µL of N2B27+RI++ without cells.

6. 100µL of N2B27+RI++ with cells was added drop by drop in each well to ensure homogeneous seeding.

7. 2 hours after seeding, cells that did not adhere were removed by very gentle pipetting and cells were fed with N2B27++ (that does not contain RI)

8. Media was changed every day until day 4 of differentiation, when cells were fixed.

### 2.3.2 D2 seeding

1. When dealing with D2 seeding protocols, we first seeded cells on a 35mm Matrigel-coated Petri Dish for the first 2 days. We used the same single-cell passaging described in 2.3.1, aiming at 1M cells in 500µL after resuspension in N2B27+RI++, that we added into a 35mm Matrigel-coated Petri-Dish filled with 1mL of N2B27+RI++. On the next day, we changed the media and removed RI.

2. After 2 days, each Petri Dish typically yields 2 to 3M cells. We then performed another single-cell passaging as described in 2.3.1, but this time we seeded cells into the wells of the Chamlide device. RI was removed 2 hours after seeding and media was changed on day 3, 4, 6

and 8. Signaling molecules specific to each experiment are indicated on a timeline next to the corresponding experiment.

## 2.4 Imaging

### 2.4.1 Immunostainings

1. Upon fixation, culture media was removed and replaced by 4% PFA. We used to include a washing step in PBS before fixation but noticed it led to colonies detachment to some extent.

2. 30 minutes after PFA fixation, cells were washed 3 times with PBS.

3. For pSMAD stainings only, a step was added to make the epitope more available. Cells were incubated in a detergent solution (1% SDS in PBS) for 30 minutes at 37°C and washed 3 times with PBS.

4. Cells were permeabilized with a blocking buffer solution (3% BSA, 1% Triton, 1% sodium azide in PBS) at 4°C overnight. We noticed that shorter incubation did not perform as well on very dense colonies.

5. Primary antibodies (see Table 2.1) were diluted in blocking buffer at the desired concentration and cells were incubated overnight at 4°C in this solution.

6. On the next day, cells were washed 3 times with PBS.

7. Secondary antibodies (see Table 2.3) and DAPI were diluted in blocking buffer at the desired concentration and cells were incubated either for 2 hours at room temperature or overnight at 4°C. We noticed that overnight incubation, although known to lead to higher noise in fluorescent signals, gave better results for DAPI penetration across the colony.

8. After 3 more washes with PBS, cells were ready for imaging.

### 2.4.2 List of primary and secondary antibodies used

Table 2.1: Primary antibodies

| Antibody | Dilution | Host | Supplier | Reference |
|---|---|---|---|---|
| Cdx2 | 1/200 | Mouse | Abcam | ab157524 |
| Cdx2 | 1/1000 | Rabbit | Abcam | ab76541 |
| Foxa2 | 1/200 | Rabbit | Cell Signaling | 8186S |
| Gbx2 | 1/300 | Rabbit | Proteintech | 21639-1-AP |
| Isl1 | 1/1000 | Goat | Neuromics | GT15051 |
| Nkx2.2 | 1/100 | Mouse | DSHB | 74.5A5 |
| Nkx6.1 | 1/100 | Mouse | DSHB | F55A12 |
| Olig2 | 1/1000 | Rabbit | Millipore | AB9610 |
| Olig3 | 1/100 | Guinea Pig | Birchmeier Lab | |
| Otx2 | 1/800 | Goat | Neuromics | GT15095 |
| Pax6 | 1/200 | Mouse | Abcam | ab78545 |
| Pax7 | 1/100 | Mouse | Santa Cruz Biotech | sc-81648 |
| pSMAD1/5 | 1/200 | Rabbit | Cell Signaling | 13820S |
| pSMAD2/3 | 1/200 | Rabbit | Cell Signaling | 18338S |
| Sox1 | 1/200 | Goat | R&D Systems | AF3369 |
| Sox2 | 1/200 | Rabbir | Cell Signaling | 3579S |
| TFAP2$\alpha$ | 1/100 | Mouse | Santa Cruz Biotech | sc-12726 |
| TFAP2$\alpha$ | 1/100 | Rabbit | Santa Cruz Biotech | sc-8975 |

Table 2.3: Secondary antibodies

| Donkey@ | Fluorophore | $\lambda(nm)$ | Supplier | Reference |
|---|---|---|---|---|
| Mouse | Alexa488 | 488 | Abcam | ab150109 |
| Goat | Alexa555 | 555 | Abcam | ab150134 |
| Rabbit | Alexa555 | 555 | Abcam | ab150062 |
| Guinea Pig | Cy3 | 568 | Jackson Immuno | 706-165-148 |

| | | | | |
|---|---|---|---|---|
| Mouse | Alexa647 | 647 | Abcam | ab150111 |
| Rabbit | Alexa647 | 647 | Abcam | ab150063 |

### 2.4.3 Microscopy

Immunostainings were imaged with two different spinning disk microscopes: - An Andor Revolution DSD2 confocal microscope owned by the team - The CSU-W1 microscope from the ImagoSeine platform (`https://imagoseine.ijm.fr/en/706/spinning-disk-confocal.htm`) was used to acquire bigger field of views For both microscopes, imaging was carried with bright field and up to 4 different wavelengths (UV, Green, Red, Far Red). Several stacks were taken to account for colony thickness (typically, 100µm with one image every 5µm).

## 2.5 Quantitative analysis of gene expression via qRT-PCR

We resorted to qRT-PCR for quantitative analysis of gene expression and followed the protocol described by [Plouhinec et al., 2020]:

1. Cells from one well, containing between 7 and 10 colonies, were dissociated in 200ul of 1M guanidinium by pipetting multiple times until the dissociation of all aggregates. The resulting solution was frozen at -20°C until all samples were collected.

2. Cell total mRNA was extracted using the RNANucleoSpin RNA extraction kit (Macherey-Nagel), and quantified using a Nanodrop.

3. Between 25 and 250ng of total mRNA were reverse transcribed (RT) using the Superscript IV VILO reverse-transcriptase (Thermo Fisher Scientific) and random hexamers according to manufacturer's instructions.

4. Gene expression was quantified by quantitative PCR on a LightCycler 480 Instrument II (Roche) using 1:250 of the reverse-transcribed mRNA sample mixed with a specific primer pair (1µM final each, Table. 2.5) and 2X KAPA SYBR FAST qPCR Master Mix (Roche) according to manufacturer's conditions. For each experiment, duplicate samples were analyzed. For each gene, the quality of the amplification was tested by quantifying its expression in a serially-diluted pool of all RT (1:10 to 1:320) to quantify amplification efficiency and target mRNA concentration relative to the RT pool in each sample.

We normalized gene expression by dividing the measured gene expression by that of the housekeeping gene *CYCLOPHYLIN A* (*CYCLO-A*).

Table 2.5: Primers used for qRT-PCR

| Gene | F/R | Sequence | Reference |
|---|---|---|---|
| *CDX2* | Forward | GAACCTGTGCGAGTGGATG | [Maury et al., 2015] |
| | Reverse | GGATGGTGATGTAGCGACTG | |
| *CYCLO-A* | Forward | CCCACCGTGTTCTTCGACAT | [Maury et al., 2015] |
| | Reverse | CCAGTGCTCAGAGCACGAAA | |
| *GBX2* | Forward | AAAGAGGGCTCGCTGCTC | [Qu et al., 2014] |
| | Reverse | ATCGCTCTCCAGCGAGAA | |
| *HOXA2* | Forward | CGTCGCTCGCTGAGTGCCTG | [Maury et al., 2015] |
| | Reverse | TGTCGAGTGTGAAAGCGTCGAGG | |
| *HOXA4* | Forward | ACGCTCTGTTTGTCTGAGCGCC | [Maury et al., 2015] |
| | Reverse | AGAGGCCGAGGCCGAATTGGA | |
| *HOXA5* | Forward | GGAGATCATAGTTCCGTGAGC | [Maury et al., 2015] |
| | Reverse | GCTGAGATCCATGCCATTGT | |
| *HOXB4* | Forward | TACCCCTGGATGCGCAAAGTTC | [Lippmann et al., 2015] |
| | Reverse | TGGTGTTGGGCAACTTGTGG | |
| *OTX2* | Forward | CCAGACATCTTCATGCGAGAG | [Lippmann et al., 2015] |
| | Reverse | GGCAGGTCTCACTTTGTTTTG | |

## 2.6 Image analysis

The image analysis described in the following section followed a standard framework. We uploaded some typical Matlab code on `https://github.com/GabrielThon/Thesis-code`.

### 2.6.1 Stitching

While the wide field of the CSU-W1 microscope enabled us to image a $700\mu m$ colony on a single field of view, this was not possible with the DSDS2 microscope, on which we had to perform $2 * 3$ or $2 * 4$ montages. Therefore, we had to resort to stitching and correct those images. Stitching was routinely performed using ImageJ implemented plugin. *Grid/Collection stitching*.

### 2.6.2 Image correction

Importantly, when montages were taken, we were confronted with the fact that the center of the colony was systematically deported to the edges of the field of view, while the periphery of the colony remained at the center of the field of view. Although moving the stage in a perpendicular plane allowed us to make sure none of the phenomena described were due to imaging artifacts, processing non-corrected images perturbed image analysis in a significant way.

#### Acquisition of the real flatfield image

To recover flatfield for post-image correction, we tested several methods. Autofluorescent plastic slides (`https://www.chroma.com/products/accessories/92001-autofluorescent-plastic-slides`) did not yield good results and mainly are not adapted to retrieve the flatfield in a confocal setup because of the thickness of the calibrating slides. We also tried to image fluorescent dextrans caught inbetween two glass slides but were faced with a similar thickness challenge.

The practical method that yielded the best results consisted in seeding hESCs in the well of a chamlide on a PDMS-coated coverslip on which Laminin521 was added uniformly (rather than stamped like in the classic micropatterning protocol), growing these cells in mTESR until confluency was reached and finally staining them with Sox2-Rabbit as primary antibody and Donkey@Rabbit Alexa 488, 555, 647 as secondary antibodies, as well as DAPI. This protocol should give a homogeneous signal since Sox2 expression is maintained in hESCs. We then took images at randomly selected positions of the sample. Averaging all the images acquired and smoothing the signal with a Gaussian filter, we should be able to get a good prediction of the microscope flatfield.

Unfortunately, most of the images taken could not be corrected with the physically-measured flatfield obtained thanks to the former method. Indeed,

best practices would require recording the flatfield in each imaging session, since it can vary in time and more drastically every time the microscope is realigned.

### Inference of the flatfield correction

Hence, we decided to infer the flatfield from our dataset thanks to a published algorithm, called BaSiC, detailed in [Peng et al., 2017]. This inference method is not ideal since one of its limitations is found when the dataset is highly-correlated and our dataset consists in montages of patterned colonies that exhibit recurrent motives. A smoothing parameter, referred to as $\lambda$ in the initial publication, can be tuned in to account for these correlations phenomena

To assess the performance of BaSiC flatfield inference from our dataset, we generated montage images of an example patterned colony and multiplied each pixel with the corresponding pixel of a known flatfield that we designed to be Gaussian. We then ran the BaSiC algorithm with different values for $\lambda$ and computed the ratio between each pixel of the inferred flatfield with the one used to generate images. This gives us an idea of whether BaSiC image correction tends to undercorrect or overcorrect images that present spatial patterns similar to those we observe in our experiments.

What comes out of this test is that the BaSiC image correction method overestimates the real flatfield at the corners of the image (leading to overcorrection), and slightly underestimates it at the borders (leading to undercorrection).

We tested whether using a high $\lambda$ value (9.5) could correct actual images from our experiments and were satisfied with the results it gave (see Fig. 2.3A). In most cases, correction seemed to improve the quality of images, except for a few sets of images taken in the far red channel (647nm) where the inferred filter distorted the images (see Fig. 2.3B). We made sure every set of images we processed did not exhibit systematic features due to correction.

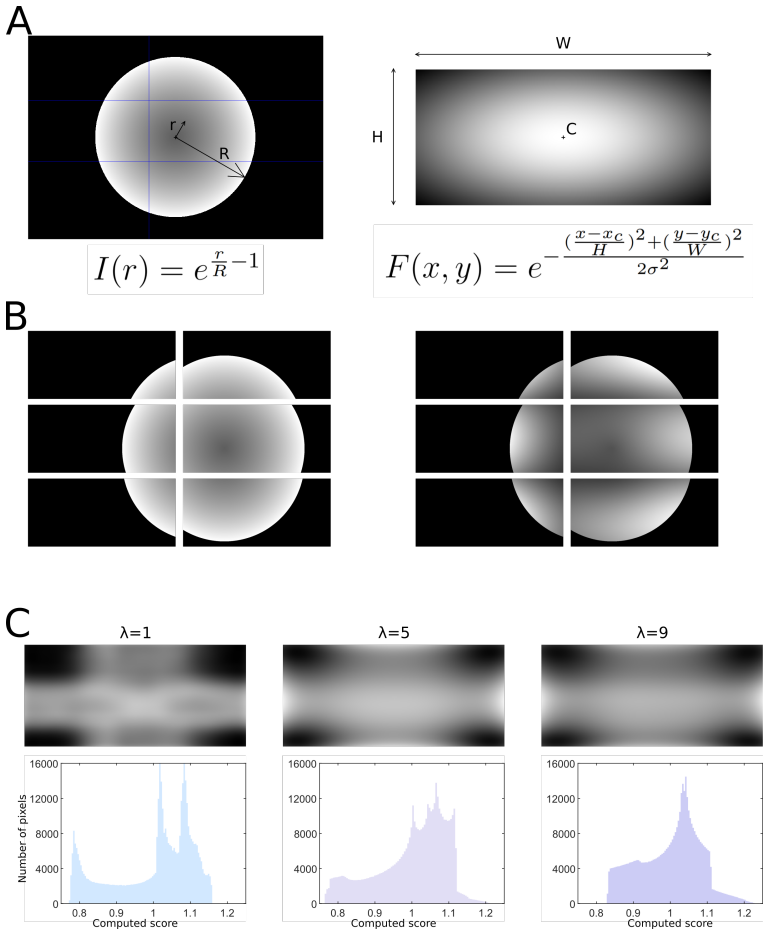


Figure 2.2: **BaSiC performances on generated montage images. A** Generated image of a model patterned colony and an anisotropic gaussian flatfield **B** Random cuts (in blue in **A**) were performed on the model colony with a 10% overlap and were distorted by the flatfield **C** Typical normalized score images and pixel distribution for $\lambda$=1,5,9 showing smoothening of the correction with persistent patterns.

### 2.6.3 Image processing

#### Montage and maximum projection of Z-Stack

We used a standard procedure to retrieve images of each colony:

1. If montages had to be performed, images were corrected with the flat-field inference method presented in 2.6.2, and hyperstacks were stitched using *Grid/Collection stitching* ImageJ plugin or ImageJ-MATLAB extension.

2. Hyperstacks were then projected along the z-axis using maximum intensity projection

In doing so, we generated one *.tif* file for each colony that contained projected images in different fluorescence channels.

### Colony border identification

DAPI images were used to identify colony border, using a global thresholding Otsu's method **graythresh**. Finetuning of the threshold was possible through a GUI **segment_cell** that was given to us by Mathieu Coppey's team.

In doing so, a binary mask was generated from the DAPI staining, and the border of the colony could be retrieved from this binary image. (see Figure 2.4A)

### Nuclear intensity

To quantify fluorescence signal across the colony, we tried to resort to nuclear segmentation on DAPI images. However, in our experimental conditions, cells are highly-packed so only a few pixels separate nuclei. Higher resolution or supervised learning on our datasets could make segmentation possible.

In order to still be able to extract quantitative information from our images, we submitted projected images to a local maxima identification algorithm **FastPeakFind** developed by Natan (`https://fr.mathworks.com/matlabcentral/fileexchange/37388-fast-2d-peak-finder`).

For each maximum that was part of the colony previously identified, we calculated the mean nuclear intensity on a disk-like structuring element,

whose radius is a tunable parameter. This amount to approximating the nucleus with a sphere of a given radius, which introduces a bit of noise in the estimated signal but already yields significant results. (see Figure 2.4B,C)

### Distance to the border of the colony

For each maximum that we identified, we computed its distance to the border of the colony. In order to do that, we used the projection algorithm **distance2curve** developed by John D'Errico (`https://www.mathworks.com/matlabcentral/fileexchange/34869-distance2curve`).

In several images, the colony did not fit within the field of view and the border could be mistaken for the border of the image. To avoid this, we removed all the maxima whose projection had been identified as a border of the image.

We added a parameter **convPixel** to convert the computed distance (in pixels) to the metric distance (in µm). For further plotting, we also added a parameter **bin** to regroup cells within a $[i * bin, (i+1) * bin]$ metric distance. Let's note that this introduces a bit of noise in the signal.

### FACS-like cell-sorting

Comparing intensity levels from one experiment to another is not trivial, since they depend on fixation, antibodies incubation or even power of the emission LED/laser.

To estimate percentages of positive cells, we used a FACS-like approach. Given a distribution of intensity levels across the sample and comparing it with a negative control, we determined a threshold above which cells were considered positive.

The negative control was either a group of cells within the colony that did not display any signal – which was mostly used when the colony was patterned – or cells from colonies using other differentiation protocols – when the colony was not patterned.

We developed a GUI **FACS_like** that allows the user to adjust the threshold of one marker and visualize positive and negative cells within a colony, and a 2D version **FACS_like_2D** to establish a correlation between two markers. Once a threshold was adjusted on one characteristic colony, it was used in all colonies of the same experiment that shared the same fluorescent marker. (see Figure 2.4E)

### Plotting of curves

For intensity profile curves, we computed the mean fluorescence over all the colonies from one representative experiment. For each fluorescent marker, we evaluated noise on an area outside of the colony and subtracted this noise. We then divided by the maximal intensity found across the set of images within the same experiment. Error shaded areas correspond to the first and third quartiles.

We removed points corresponding to distances for which less than a given number of cells ($\sim 20$) had been identified (generally near the center), that were leading to very noisy signal mostly due to binning.

For percentage curves, we computed the mean percentage over all the colonies from one or several biological replicates of the experiment.

### Clustering of curves

We wanted to classify colonies in different categories depending on the signal of a given marker. Is the distribution flat? Are there cells only at the center, or at the border? We first thought of two statistical indicators of the distribution of cells that could discriminate between colonies:

- The mean distance from positive cells to the border of the colony. For a homogeneous disk of radius R: $D_{center} = \frac{\int_0^R (r^2 dr)}{\int_0^R (r dr)} = \frac{2R}{3}$ so $D_{border} = R - \frac{2R}{3} = \frac{R}{3}$. While this indicator can discriminate between a homogeneous distribution ($D_{border} = \frac{R}{3}$) and one where positive cells are located at

the periphery ($D_{border} = 0$) or at the center ($D_{border} = R$) of the colony, it scores badly for two-peaked distribution.

- An entropy-like parameter to rank how ordered the distribution is. Let $N$ be the number of bins. Stemming from the curve representing the percentage of positive cells in function of the radius, one can normalize it into a radial probability distribution $\{p_i\}_{i=1..N}$. The curve that we get can be viewed as followed: let's place ourselves along one radius of a colony; what is the probability, given a positive cell, that its distance to the border of the colony is within the interval $[bin * (i-1), bin * i]$. One can then compute a rescaled Shannon entropy $S = \frac{-\sum_{i=1}^{N}(p_i log(p_i))}{log(N)}$. Its value should be 1 for a homogeneous distribution and 0 for a peaked distribution. While this estimator is good to tell how localized the signal is, it loses spatial information. For example, two peaked distributions at different distances will similarly give a null value.

We finally opted for a third indicator that we thought adapted to our problem, which consists in computing distances between radial probability distributions thanks to optimal transport theory. We found this distance to be relevant in our case since it incorporates a mapping of the space, with higher costs involved when "moving" a positive cell from the border to the center of the colony than to a neighbor location.

Practically, we computed the 1-Wasserstein distance for each pair or colony, by using the **ws_distance** Matlab function found on `https://github.com/nklb/wasserstein-distance`. We then built a hierarchical cluster tree using the **linkage** function, and set a threshold to form n clusters (starting at n=2) with the **cluster** function. We then plotted the curves assigned to different clusters together to see if curves within each cluster behave similarly. If several outliers remained, we increased the number of clusters to describe our dataset more accurately.

It is important to note that whenever a curve represents a "radial prob-

ability distribution", it does not account for the global number of positive cells, since this information is lost in the rescaling step.

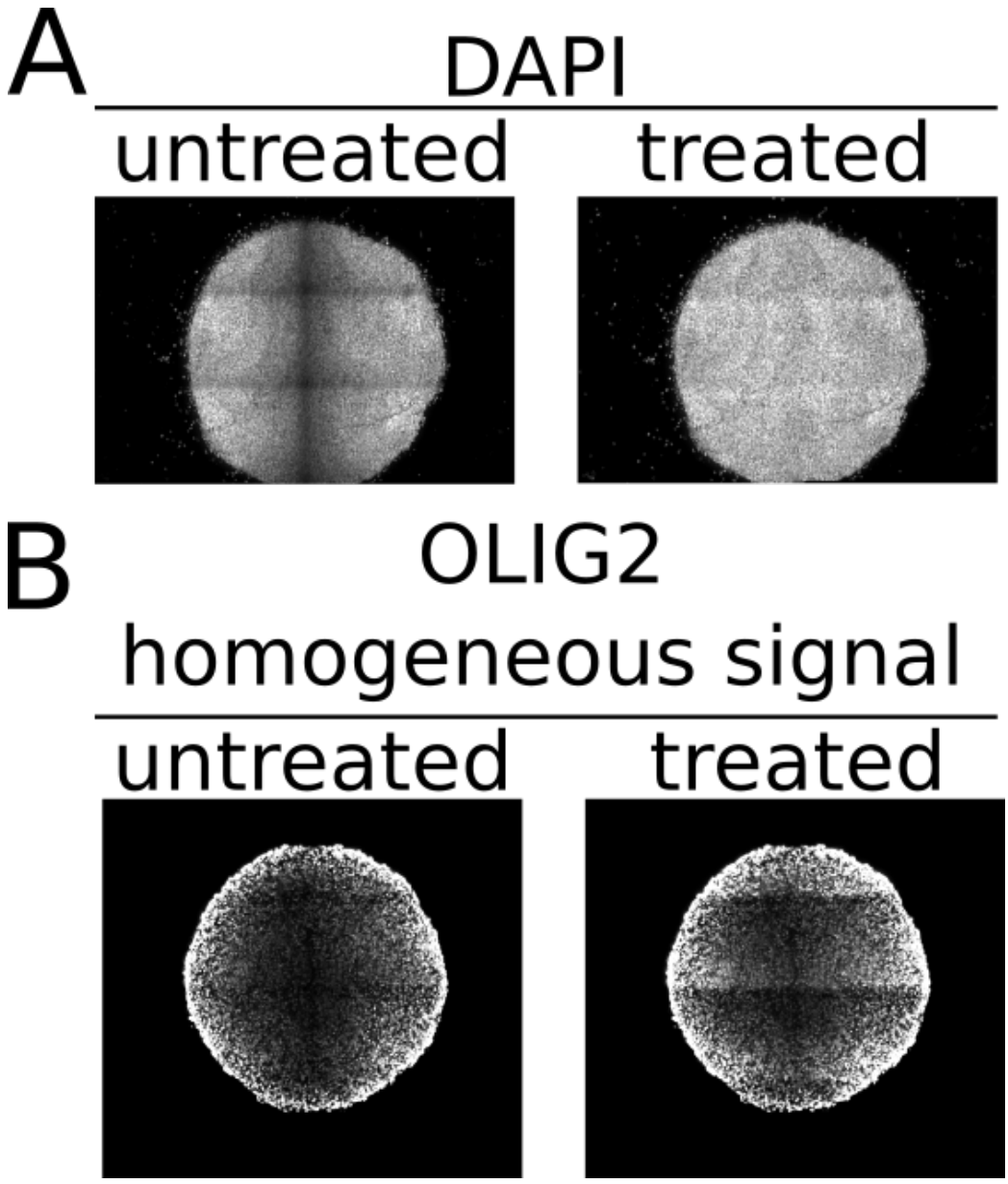


Figure 2.3: **Correcting stitched images with BaSiC. A** Correction of the DAPI signal in stitched images achieved by the BaSiC algorithm. **B** Example of treatment with persistent features. Here, the upper right and left pixels seem to be undercorrected.

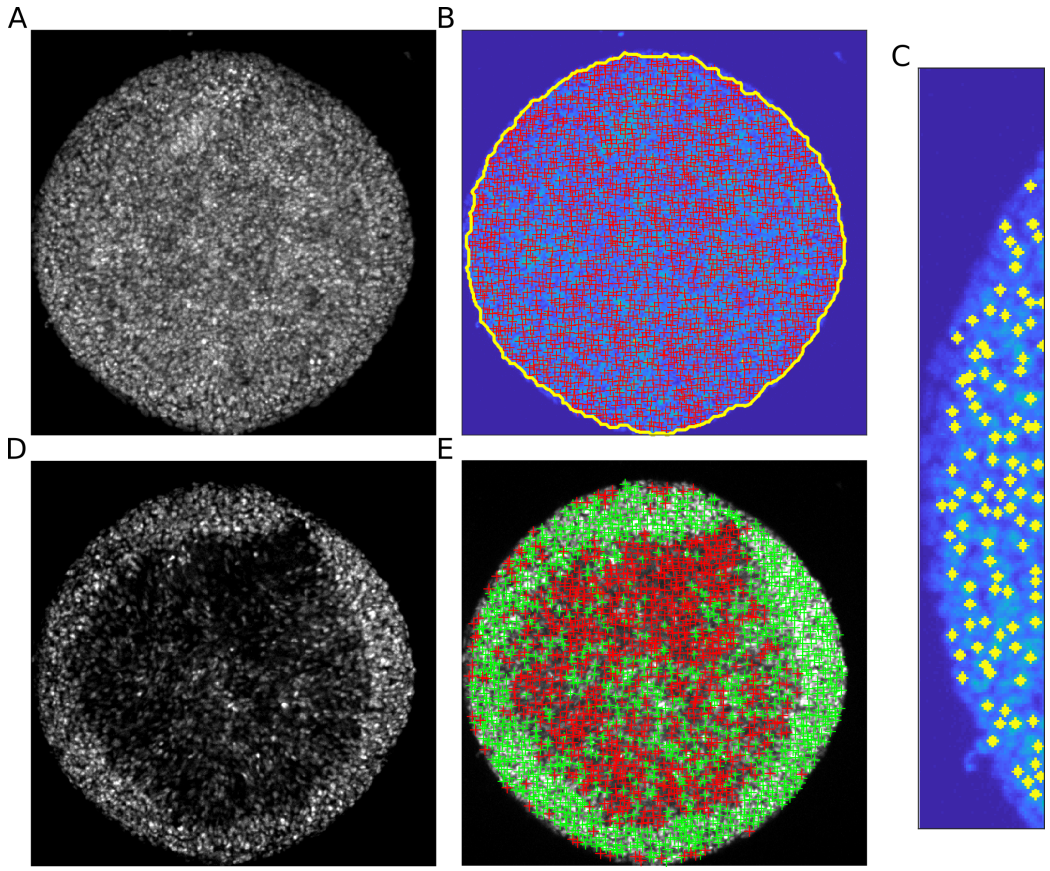


Figure 2.4: **Processing images to extract quantitative data. A** DAPI image of a colony submitted to BMP stimulation (10ng/mL from D3 to D9). **B** Extraction of the border of the colony (in yellow) and identification of local maxima (in red) from the DAPI image **C** Zoom on a region of the colony enables tuning of the radius of the sphere (in yellow) before intensity computation. **D** Corresponding TFAP2$\alpha$ staining. **E** FACS-like tuning discriminates between positive (green) cells and negative (red) cells.

# Chapter 3

# Spinal cord patterning on micropatterned substrates

This chapter corresponds to the main results from our investigation of neural differentiation on micropatterned substrates and is the core of the thesis.

With advice from Vanessa RIBES and Stéphane NEDELEC, we adapted neural differentiation protocols to micropatterned substrates in order for them to be suited to investigate the dorso-ventral patterning of the neural tube.

We decided to organize this part as a short report that we would like to submit for publication in the near future. We did not include a Material and Methods section to avoid too much repetition with the Material and Methods part of the thesis.

# Abstract

During embryonic development, the neural tube is patterned along its dorso-ventral (DV) axis by antiparallel gradients of BMP, Wnt and SHH. While classical experimental models to study DV patterning of the neural tube can provide clear evidence of the implication of these pathways, they are less efficient in probing how cells respond to them in a quantitative and time-trackable manner. In this paper, we tested whether neural specification from hESCs on micropatterned substrates can be used to overcome these issues. We first identify conditions to generate pure spinal neural progenitor populations from hESCs and we evaluate how colonies respond to dorsalizing and ventralizing morphogenetic signals provided in bulk. We report that neural progenitors on micropatterned substrates are more prone to differentiate into dorsal fates due to endogenous BMP, Wnt and Activin/Nodal signaling. We then assess how dorsal cues of BMP and ventral cues of SAG, an agonist of SHH, are interpreted and lead to patterns at the scale of the colony. In the case of ventral patterning, we highlight the importance of Activin/Nodal in the establishment of an OLIG2 pattern. All in all, micropatterns substrates and their tendency to unveil endogenous signaling appear like an interesting option to study *in vitro* the spatial self-organization of neural progenitors.

# Introduction

The function of many organs holds in the generation of multiple cell types precisely arrayed in the tissue. This is well exemplified in the generation of thousands of distinct types of neurons in appropriate numbers and at precise locations in the developing spinal cord, which underlies the formation of neural circuits encoding our locomotion and sensory senses [Jessell, 2000]. The precursors of these neurons originally lie in the caudal lateral epiblast [Henrique et al., 2015]. This tissue is composed of naive progenitors, that can either enter the primitive streak and give rise to mesodermal and endodermal cells or be pushed towards more anterior regions where they acquire a pre-neural progenitor state (PNP), marked by the transcription factors SOX1 and PAX6. Transient CDX2 expression was also observed in the caudal part of the neural tube of the mouse embryo prior to E12.5 [Sanchez-Ferras et al., 2012] This later state is then converted into a full neurogenic progenitor (NP) state.

During their differentiation, NPs acquire a specific identity depending on their position along the dorso-ventral (DV) axis in the neural epithelium. As such, 11 molecularly distinct progenitor subtypes can be distinguished (, dorsal progenitors (dp1-6), ventral progenitors (p0-3), motoneuron progenitors (pMN)), each of which will generate a limited number of neurons. This pattern of differentiation mainly emerges in response to two antiparallel morphogen gradients – BMP in dorsal versus SHH in ventral – which together provide positional information to the neural progenitors [Sagner and Briscoe, 2019]. Yet, there are multiple other pathways whose role at specific times during neural differentiation has been pointed out, such as retinoic acid (RA) secreted by the somites or WNT secreted by the roof plate. Activin/Nodal was also reported to influence the pace of maturation of neural progenitors [Wind et al., 2021; Sagner et al., 2020] and to act as a morphogen in the patterning of the secondary neural tube [Gonzalez-Gobartt et al., 2021]. To what extent the combined positional and temporal information provided by

these signals enables robust development of the neural tube remains to be fully understood [Zagorski et al., 2017].

To address this question, several *in vitro* models have been developed in order to get around the difficulty of working in animal models, where the tissue can be poorly accessible, let alone in humans. The knowledge of how the different neural identities are specified *in vivo* has been used to define guided differentiation protocols to derive populations of cells enriched with a single or few of the 13 spinal NP subtypes from pluripotent stem cells (PSCs) or embryonic stem cells (ESCs) [Lai et al., 2016]. However, these protocols do not allow the reproduction of both neuronal diversity and spatial organization found *in vivo* yet. Both are essential to ensure the formation of functional microcircuits, as recently evidenced by the increased activity and neuromuscular innervation of transplanted MNs if they are in the presence of interneurons. [Magown et al., 2017]

A successful attempt to partially recover spatially organized neural diversity was obtained when deriving organoids from PSCs or ESCs, which rely heavily on non-adherent culture conditions and limited diffusion of the morphogen of interest [Meinhardt et al., 2014; Duval et al., 2019]. DV polarisation of cysts has been reported in some instances [Zheng et al., 2019], but the mechanisms underlying how polarisation occurs are hard to unveil, given that the phenomenon occurs stochastically and that movements of cells within the cysts are hard to track because of 3D and floating conditions.

A promising alternative experimental setup that generates spatially organized structures and is well fitted for microscopy is to be found in growing cells on micropatterned substrates [Warmflash et al., 2014]. This technique was first used to study germ layer specification and later adapted to investigate patterning of the anterior ectoderm. On circular patterns, cells acquire distinct cell fates depending on their position along the radial axis, which can be explained by differential sensitivity to endogenous signaling [Xue et al., 2018; Britton et al., 2019].

These last studies focused on the patterning of the ectoderm rather than that of the spinal cord. Here, we use the micropatterned substrates experimental setup to study how DV specification arises from an initially homogeneous population of spinal progenitors. First, we propose a 4-day protocol to derive a pure population of naïve spinal progenitors on micropatterns. Then, we investigate the "default" identities acquired by these progenitors. Surprisingly we observe by default a more dorsal identity than in other model systems, and suggest how endogenous signaling might be responsible for those differences. Finally, we study how dorsalization signals (via BMP) or ventralization signals (via SAG) are translated into cell fate organization at the level of a colony, and we show that patterns can be observed in both cases. Taken together, this study highlights that self-organization capabilities of the progenitors rather than passive patterning from the organizing gradients could be involved in the generation of a broad diversity of neurons and propose an experimental setup that is well designed to decipher how nodes of the morphogenetic network are linked together.

# Results and discussion

## Homogeneous population of caudal spinal progenitors generated on micropatterned substrates

In order to investigate micropatterned substrates based spinal DV patterning, we used a previously standardized differentiation protocol of human embryonic stem cells (hESCs) into naive spinal progenitors [Maury et al., 2015; Mouilleau et al., 2021]. It is based on the combined addition to neural differentiating N2B27 medium of dual SMAD inhibitors (LDN-193189 and SB-43154), activation of WNT signaling (CHIR-99021) and retinoic acid (RA) (Fig. 1A). This protocol was sufficient to orient cells plated onto conventional culture dishes in 4 days towards a caudal neural state characterized

by the pan-neuronal markers PAX6 and SOX1 (Fig. S1A).

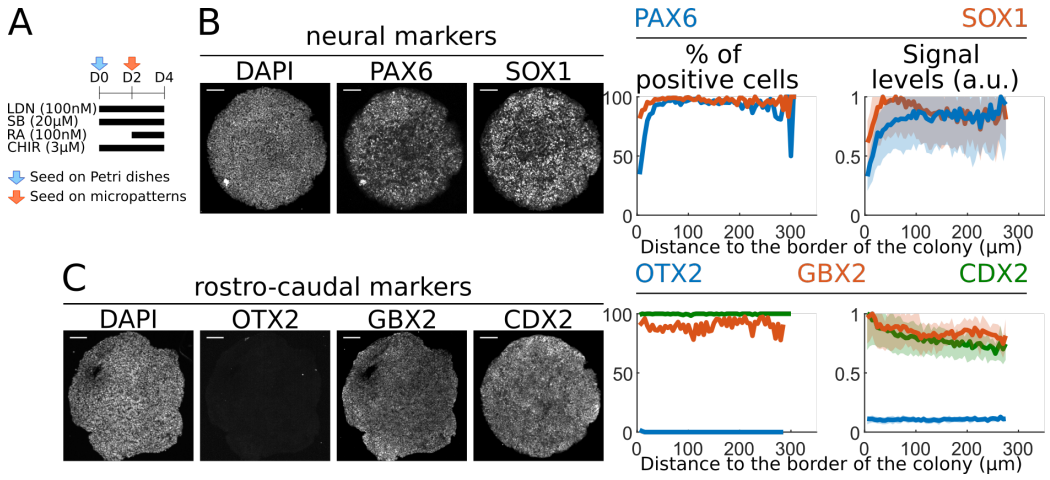


Figure 1: **Generation of a homogeneous population of spinal progenitors.** **A** The differentiation protocol used to generate a homogenous pool of naive spinal progenitors. **B** Immunostainings for the neural markers PAX6 and SOX1 and DAPI staining on cells differentiated along the protocol in A on day 4 of differentiation representative of n=10 colonies obtained in 3 independent experiments. Quantifications of the % of cells expressing these markers (left graph) and of the expression levels of these markers (right graph) along the radius of the colonies (lines: mean value; bars: first and third quartiles.; n=4 colonies of 1 experiment). **C** Immunostainings for the rostro-caudal markers OTX2, GBX2 and CDX2 (n=9 for OTX2 and GBX2; n=10 for CDX2, 3 independent experiments). Quantification on n=1 colony of 1 experiment for OTX2 and GBX2, and on n=4 colonies of 1 experiment for CDX2. Scale bar=100µm.

Micropatterned substrates used consisted of 700µm diameter Laminin521-coated islands on flat poly-dimethylsiloxane (PDMS) surfaces. hESCs were seeded at high density (500k/cm$^2$ upon seeding, which gave $\sim$ 2000 cells in each 700µm colony after removal of cells that did not adhere) onto these micropatterned substrates and allowed to differentiate. After 4 days, cells expressing CDX2, PAX6 and SOX1 were detected in the colonies (Fig. S1B). However, the level of expression of these markers was modulated depending

on the position of cells along the radial axis of micropatterned substrates. Inner cells adopted a SOX1$^{+}$; PAX6$^{+}$; CDX2$^{low}$ caudal neural state, while cells at the colony border were CDX2$^{high}$ but PAX6$^{low}$ and SOX1$^{-}$. This is reminiscent of previously described self-organized concentric patterns of neural cells surrounded by non-neural ectodermal cells upon differentiation of hESCs into ectoderm on micropatterns [Xue et al., 2018; Britton et al., 2019]. These concentric patterns of distinct cell fates complexified the study of the cell diversification process operating in neural cells only.

As we wanted to study DV patterning of neural progenitors, we wanted to start with a homogeneous population of unprimed neural progenitors. Therefore, we opted for seeding cells on micropatterned substrates at a later stage of differentiation. Passaging cells on day 2 has been used in protocols to derive NPs in adherent monolayers [Gouti et al., 2014]. We started our differentiation on conventional culture dishes, dissociated and seeded the cells on micropatterned substrates after the first two days of differentiation (Fig. 1B). On day 4 of differentiation, all cells harbored a CDX2$^{+}$; SOX1$^{+}$; PAX6$^{+}$ caudal neural progenitor state and the levels of expression of these markers were homogeneous except for a few cells at the periphery (Fig. 1B,C). We investigated the antero-posterior identity of these cells further by monitoring by immunofluorescence the expression of the anterior marker OTX2 and the hindbrain and spinal cord marker GBX2 and by quantitative real-time (qRT) PCR of several HOX genes. Colonies expressed *CDX2*, *GBX2*, *HOXA2* to *HOXA5* and *HOXB4* and not the anterior marker *OTX2*, and thus can be considered as related to spinal progenitors (Fig. 1B, S1C,D). As a comparison, progenitors seeded on micropatterned substrates and not submitted to the caudalizing molecule CHIR-99021 were OTX2$^{+}$, GBX2$^{-}$, CDX2$^{-}$ and expressed much lower levels of *HOX* genes than those cultured with CHIR-99021 (Fig. S1C,D).

Hence, we identified a method to generate micropatterned substrates containing homogeneous hESC-derived caudal neural progenitors. Seeding of

differentiating hESCs previously routed to an ectodermal state – on day 2 of differentiation – avoids a self-organizing patterning of hESCs on micropatterned substrates [Xue et al., 2018; Britton et al., 2019].

## Two distinct dorsal spinal phenotypes spontaneously emerge on micropatterned substrates

We next assessed the DV identity of hESC-derived spinal progenitors that were allowed to differentiate on micropatterned substrates in the presence of RA up to day 9 (Fig. 2A). We immuno-labeled a few transcription factors defining specific spinal progenitor pools [Lai et al., 2016] (Fig. 2B). None of the cells harbored a ventral state, as NKX6.1 (a FP to p1 marker) was hardly detected in day 9 colonies (Fig. S2Di). Instead, all the cells expressed the pan dorsal marker PAX7 (Fig. 2C, S2Dii). This is reminiscent of many neural differentiation protocols where PSC-derived neural cells adopt a dorsal state by "default" [Meinhardt et al., 2014; Duval et al., 2019].

We next monitored OLIG3 expression, which marks the dp1 to dp3 subpopulations of dorsal cells [Lai et al., 2016] and is dependent on the activity of WNT and BMP signals [Zechner et al., 2007]. Unexpectedly, OLIG3$^+$ nuclei were present in all colonies despite the absence of exogenous dorsalizing cues in the medium (Fig. 2A,C). In 43% of micropatterned colonies, OLIG3 was homogeneously expressed throughout the colonies (Fig. 2C, top panels). In the same number of colonies, its expression was restricted to a row of 2-3 cells at the periphery (Fig. 2C, bottom panels). In the remaining colonies, in addition to the outer ring of OLIG3$^+$ cells, a few additional OLIG3$^+$ cells were observed within the colonies (Fig. 2C, middle panels).

We then tested the implication of several endogenous signaling cues in generating these two discrete dorsal states. For this, we exposed cells from day 4 to day 9 to LDN, SB and iWP2, which are respectively BMP, Activin/Nodal and WNT signaling inhibitors [Boergermann et al., 2010; Byfield et al., 2004; Chen et al., 2009]. Those three signals play a key role

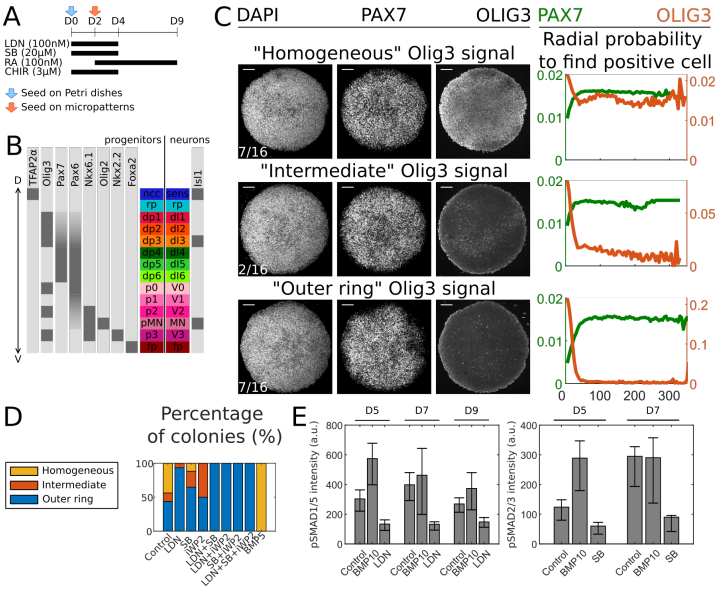


Figure 2: **Default fate of neural progenitors on micropatterns. A** Protocol used to observe the "default" fate of neural progenitors on micropatterns. **B** Expression of DV markers for neural progenitors and neurons that were used in this article. **C** Clustering of default condition colonies according to their OLIG3 distribution profile. Immunostainings for PAX7 and OLIG3 and mean quantification of the radial probability to find positive cells for each phenotype. (n=16 colonies of 4 independent experiments). **D** Percentage of colonies that were clustered into one of the three phenotypes for default ("Control") and inhibition conditions (n=16,15,17,14,6,7,9,8,2 colonies of 4 independent experiments from left to right). BMP5 corresponds to a stimulation of BMP4 at 5ng/mL from day 4 to day 9 and was used as a positive control for homogeneous signaling as later shown in Fig.3A. **E** Mean intensity for pSMAD1/5 and pSMAD2/3 over the whole colony at different timepoints and for different conditions (n=10,10,10,9,6,3,10,9,10 colonies of 1 experiment from left to right for pSMAD1/5 and n=10,10,9,9,8,9 colonies of 1 experiment from left to right for pSMAD2/3). BMP10 corresponds to a stimulation of BMP4 at 10ng/mL from day 4 to day 9. Scale bar=100µm.

in cell fate specification of progenitors laying in the dorsal part of the neural tube [Le Dréau and Martí, 2012; Sagner et al., 2020; Gonzalez-Gobartt et al., 2021]. Exposure to each of these inhibitors on their own – and even more when combined – inhibited the generation of a homogeneous OLIG3$^+$ state, with BMP signaling inhibition having the strongest negative impact on OLIG3 expression (Fig. 2D, S2A). Hence, endogenous WNT, BMP and Activin/Nodal signaling is operating in the colonies and impact cell fate decisions. Surprisingly, in the presence of any of these small molecules, an outer ring of OLIG3$^+$ cells always persisted (Fig. 2D, S2A). It remains to be determined whether the persistence of OLIG3 induction in outer cells subjected to the inhibitors is explained by specificities in their differentiation timing or in the activity of effectors downstream of dorsalization signals [Xue et al., 2018].

To confirm the existence of endogenous BMP and Activin/Nodal signaling in the default condition colonies, we monitored the activity of downstream effectors of these signaling pathways. We fixed colonies on different days and stained them for pSMAD1/5 (for BMP) and pSMAD2/3 (for Activin/Nodal). We then compared their level of expression with conditions where the corresponding signaling pathway was inhibited, and used BMP stimulation at 10ng/mL from day 4 to day 9 as a positive control (Fig. 2E). Both pSMAD1/5 and pSMAD2/3 were detected in spinal progenitors on micropatterned substrates as soon as day 5 of differentiation and this expression was inhibited respectively by LDN and SB. This confirmed that cells grown in these conditions displayed ongoing BMP and Activin/Nodal signaling. While BMP signaling was rather constant during the course of differentiation, we observed a progressive build-up of Activin/Nodal signaling. Quantification of these signals in individual colonies showed different levels of pSMAD1/5 signal on day 7 (Fig. S2B), as well as spatial dynamics of pSMAD1/5 and pSMAD2/3 signals. This could account for the different phenotypes we observe in Fig. 2C, with higher endogenous levels of pSMAD1/5 leading to

more dorsal fates observed in "homogeneous" colonies. A more convincing correlation would be established using live imaging of a pSMAD1/5 reporter cell line and staining for OLIG3 on day 9.

Intriguingly, endogenous signals were also implicated in the establishment of PAX7$^{+}$; OLIG3$^{-}$ state. Inhibition of each of the signals decreased the expression of PAX7 throughout colonies and inhibiting both BMP and Activin/Nodal signaling almost blocked the induction of PAX7 (Fig. S2C). Cells submitted to combined inhibition of the BMP, Activin/Nodal and WNT inhibitors did not display an increase in the ventral marker NKX6.1 and were still positive for PAX6, although its expression was decreased (Fig.S2D).

Altogether, our data show that in contrast to dp4-6 default differentiation operating in 3D organoids [Meinhardt et al., 2014; Duval et al., 2019], 2D micropatterns can favor the activation of more dorsal dp1-3 identities on account of endogenous signaling.

## Organized and dorsalized cell fates within colonies subjected to BMP4

We next investigated whether we could dorsalize naive caudal spinal progenitors on micropatterned substrates after exposure to exogenous BMP4. In view of experiments demonstrating the morphogenetic effects of the concentration, duration and timing of exposure to BMP4 [Sagner and Briscoe, 2019], we modulated these exposure parameters (Fig. 3) and tested the effects of BMP4 stimulation between day 4 and day 9 at four distinct concentrations ranging from 1ng/mL to 10ng/mL. Alternatively, we modulated the time at which BMP4 was added to the differentiation medium and then retained until day 9. The response of cells was evaluated with three markers, including PAX7, OLIG3, TFAP2$\alpha$. TFAP2$\alpha$ is a marker for both neural crest cells (NCCs) and dorsal interneurons [Mitchell et al., 1991; Gard et al., 2017] (Fig. 3). In control conditions, $\sim$ 15% of the cells are TFAP2$\alpha^{+}$ and are probably dorsal interneurons. This percentage drops in colonies inhibited with LDN,

SB or iWP2 (Fig. S3A,B).

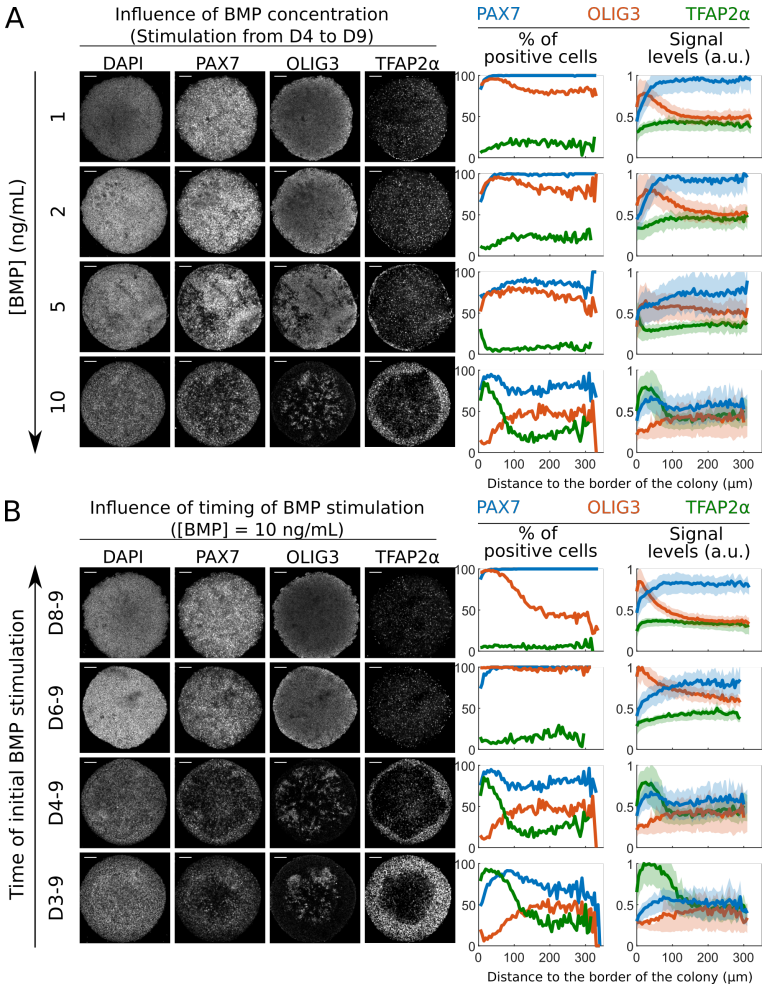


Figure 3: **Dorsalization of neural progenitors with BMP. A** Characteristic immunostainings of PAX7, OLIG3 and TFAP2$\alpha$ for increasing concentrations of BMP from day 4 to day 9 and quantification of signals (n=8,8,9,7 for [BMP]=1,2,5,10ng/mL). **B** Characteristic immunostainings of PAX7, OLIG3 and TFAP2$\alpha$ for different timing of exposure of BMP at 10ng/mL and quantification of signals (n=9,4,7,6 for D8-9,D6-9,D4-9,D3-9). Scale bar=100µm.

In contrast with the condition in the absence of BMP4, where colonies

with two distinct dorsal fates could be detected (Fig. 2), upon exposure to low BMP4 concentration (1-2ng/mL) or high but brief exposure (10ng/mL from day 6 to day 9), all colonies were composed of a homogeneous population of OLIG3$^{+}$; PAX7$^{+}$; TFAP2$\alpha^{-}$ dp1-dp3-like progenitors (Fig. 3A, B).

Both increasing BMP4 concentration or starting the exposure to high BMP4 earlier than day 6 generated self-organizing patterns of cell fates, in which inner cells were OLIG3$^{+}$; PAX7$^{+}$; TFAP2$\alpha^{-}$ dp1-dp3-like progenitors and outer cells were OLIG3$^{-}$; PAX7$^{+}$; TFAP2$\alpha^{+}$ NCC-like cells (Fig. 3A, B). The thickness of the peripheral ring of NCC-like cells further increased when increasing BMP concentration or advancing the time of BMP4 exposure (Fig. 3A,B).

We next wondered whether these patterns of BMP-dependent cell types could be explained by a spatial modulation of BMP signaling throughout colonies, as previously shown for gastruloids [Warmflash et al., 2014; Etoc et al., 2016]. Immunolabeling for pSMAD1/5 of colonies exposed to 10ng/mL of BMP4 on day 5, 7 and 9 indicated that after 3 days of exposure to BMP4, only a ring of cells at the periphery of the micropatterned substrates maintained an active BMP signaling (Fig. S3C). Hence, the concentric generation of distinct dorsal states on micropatterned substrates echoes the spatial and temporal modulation of the BMP signaling within colonies, as previously shown in organoids [Duval et al., 2019].

Thus, differentiating naive spinal progenitors on micropatterned substrates in the presence of BMP4 represents a great means by which robust patterns of concentrically organized dorsal cells can be generated.

## Ventralization of cells under SAG ventral stimulation and the implication of Activin/Nodal

In the absence of external cue simulation, no ventral neural progenitors were derived in day 9 micropatterned colonies (Fig. 2D). To produce such cells we exposed naive caudal neural progenitors to Smoothened Agonist (SAG) – an

agonist of SHH – from day 4 to day 9. We tested several concentrations of SAG ranging from 10nM to 1µM as this parameter is sufficient to generate distinct ventral cell states in chick caudal neural plate explants [Dessaud et al., 2008]. The state of cells was assessed using antibodies against NKX6.1, OLIG2, NKX2.2 which are FP to p2, pMN and p3 markers, respectively [Lai et al., 2016].

The generation of colonies containing mostly NKX6.1$^+$ ventral cells was only seen at high concentrations of SAG (500nM-1000nM) (Fig. 4A). Even at these high concentrations, only a few individual cells were stained with the ventral-most p3 marker NKX2.2. Induction of this protein could only be seen upon an early stimulation of the SHH pathway (as from day 2) and without adding RA to the culture media, and this protocol also yielded FOXA2$^+$ cells that could correspond to floor plate cells (Fig. S4A,B). Similarly, the number of OLIG2$^+$ cells was unexpectedly low, compared to those that could be produced following the same differentiation protocol in 3D-embroid bodies [Maury et al., 2015; Mouilleau et al., 2021]. Furthermore, cells that expressed this marker were confined to the periphery.

This self-organized pattern of OLIG2$^+$ cells was unexpected as SAG is a small molecule and thus we can expect it to diffuse freely as opposed to BMP4. This first prompted us in assessing the temporal dynamics of OLIG2 induction. We stimulated colonies with 500nM of SAG and stained for OLIG2 at different days to catch its dynamic of expression that led to the pattern. On day 5, no OLIG2$^+$ cells are detected in the pattern (Fig. 4B). On day 7, OLIG2$^+$ cells are detected in the whole colony, with slightly more cells at the border ($\sim$ 50%) than at the center ($\sim$ 20%). On day 9, OLIG2$^+$ cells are only detected within 80µm from the border of the colony. These results suggest a temporal restriction of the pattern to the border of the colony.

We wondered whether spatial patterns of SHH activity in colonies could lead to this restriction of OLIG2$^+$ cells to the border of the colony. For this, we transfected hESCs with a genome integrating plasmid ePiggyBac

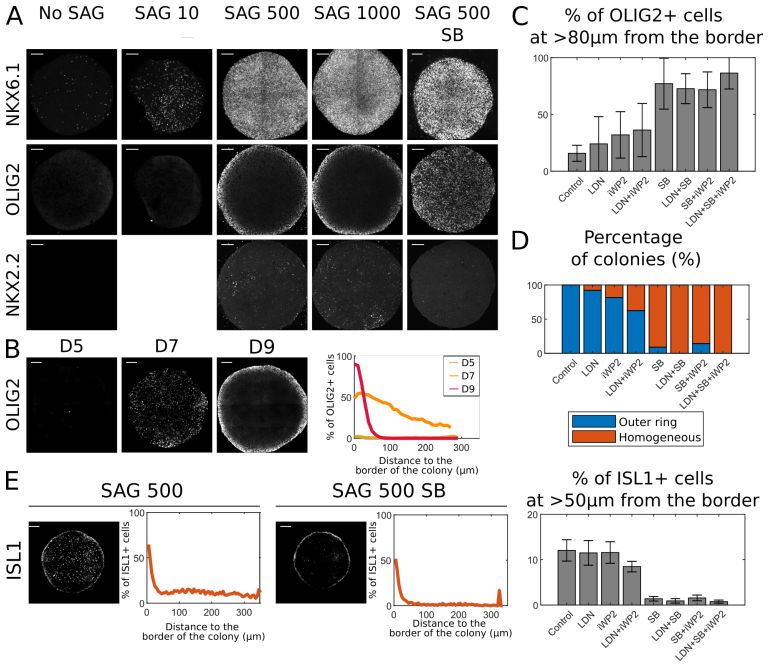


Figure 4: **Ventralization of neural progenitors with SHH. A** Immunostainings for NKX6.1, OLIG2 and NKX2.2 for increasing concentrations of SAG and for SB inhibition at [SAG]=500nM (n=10,6,22,7,4 colonies for NKX6.1, n=10,6,39,7,12 colonies for OLIG2 and n=4,0,31,5,14 colonies for NKX2.2). **B** Timecourse of OLIG2 signal in [SAG]=500nM colonies (n=10,10,20). **C** Percentages of OLIG2$^+$ cells excluding cells within 80µm from the border of the colony (n=11,11,8,8,8,7,7,11 colonies from left to right). **D** Clustering of SAG500 colonies exposed to different inhibitors (n=12,13,11,8,11,7,7,11 colonies from left to right). **E** Immunostainings for ISL1 and mean profile of positive cells for SAG500 (n=11) and SAG500+SB (n=8) colonies. Percentages of ISL1$^+$ cells excluding cells within 50µm from the border of the colony (n=11,11,8,8,8,7,7,11 colonies). Scale bar=100µm.

[Lacoste et al., 2009] carrying a Gli transcriptional reporter transgene called GBS. We did not manage to get a stable monoclonal expression and worked with a polyclonal population where fluorescent signal was only detected in a few percent ($\sim$ 2-3%) of the cells after puromycin selection. Statistically, we hypothesized that the distribution of GBS$^+$ cells averaged over a large

number of colonies should mimic the response to SHH across the colony (Fig. S4C). The results seem to indicate that the response to SHH is increasing from day 5 to day 9, and a shift from a rather homogeneous signal on day 7 to a stronger signal at the edge on day 9. The restriction of OLIG2$^+$ cells to the border of the colony appears correlated with a decrease of the SHH response in the middle of the colonies. However, the method we used suffers from low stats and this result should be confirmed (see paragraph 4.1.4 in the discussion chapter). Sustained SHH signaling is required for the maintenance of pMN identity in explants [Dessaud et al., 2010] and fate reversal towards more dorsal identities because of reduced SHH signaling might be taking place at the center of SAG500 colonies.

Given that endogenous signaling of the BMP, WNT and Activin/Nodal pathways appeared to be involved in cell specification of default conditions, we wondered whether the patterning of OLIG2 could be explained by dorsalizing signals. Therefore, we submitted colonies to LDN, SB and iWP2 inhibition in addition to SAG (500nM). Surprisingly, while LDN and iWP2 did not have any impact on the OLIG2 pattern, all conditions including SB inhibition led to a more homogeneous OLIG2 signal (Fig. 4A). Although in some colonies, cells at the center of the colony displayed a lesser intensity of OLIG2 than cells in the periphery, the number of positive cells at the center – obtained by removing cells whose nucleus was at a distance of 80µm or less to the border of the colony – was significantly increased in SB conditions (Fig. 4C). We clusterized colonies into two groups: each colony was assigned to a "homogeneous" or an "outer ring" distribution. Most of the SB-treated colonies fell under the homogeneous category, whereas non-treated colonies were mostly outer ring phenotypes (Fig. 4D). More GBS$^+$ cells were observed at the center of SB-treated colonies on day 9 (Fig. S4C), suggesting that Activin/Nodal inhibition could help maintain a higher response to SHH at the center of the colony and lead to sustained expression of OLIG2 in SB-treated colonies. Again, this observation needs to be confirmed with a

more sensitive measurement of the SHH activity in colonies.

Activin/Nodal has been described as involved in the maturation of neurons: its stimulation leads to a high percentage of late expressed genes such as Sox9, Nfia, Nfib and Nfix while its inhibition increases the expression of early expressed genes such as Lin28a and Lin28b [Sagner et al., 2020]. We asked ourselves the question of whether the OLIG2 pattern could be explained by temporal differences in the pace of maturation of progenitors along the radius of the colony. We decided to stain colonies after 9 days of differentiation with the mature motoneuron marker ISL1 (Fig. 4E). At this stage, mature neurons only seldom, and further differentiation involving Notch inhibition with DAPT is necessary to induce neuron maturation with high efficiency. Some non-nuclear signal appeared at the border of the colony, which we disregarded for our analysis. Colonies without SB inhibition had $\sim$ 10 % of ISL1$^{+}$, whereas SB inhibited colonies were mostly ISL1$^{-}$, confirming that SB inhibits differentiation of motoneurons. However, in the absence of SB, ISL1$^{+}$cells were distributed homogeneously across the colony, so there does not appear to be higher maturation of motoneurons at the center of the colony that could account for OLIG2 downregulation. NKX6.1 homogeneous expression in SAG500 colonies (Fig. 4A) also seems to indicate the persistence of a progenitor state and argue against the formulated hypothesis. More systematic characterization of the DV status and the temporal status of cells in each condition is required to understand how the OLIG2 pattern arises in SAG500 colonies.

# Conclusion

Neural progenitors can be cultivated on micropatterned substrates and their DV identities can be probed in the absence or in the presence of exogenous stimulation. This leads to surprising observations: a “default” dorsal fate regulated by endogenous BMP, WNT and Activin/Nodal signaling, the

emergence of NCC-like fates in a dose and time-dependent manner under BMP stimulation, and a pattern of OLIG2$^+$ pMN under SAG stimulation that originates from a lesser response to the SHH pathway at the center of colonies and seems to be homogenized in the presence of Activin/Nodal inhibition.

While the mechanisms leading to patterning in all of these scenarios are not fully resolved, we would like to state that micropatterns tend to exacerbate endogenous signaling due to the high densities necessary to generate patterns, and we believe that this experimental setup can unveil some new interactions between signaling pathways in the specification of DV identities amongst neural progenitors.

## Supplementary Figures

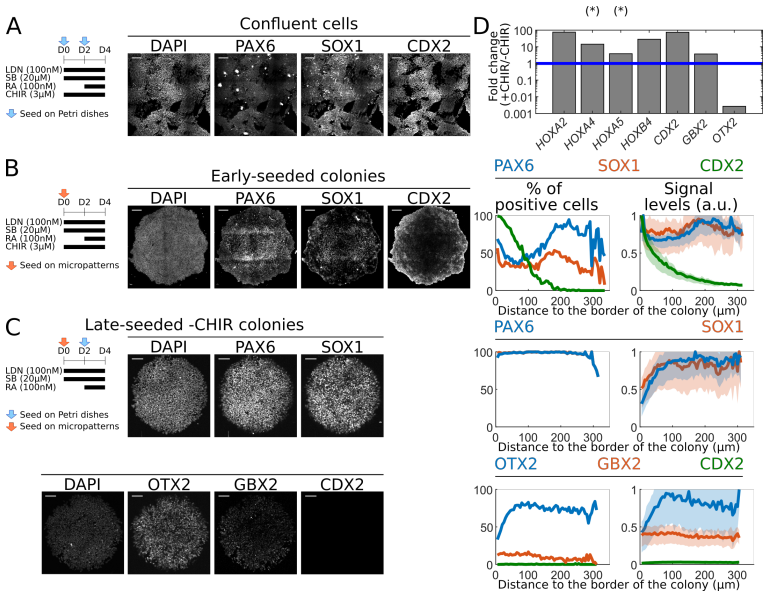


Figure S1: **Supplementary Figure 1.** **A** Immunostainings for PAX6, SOX1 and CDX2 and DAPI staining on day 4 of differentiation of cells differentiated on Petri Dish using the protocol schematized on the left, representative of n=6 field of views obtained in 2 independent experiments. **B** Immunostainings for PAX6, SOX1 and CDX2 and DAPI staining of cells when seeding cells on micropatterns on day 0 representative of n=7 colonies obtained in 4 independent experiments. Quantification on n=2 colonies within 1 experiment. **C** Immunostainings for PAX6, SOX1, OTX2, GBX2 and CDX2 in the absence of CHIR stimulation (n=18 for PAX6,SOX1; n=17 for CDX2; n=12 for OTX2 and GBX2). Quantification on n=8 colonies within 1 experiment for PAX6 and SOX1, and on n=7 colonies within 1 experiment for CDX2, OTX2 and GBX2. **D** Ratio of mRNA levels of expression of the indicated genes relative to CycloA transcripts on day 4 in cells differentiated on micropatterned substrates with CHIR (Fig. 1A) and without CHIR (Fig. S1C). Mean from two technical replicates from one biological sample. (*) means we lacked data on day 4 and used a sample on day 5 as a proxy (media from day 4 to 5 contained only LDN, SB and RA in both conditions). Scale bar=100µm.

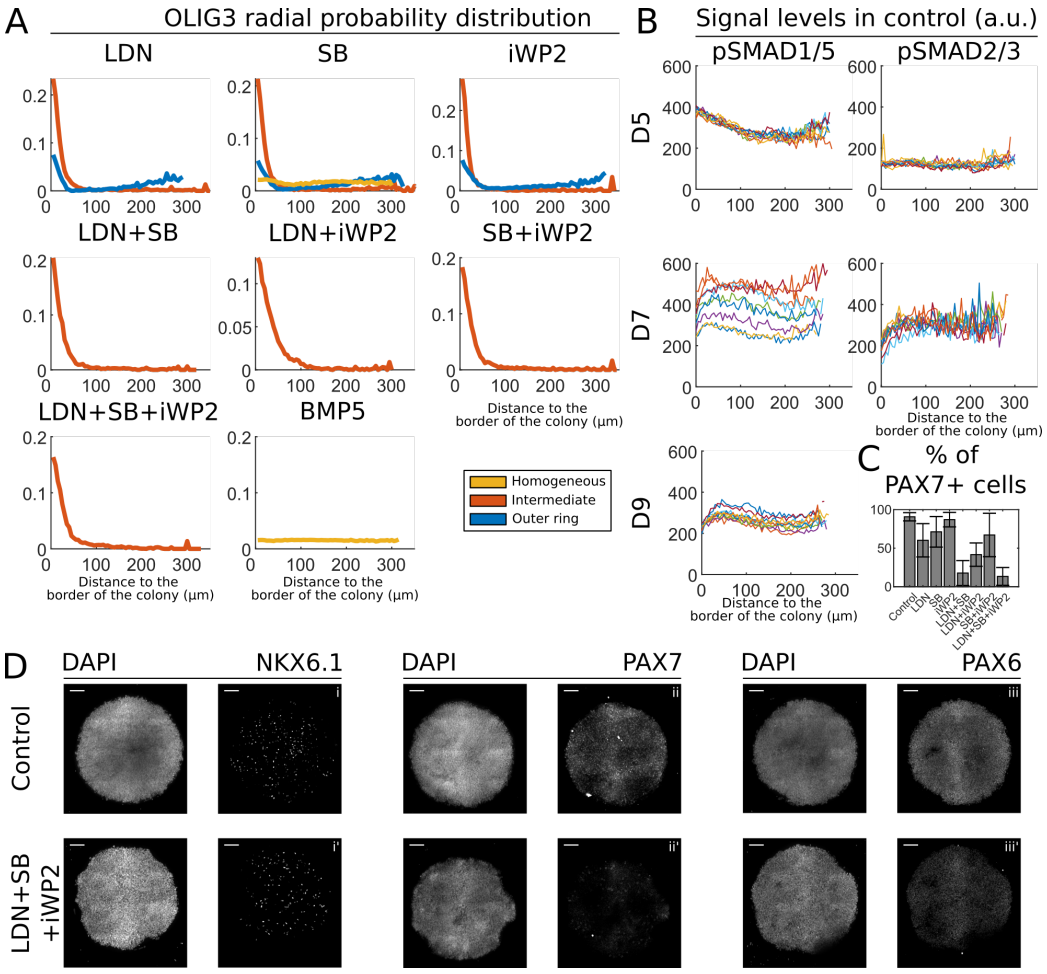


Figure S2: **Supplementary Figure 2.** **A** OLIG3 radial probability distribution in D9 spinal progenitors grown as in Fig. 2D (line: mean value in colour-coded clusters). **B**. pSMAD1/5 and pSMAD2/3 intensity profiles for colonies in the "default" condition (n=10,9,10 colonies for pSMAD1/5 D5,7,9 and n=10,9 colonies for pSMAD2/3 D5,7). **C** Percentages of PAX7$^+$ cells in "default" condition and with inhibitors (n=16,15,17,14,6,7,9,8). **D** Immunostainings for PAX7, NKX6.1 and PAX6 in "default" condition and under triple inhibition (n=26,20,10 colonies for Control, n=18,10,10 for triple inhibition). Scale bar=100µm.

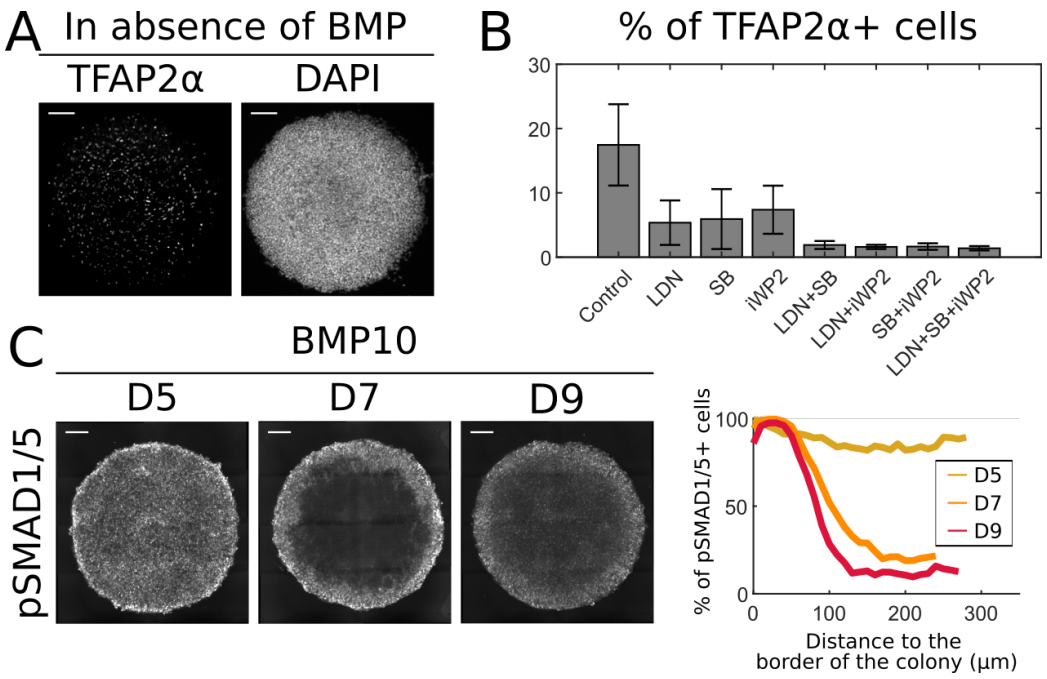


Figure S3: **Supplementary Figure 3. A** Immunostaining for TFAP2$\alpha$ and DAPI staining in "default" condition. **B** Quantification of TFAP2$\alpha^+$ cells in "default" condition and with inhibitors (n=16,15,17,14,6,7,9,8 colonies from left to right). **C** Immunostainings for pSMAD1/5 in colonies stimulated with BMP from day 4 until fixation on day 5, 7 or 9. Mean expression profile across the colony (n=10,6,9 for D5,D7 and D9). Scale bar=100µm.

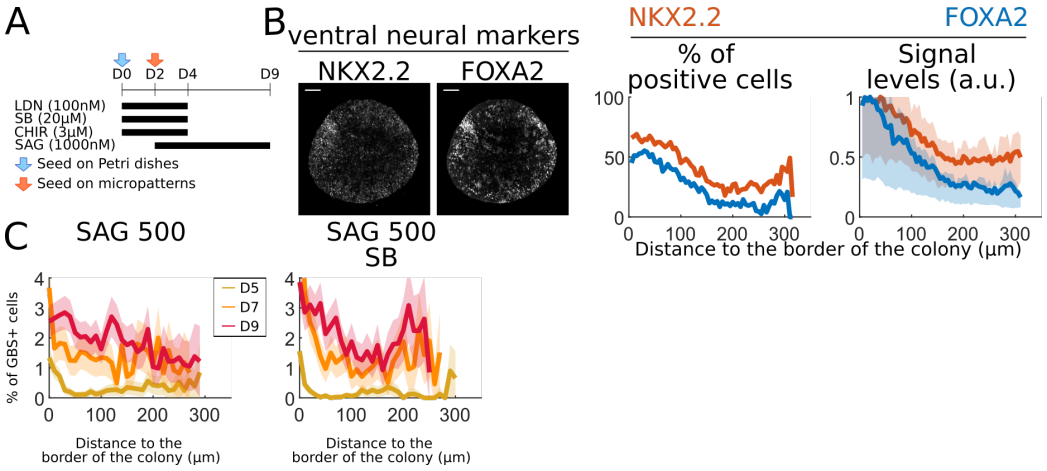


Figure S4: **Supplementary Figure 4.** **A** Floor plate generation protocol, including high SAG concentration (1000nM) and no RA stimulation. **B** Immunostainings of NKX2.2 and FOXA2 observed with this floor plate generation protocol. Quantification of the signal on 5 colonies from the same experiment. **C** Quantification of GBS$^+$ cells in colonies exposed to [SAG]=500nM fixed on day 5, 7 and 9 (n=20,10,18). Scale bar=100µm.

# Chapter 4

# Discussions and perspectives

The results we presented in the former chapter can be seen as exploratory work to assess how suited micropatterned substrates are to differentiate neural progenitors. When we explained why we consider micropatterned substrates as an appealing alternative to investigate the dorso-ventral patterning of the neural tube, we insisted on its potential to have tight control of stimulation and to track fates temporally.

We will organize our discussion along the three following points:

- What comes out of the exploratory work conducted on micropatterned substrates and how could it be continued?
- How much control of stimulation do we actually have and how could we envision improving this control?
- How can timetracking be implemented in micropatterns experiments?

During the discussion, we will also present some preliminary experiments that we were able to conduct during the thesis project to overcome limitations of micropatterns.

## 4.1 Micropatterned substrates

In Fig. 4.1, we present the main points we want to articulate the discussion on our results on micropatterned substrates around.

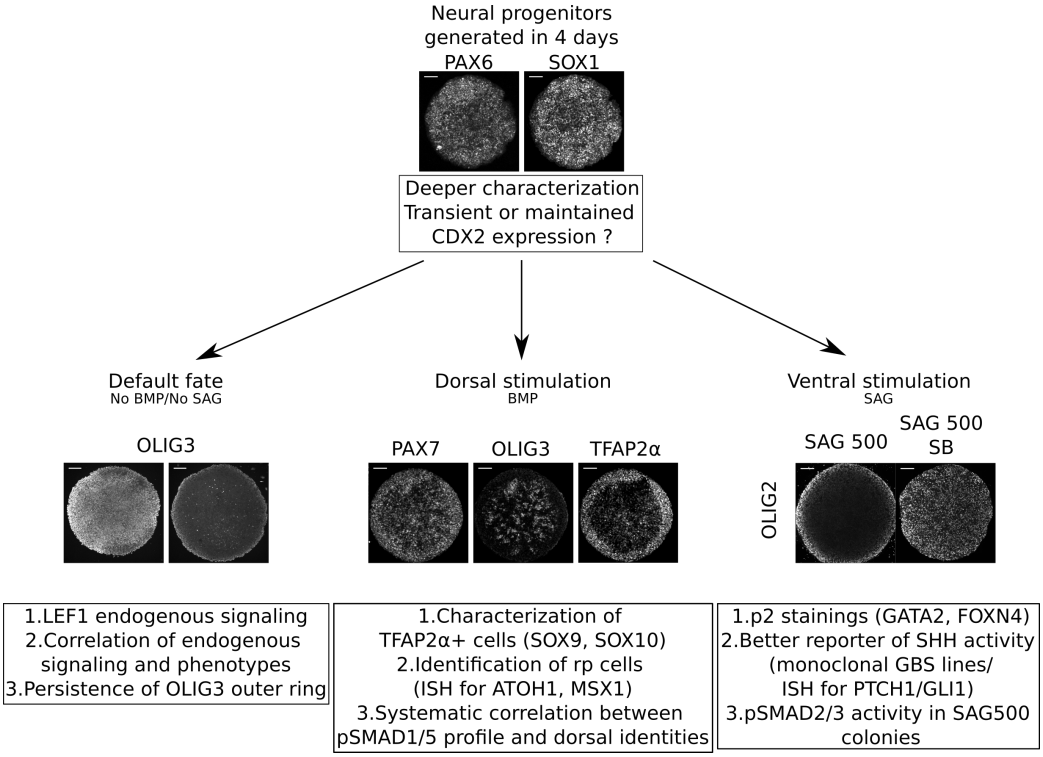


Figure 4.1: **Plan of the discussion of main results.** Outline of the discussion with results from the article and corresponding points discussed in this section.

### 4.1.1 D4 neural progenitors

We described a protocol to generate $PAX6^+/SOX1^+$ neural progenitors on micropatterned substrates using a 4-day protocol. We propose a few possibilities to characterize them better.

- The dynamic of expression of PAX6 and SOX1 could be refined by stainings on D3 and D5. What is the temporality of the apparition of these markers in our experimental setup? Have we reached maximal expression of these markers on D4 or could we benefit from extending the protocol?

- Similarly, unveiling the dynamic expression profile of CDX2 could precise the identity of neural progenitors. Is CDX2 expression only transient as observed *in vivo* [Sanchez-Ferras et al., 2012]?

- Repeats of qRT-PCR for *HOX* genes would be needed to confirm the one from our main results, which only stems from one experiment. Are more caudal *HOX* genes such as *HOXC6*, *HOXC8* and *HOXC9* also expressed in neural progenitors generated with our protocol?

### 4.1.2 D9 default fate

We observed and quantified bistable OLIG3 expression profiles in the absence of exogenous BMP stimulation, and showed that BMP, Activin/Nodal and WNT inhibitions oriented colonies towards "outer ring" phenotypes. We started to investigate the dynamics of the BMP and Activin/Nodal pathways and noticed levels of endogenous signaling in colonies that might be correlated with the OLIG3 expression profile.

- We did not look at WNT endogenous signaling although WNT inhibition had an impact on the OLIG3 expression profile. Could we monitor WNT endogenous signaling with LEF1 stainings between D4 and D9?

- Correlating endogenous signaling and OLIG3 expression profiles is not trivial. The latter could result from the integration of signals between D4 and D9. Furthermore, we cannot fix a colony before D9 and guess what phenotype it would have resulted in. It would still be a good

sign if statistics over the appropriate number of colonies showed a bimodal distribution within the dynamics of endogenous signaling pathways that would match the bimodal distribution of OLIG3 expression profiles. Reporter cell lines for the activity of the different pathways involved could also enable us to monitor signals from D4 to D9, then fix and stain cells for OLIG3 in search for a causality effect. We will present in 4.3.1 how we are currently trying to generate reporter cell lines to monitor signaling pathways activity.

- We were not able to explain the persistence of an OLIG3 2-3 cells wide ring in colonies where dorsalizing signals were inhibited. Can we be sure that these cells do not come from an existing prepattern of identities? D4 colonies seem to have fewer PAX6$^+$ cells at the very periphery, which might differentiate into this OLIG3$^+$ ring. This raises a larger question of edge effects in micropatterns. Could mechanical constraints exerted on cells at the periphery, and mediated via the YAP/TAZ pathway or from modulation of the BMP signaling pathway by mechanical forces independent of the YAP/TAZ pathway – such as suggested by [Xue et al., 2018] – be responsible for this OLIG3$^+$ ring?

### 4.1.3 Dorsal stimulation with BMP

We explored the effect of timing and concentration on dorsal neural identities and were able to modulate the size of a ring of TFAP2$\alpha^+$ cells by varying exposure to BMP.

- The state of TFAP2$\alpha^+$ cells is not completely solved. As explained in the result section, both NCC and dorsal interneurons express TFAP2$\alpha$. Immunostainings for specific NCC markers, such as SOX9 or SOX10, would help solve this ambiguity. We tried to stain colonies for SOX10 and cells were negative but we lacked an appropriate positive control. Colonies derived from protocols described by [Britton et al., 2019]

where a SOX9 ring appears could be used as a positive control.

- At high BMP concentrations, we described patches of $PAX7^+$, $OLIG3^+$ at the center of the colony, and suggested cells negative for these markers to be roof plate cells. It would be interesting to perform *in situ* hybridization for the roof plate markers ATOH1 or MSX1 to test this hypothesis. One could also investigate why fates are organized in patches rather than concentric rings, and whether signals secreted by roof plate cells can explain this organization.

- Finally, we started to look at pSMAD1/5 activity in one condition (BMP 10ng/mL D4-9). One could try to do it in a more systematic way and explore conditions that lead to different sizes of the $TFAP2\alpha^+$ ring, in the attempt to establish a correlation between pSMAD1/5 signals and the size of this ring.

### 4.1.4 Ventral stimulation with SAG

In the case of ventral stimulation with SAG, we witnessed the emergence of an OLIG2 pattern that we could not fully account for. Differential SHH signaling across the colony seems like the more direct explanation, but even then, what leads to this pattern of SHH activity might prove important. We also reported that Activin/Nodal inhibition could modify the OLIG2 pattern and SHH activity.

- In SAG500 conditions, we would like to have additional stainings for cells at the center. We know that they are $NKX6.1^+$, $OLIG2^-$, $NKX2.2^-$ so we assume they are p2 progenitors. We think our observations could be strengthened by GATA2 or FOXN4 stainings for p2 progenitors. We would need to find antibodies or resort to *in situ* hybridization.

- We presented the results on SHH signaling obtained with a GBS polyclonal cell line where only a few percent of cells displayed fluorescence.

We think that the amount of positive cells is too low to reveal a statistical difference but we decided to show them since they could help us think of models for how OLIG2 patterning occurs. Better results could be obtained from a monoclonal GBS line sensitive to SAG stimulation. An alternative could also lie in *in situ* hybridization for downstream effectors of the SHH pathway, such as PTCH1 and GLI1.

- Finally, one would have to come up with a model to explain how Activin/Nodal changes the OLIG2 pattern. At the very end of the thesis project, we investigated pSMAD2/3 dynamics in SAG500 and SAG500+SB conditions. It seems that pSMAD2/3 is upregulated in the SAG500 condition, but signals are very low and noisy and we could not infer any spatial profile of Activin/Nodal signaling yet. One would have to analyze the data we generated in detail and see whether a model taking these observations into account can be formulated.

## 4.2 Controlling stimulation

### 4.2.1 Limitations of micropatterns

When it comes to controlling stimulation, what occurs on micropatterns does not seem so straightforward. While providing the morphogen in bulk leads to reproducible patterns, the patterning process relies on gradients of activities of the downstream response to signaling pathways. On the one hand, this is a strength of micropatterns that allows us to recover spatial organization. On the other hand, this complicates analysis and interpretation: for each spatial organization we observe, we need to identify which signaling pathways are involved and quantify their downstream response. One could say that we reconstruct a one-to-one correspondence between the activity levels and the ensuing spatial organization more than we control stimulation.

### 4.2.2 Patterning in micro-transwells

Two mechanisms leading to a graded interpretation of bulk stimulation on micropatterns have been analyzed by [Etoc et al., 2016] and presented in 1.4.1. One is differential receptor accessibility: in the case of BMP, receptors are located at the basal side of the membrane and not accessible when stimulating cells apically with BMP. Basal stimulation was sufficient to ensure a homogeneous pSMAD1/5 profile. Another one is the secretion of inhibitors. Models explaining the profile of inhibitor expression consider that it is lost at the edge of the colony. In both cases, this can be attributed to an "edge effect" of the colony.

We took advantage of an experimental setup that was designed by Tom Wyatt, a post-doc in the team, to stimulate monolayers of cells locally and from the basal side, referred to as "micro-transwells" (Fig. 4.2A). Cells are seeded on a porous membrane in the bottom compartment of a transwell. In the top compartment, a PDMS structure is bounded to the membrane (Fig. 4.2B). It contains seven "micro-transwells" that do not communicate and can be filled with a solution of a given concentration of morphogen. Practically, a hole needs to be punched in one of the micro-transwells to equilibrate pressure. Furthermore, the edge effect is avoided by making sure the monolayer extends beyond the stimulated part.

Cells represented in green (Fig. 4.2A) can sense the morphogen diffusing through the porous membrane from their basal side. This setup is extremely interesting when interested in endogenous signals secreted by cells in response to stimulation. Indeed, in the case where cells secret a signal from their apical side (*e.g.* WNT) when stimulated (*e.g.* with BMP), one can study how neighboring cells – in red on the figure – integrate the endogenous signal without being stimulated by the primary signal.

For this experimental setup to work, it is important to make sure that the morphogen provided in the top compartment does not diffuse through cells and reach the bottom compartment. Therefore, one has to work with

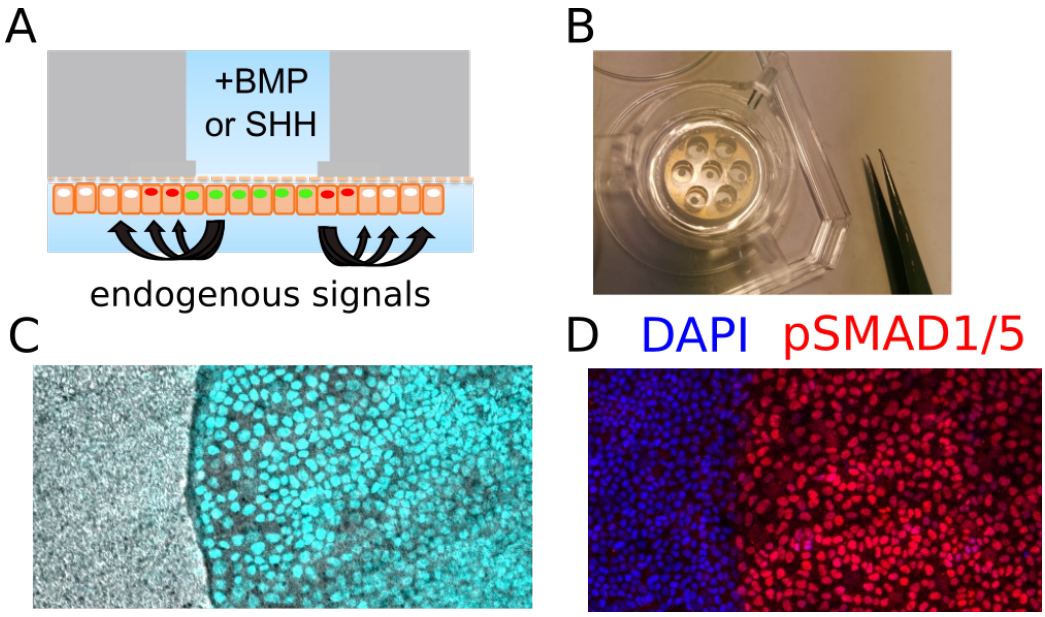


Figure 4.2: **The setup for micro-transwells experiments. A** Basal and local stimulation of green cells is achieved by diffusion of a morphogen provided in the top compartment of a transwell through a porous membrane. Stimulated cells (in green) may secret endogenous signals in response to this primary stimulation and induce differentiation of neighboring cells (in red). **B** Photo of the device with 7 micro-transwells. Light regions in each micro-transwell correspond to membrane coated with PDMS and darker regions to membrane without PDMS. **C** Overlapping bright field (BF) and pSMAD1/5 fluorescent image of cells on the micro-transwells setup stimulated with BMP4. Cells cover the whole field of view, but only cells on the membrane without PDMS (right of the image and darker in BF) respond to BMP stimulation. **D** DAPI and pSMAD1/5 stainings on the micro-transwells setup.

macromolecules like SHH rather than small agonists like SAG.

Why did we decide to use this setup to study neural progenitors differentiation? We thought it could give a hint at whether mechanisms of basal receptor localization and inhibitor secretion described for BMP are also responsible for the emergence of patterns of dorsal identities in neural

progenitors on micropatterned substrates stimulated with BMP. As for SHH stimulation, we wondered whether basal stimulation could solve the decrease in SHH signaling observed at the center of the colony.

### Description of the protocol

We do not describe the realization of the micro-transwell device that was carried out by other members of the team, but we explain the process of seeding and cultivating cells on this device.

- We tried to place ourselves in very similar conditions to those we used on micropatterns. During the first two days of differentiation, cells were plated on Petri Dish (1M cells per 35mm Petri Dish).

- On day 2 of differentiation, we seeded cells on the micro-transwells device. To achieve that, we worked with the transwell upside down and treated the bottom part of the membrane by applying successively on each micro-transwell a drop of Laminin-521 at a concentration of 20µg/mL in PBS++ for 1 hour, then a drop of a solution of 1% Pluronic F-127 in PBS++ for 45 minutes, and finally a drop of DMEM-F12 to avoid drying. We made sure that drops did not merge so that cells from different micro-transwells will form independent monolayers.

- We then dissociated D2 cells in Accutase+RI, resuspended them in N2B27+RI++, and deposited 18µL drops containing 100k cells on each micro-transwell. We clipped the transwell in a 6-well plate, still upside down.

- After 45 minutes in the incubator, we flipped the 6 well-plate and filled the bottom compartment and the micro-transwells with N2B27+RI++.

- After another 45 minutes, we removed RI and cells that did not attach to the membrane by aspirating media from the top compartment, taking the transwell out of the 6-well plate, gently flushing N2B27 media

on the transwell held with a 90° angle (to avoid cells detaching because of gravity), then moving it in another well of the 6-well plate and filling the bottom and top compartments with N2B27++ (without RI).

- We changed the media on day 3,4,6 and 8 according to experimental conditions.

**BMP stimulation of neural progenitors**

We stimulated monolayers of cells on micro-transwells in the absence of BMP and at different concentrations of BMP4 (1, 5 and 10ng/mL) from day 4 until fixation on day 7 or 9. We stained for PAX7 and OLIG3 to monitor dorsal identities (Fig. 4.3).

If we look at the dynamics of stimulated cells in response to BMP stimulation, we notice that PAX7$^+$, OLIG3$^+$ dp1-3 identities appear as of day 7 at concentrations of BMP ranging from 1 to 10ng/mL. On day 9, the OLIG3 signal in the stimulated region seems to be kept rather homogeneous at low concentrations (1ng/mL) and to disappear at high concentrations (5-10ng/mL). A possible scenario is that cells at high concentrations went through a transient dp1-3 state before dorsalizing further into roof plate or NCC identities, while at low concentrations, they stopped at the dp1-3 state.

It is not clear to draw a correspondence between the concentrations of BMP in micro-transwells experiments and on 2D micropatterned substrates: in the first case, BMP is provided through the porous membrane from the basal side; in the second case, BMP is provided in bulk from the apical side. Other experimental work on gastrulation within the team seems to indicate that cells respond better to BMP on micro-transwells – meaning that lower concentrations are needed to achieve similar differentiation. This is in line with basal localization of receptors and uniform accessibility of BMP receptors when stimulating basally.

We were expecting cells far from the stimulated region to exhibit PAX7$^+$, OLIG3$^-$ dp4-6 identities on day 9 in all conditions. Indeed, these cells far

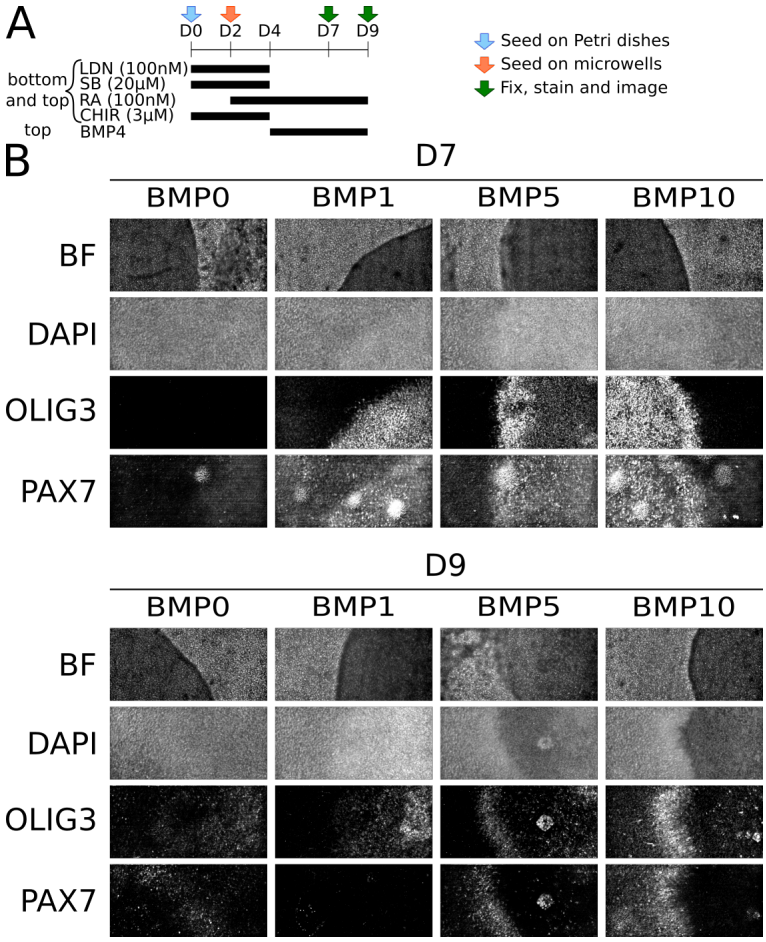


Figure 4.3: **BMP stimulation of neural progenitors on micro-transwells. A** Protocol used to study BMP stimulation of neural progenitors on micro-transwells. BMP is only provided in the top compartment. **B** BF images, DAPI stainings and immunostainings for OLIG3 and PAX7 on cells on micro-transwells stimulated with different concentrations of BMP4 (0, 1, 5 and 10ng/mL) from D4 until fixation on D7 or D9. The stimulated region corresponds to the darker region on BF images.

from the stimulated region do not sense BMP but are provided with all the conditions leading to "default" neural identity. From images of the stainings, it is hard to clearly state that these cells are PAX7$^+$. This could be due to

bad PAX7 staining in this experiment: at D9, we witness a very low and noisy PAX7 signal, and at D7 some debris diffusing light in the PAX7 channel (Fig. 4.3, PAX7 staining).

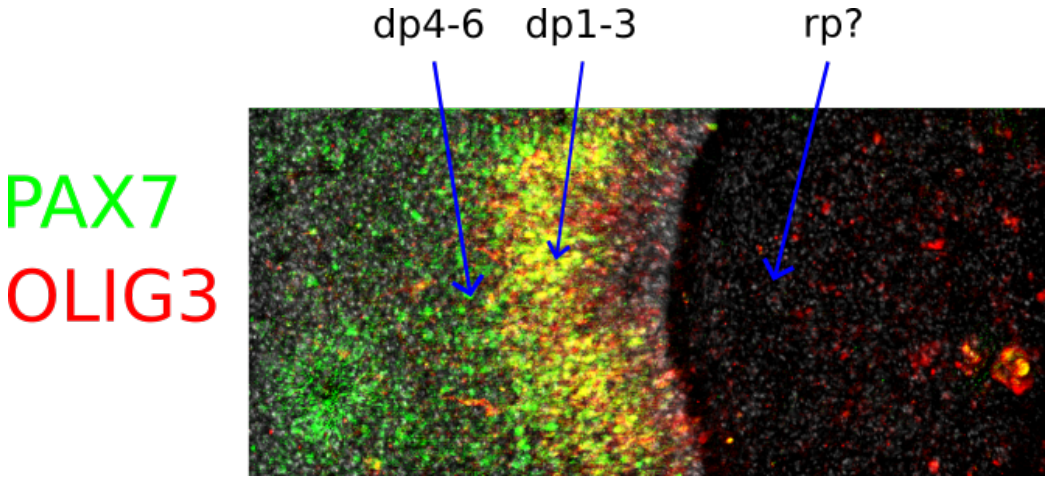


Figure 4.4: **Gradients of expressions at micro-transwell boundaries.** Annotated composite image of the OLIG3/PAX7 stainings on day 9 for stimulation of BMP of 10ng/mL from day 4 to day 9.

Last but not least, the OLIG3/PAX7 state in the cells close to but out of the stimulated region at high concentrations of BMP raises interesting questions. If we look at the composite image of the D9-BMP10 condition (Fig. 4.4), we witness a ring of OLIG3$^+$, PAX7$^+$ cells (in yellow) and then a ring of OLIG3$^-$, PAX7$^+$ cells (in green), establishing a gradient of dorsal identities on a tissue that is only a few cells thick. Several scenarios can explain this observation:

- Endogenous signals secreted by stimulated cells and patterning neighboring tissues. *In vivo*, the roof plate secrets BMP and WNT that pattern the dorsal part of the neural tube [Lee and Jessell, 1999]. It seems that the gradient of dorsal identities appears on day 9 at high concentrations of BMP (5-10ng/mL), and we hypothesized these conditions might lead to putative roof plate cells in the stimulated region.

Therefore, endogenous signals may be secreted by cells in the stimulated region and pattern neighboring tissues. One could try to directly monitor the production of endogenous signals in the stimulated region or indirectly observe the response of neighboring cells to these pathways. Adding inhibitors of each pathway in the bottom compartment could also be an interesting experiment, but one would have to be very careful to check that this does not impact the differentiation of cells within the stimulated region as well.

- Cells progressively moving out of the stimulated region. OLIG3$^{-}$, PAX7$^{+}$ cells would initially be in the stimulated region and moved out during the experiment, so they experienced a temporal step function from a BMP stimulation to no BMP stimulation. The same would apply for OLIG3$^{+}$, PAX7$^{+}$ cells, but they would have been exposed to BMP for a longer duration. To test this hypothesis, one would need to perform live imaging and tracking of cells during the 7 days that they spend on micro-transwells.

- A sharp gradient of BMP at the edge of the stimulated region that translates into a local gradient of dorsal identities. pSMAD1/5 immunostainings could be used to test this hypothesis. However, in Fig. 4.2C, although the experimental conditions under which this image was taken are different, it seems that the delineation between the stimulated and non-stimulated region is very clear and does not allow for a BMP gradient that could span over several cells outside the stimulated region. Also, pSMAD1/5 immunostainings would not be able to discriminate between exogenous BMP stimulation and possible endogenous BMP signaling presented in the first hypothesis.

All in all, these few results on BMP stimulation on micro-transwells hint that this setup can provide a lot of information within a single experiment, by looking at several regions of interest: the stimulated region, the neighboring

region and the region far from stimulation. On top of that, looking at identities at the edge of the monolayer in the non-stimulated region could also be a means to assess the influence of the border of the colony and compare it with experiments on micropatterned substrates.

### SHH stimulation of neural progenitors

As we mentioned in the introduction of this section, we need to use macromolecules in micro-transwells experiments, so that there is no diffusion between the top and bottom compartments. We conducted ventral stimulation experiments by using a recombinant human high activity SHH protein from R&D Systems (`https://www.rndsystems.com/products/recombinant-human-sonic-hedgehog-shh-protein-high-activity_8908-sh`). Its activity was estimated by the manufacturer thanks to alkaline phosphatase production by mesenchymal stem cells and from the curve provided on the website, we could estimate an $I_{50}$ value in the order of magnitude of $\sim$ 10ng/mL and a saturation value at $\sim$ 100ng/mL (Fig. 4.5),

We first performed a dose-response experiment to SHH on micropatterned substrates (Fig. 4.6), by submitting colonies to SHH concentrations of 20, 50, 100 or 200ng/mL from day 4 to day 9. We witnessed a contraction of colonies at 20 and 50ng/mL that is likely due to an experimental problem.

Judging from the expression of NKX6.1, only a few neural progenitors are ventralized at 20ng/mL, and this number increases at 50ng/mL and 100ng/mL, concentrations at which NKX6.1 expression is present in all neural progenitors. The patterned OLIG2 expression profile at 100ng/mL and 200ng/mL resembles that of colonies stimulated with SAG at 500 and 1000nM from day 4 to day 9. We did not check for an effect of SB inhibition on SHH-stimulated colonies. The results from this dose-response experiment seem to show that the OLIG2 pattern is obtained at SHH concentrations at which the activity of the SHH pathway is saturated (Fig. 4.5).

The OLIG2 staining at 20ng/mL is also surprising, since the very few

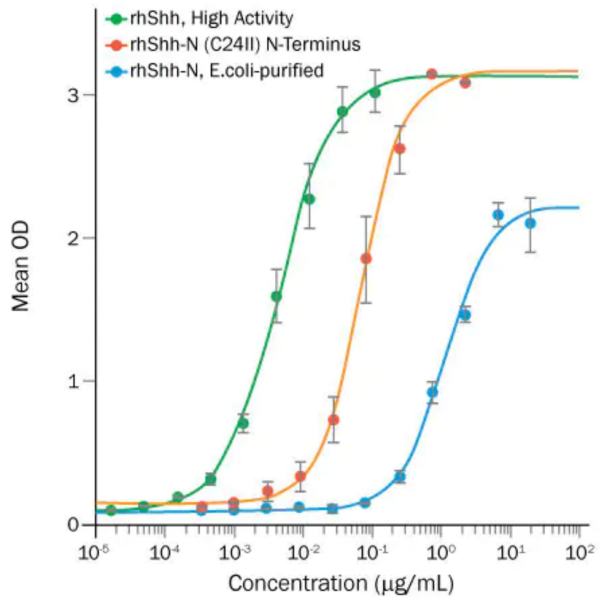


Figure 4.5: **A recombinant human high activity SHH protein.** Estimation of activity of *rhShh, High activity* (green curve) by alkaline phosphatase production in mesenchymal stem cells. It is compared to two other forms of recombinant SHH proteins (red and blue curves).

OLIG2$^+$ cells that appear are exclusively located at the periphery of the colony. It might be interesting to compare it to OLIG2 expression for SAG concentrations in the range of 100nM – we only used 10nM or 500nM – to see if this pattern is more pronounced in SHH than in SAG conditions and if this can be linked with SHH being a macromolecule and leading to diffusion-limited mechanisms.

Confident that the high activity SHH recombinant protein displayed a similar behavior than SAG, we switched to micro-transwells and conducted two dose-response experiments: one in the presence of RA to generate ventral progenitors (Fig. 4.7), and another one in the absence of RA and with earlier SHH stimulation to generate floor plate and p3 progenitors (Fig. 4.8).

In the presence of RA (Fig. 4.7), no ventral NKX6.1$^+$ progenitors were

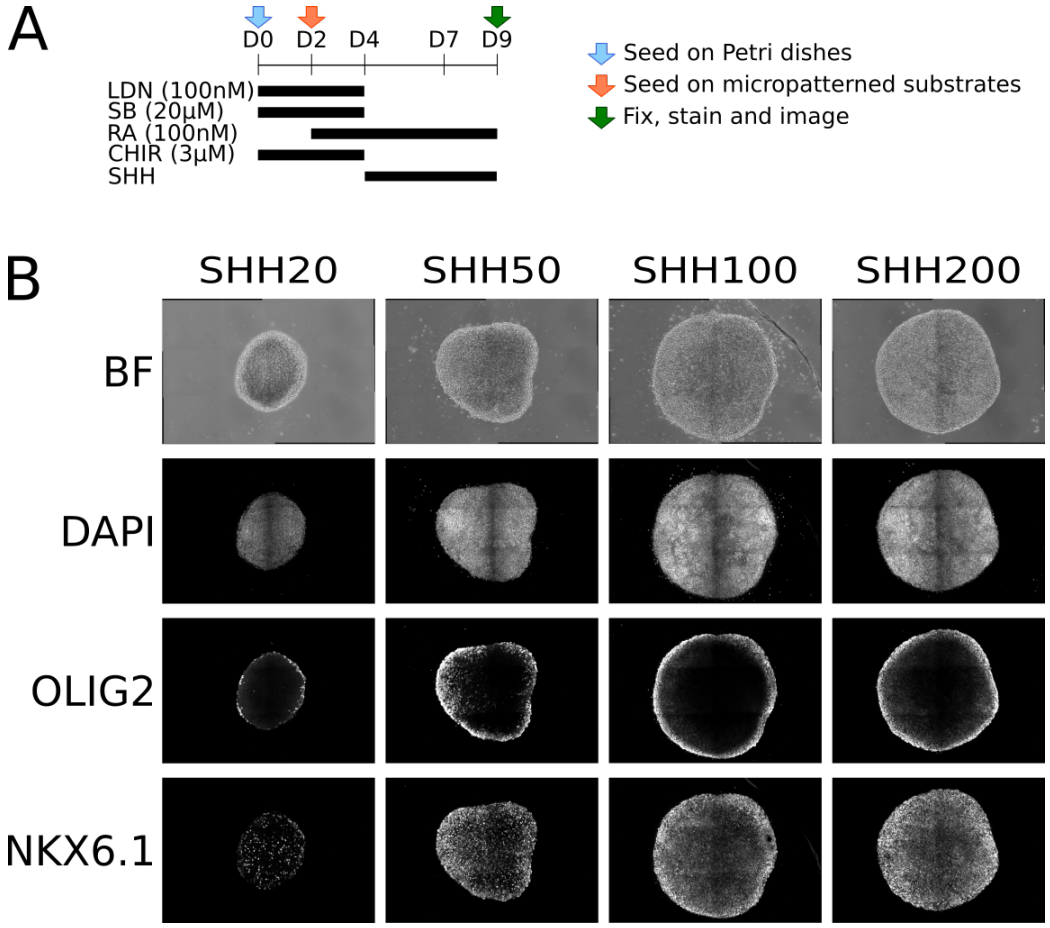


Figure 4.6: **SHH dose-response experiment on micropatterns. A** Protocol used on micropatterned substrates in the dose-response experiment to SHH. **B** D9 BF images, DAPI stainings and immunostainings for the ventral markers OLIG2 and NKX6.1 for different concentrations of SHH (20, 50, 100 and 200ng/mL).

seen without SHH and at a concentration of 20ng/mL. The first NKX6.1$^+$ cells appeared at a concentration of 50ng/mL of SHH, and OLIG2$^+$ cells were seen in the stimulated region. High concentrations of 100ng/mL and 200ng/mL led to a high and homogeneous expression of OLIG2. We noticed a higher signal at 100ng/mL compared to 200ng/mL. We wonder whether this

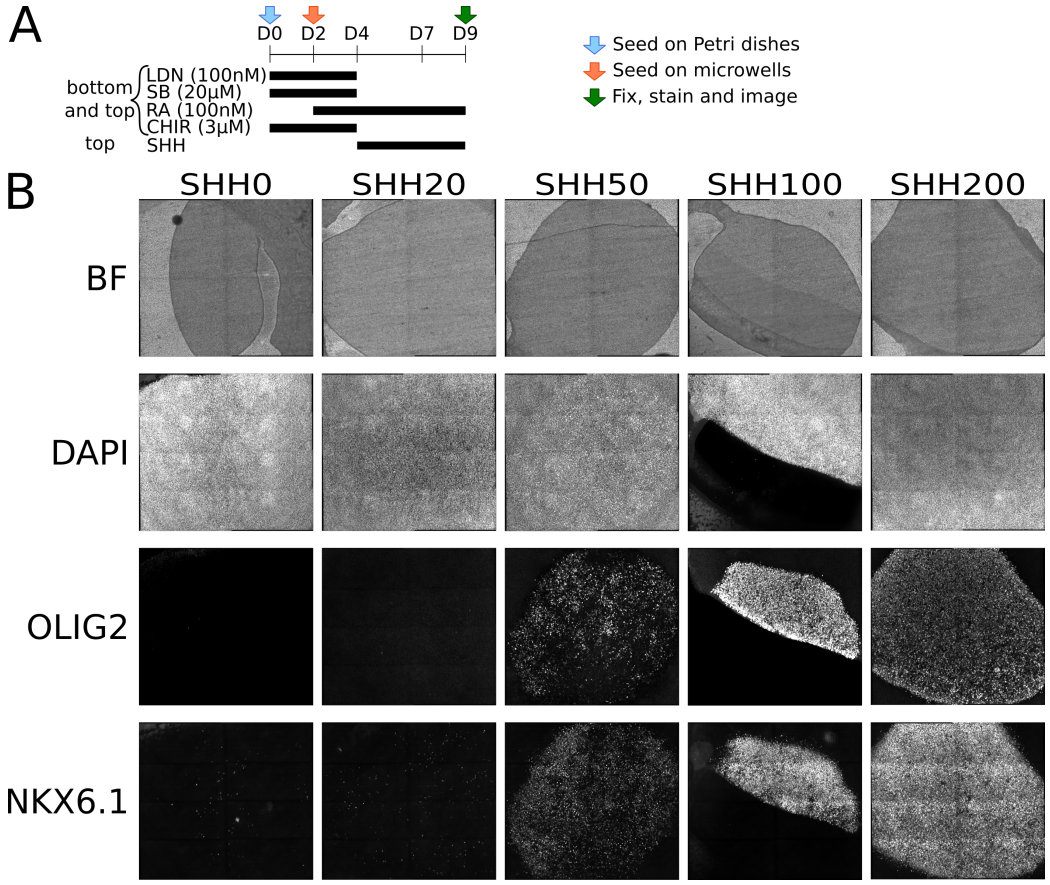


Figure 4.7: **SHH stimulation of neural progenitors on micro-transwells. A** Protocol used to study SHH stimulation of neural progenitors on micro-transwells. SHH is only provided in the top compartment. **B** BF images, DAPI stainings and immunostainings for the ventral markers OLIG2 and NKX6.1 on cells on micro-transwells stimulated with different concentrations of SHH (0, 20, 50, 100 and 200ng/mL) from D4 to D9. The stimulated region corresponds to the darker region on BF images.

could mean that cells at 200ng/mL downregulate the pMN marker OLIG2 and switch on the p3 marker NKX2.2. Additional stainings for NKX2.2 would be necessary to further investigate this hypothesis.

In the absence of RA and under early SHH stimulation, we stained cells

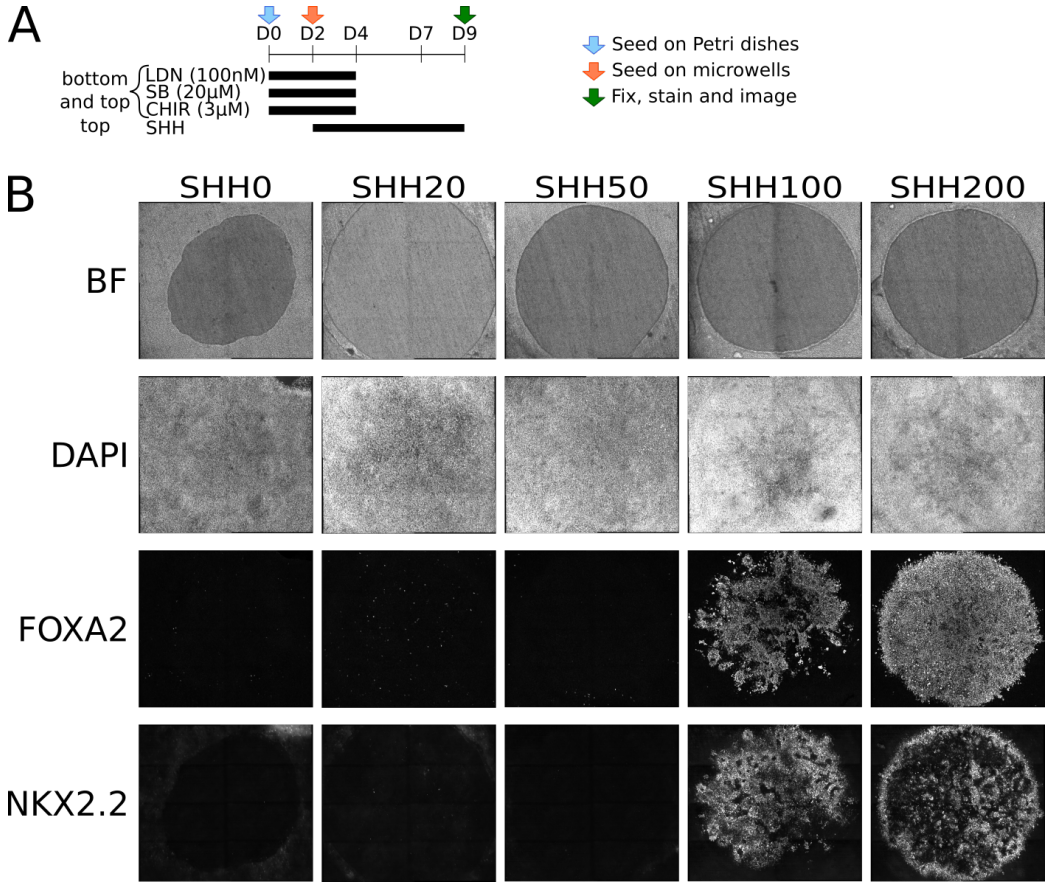


Figure 4.8: **Floor plate generation on micro-transwells. A** Protocol used to study SHH stimulation of floor plate and p3 progenitors on micro-transwells. Note that SHH is only provided in the top compartment as of D2 and no RA is added to the differentiation media. **B** BF images, DAPI stainings and immunostainings for the floor plate marker FOXA2 and the p3 marker NKX2.2 on cells on micro-transwells stimulated with different concentrations of SHH (0, 20, 50, 100 and 200ng/mL) from D2 to D9. The stimulated region corresponds to the darker region on BF images.

for the p3 progenitor marker NKX2.2 and the floor plate marker FOXA2 (Fig. 4.8). No NKX2.2$^+$ or FOXA2$^+$ cells were observed for concentrations of 50ng/mL or less.

At 100ng/mL, patches of NKX2.2$^+$ cells and FOXA2$^+$ cells were seen in the stimulated region. Some colocalization between the two markers was observed, and their relative levels of expression were very diverse (Fig. 4.9). This colocalization is reminiscent of the transient NKX2.2$^+$/FOXA2$^+$ floor plate in E2 chick embryos, before downregulation of NKX2.2 happens at E3 [Mansour et al., 2014]. At 200ng/mL, almost all cells are FOXA2$^+$, while NKX2.2 remains expressed in patches of cells. Later immunostainings would be useful to check whether identities get refined later on.

At 200ng/mL, we also noticed more NKX2.2$^+$ cells at the border of the stimulated region. Most of these cells were located out of the stimulated region (upper part of the image). Similar scenarios as those explained in the BMP stimulation subsection could apply. In this case, the floor plate secrets SHH once specified, and it would be interesting to see if cells in the stimulated region secret SHH.

We were rather impressed with the homogeneity and the precision basal stimulation could achieve, even more in the case of SHH. *In vivo*, neural progenitors are polarized in the neural tube, and their apical membranes face the ventricular lumen of the neural tube [Kosodo and Huttner, 2009]. SHH is secreted by the notochord and the floor plate and concentrates in the apical region [Chamberlain et al., 2008], where the primary cilia – the structure that initiates the response to SHH signaling – is also located [Tuson et al., 2011]. It would then seem more appropriate to stimulate neural progenitors from their apical side rather than from their basal side. Yet, basal stimulation on micro-transwells seems to yield a homogeneous OLIG2 population while apical stimulation on micropatterned substrates leads to a patterned OLIG2 profile. To understand better what is happening, it would be interesting to stain cells with polarity markers, such as PAR3 or ZO-1.

In this section, we presented a few preliminary results on the differentiation of neural progenitors on micro-transwells. We think further experiments on this system could help disentangle how signaling pathways are

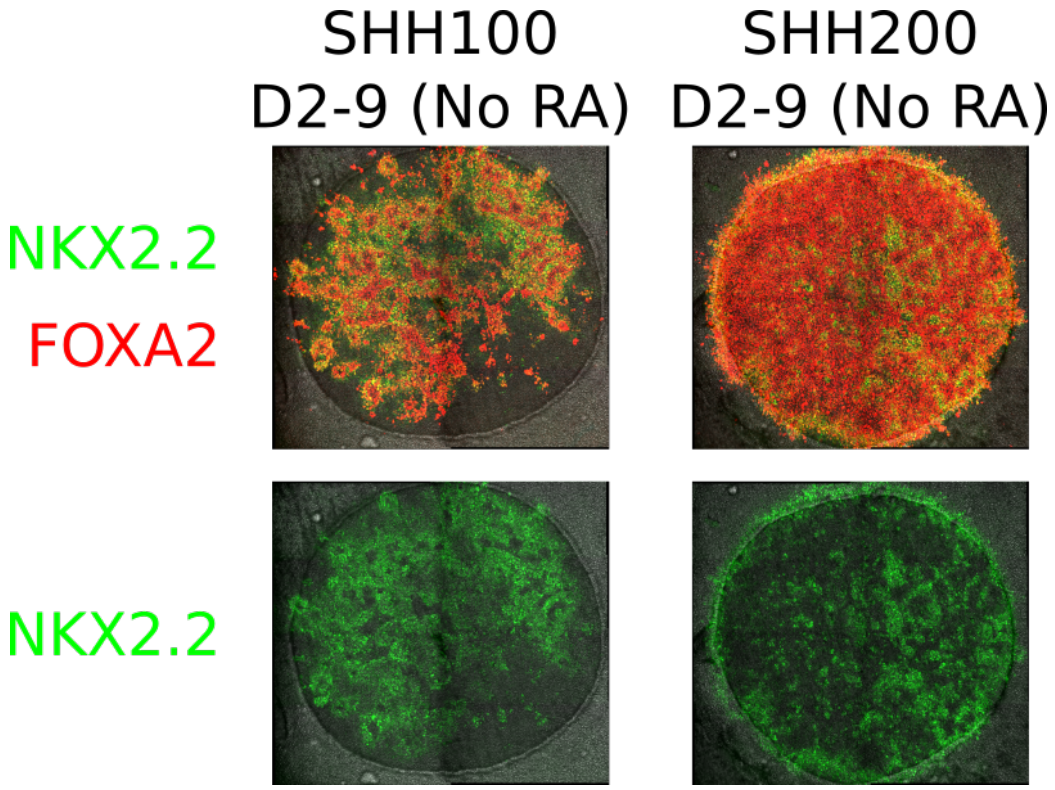


Figure 4.9: **Colocalization of NKX2.2 and FOXA2 in floor plate cells.** Composite images of the NKX2.2/FOXA2 stainings on day 9 for stimulation of SHH of 100ng/mL and 200ng/mL from day 2 to day 9 and in the absence of RA.

transduced and to discriminate between the consequences of direct stimulation and secondary secreted signals, as well as generate datasets that are rich since different regions of a single experiment are submitted to different signals.

### 4.2.3 Towards a controlled graded basal stimulation?

While micro-transwells allow for a better one-to-one correspondence between the stimulation exerted on the cells and the identities of neural progenitors,

its major problem is that spatial organization is somehow lost. The region close to but out of the stimulating zone can present gradients of endogenous signals and be studied, but the other regions respond to a unique concentration of morphogen.

The ideal setup to study neural differentiation would allow controlled basal stimulation and the possibility to impose gradients of concentration that translates into gradients of identities. It would be even greater if we could impose antiparallel gradients that mimic the gradients of SHH and BMP in the neural tube.

During his postdoc in the team, Tom Wyatt developed a system that is meant to meet all these criteria (Fig. 4.10). To generate gradients of tunable shapes, he used a microfluidic network described by [Dertinger et al., 2001]. Three inputs and multiple branching points allow for progressive mixing of the media. This results in a gradient in a wide channel once the mixing streams are combined. Mixing of fluorescent dextrans was used as a proof of concept. Similarly to micro-transwells, basal stimulation of cells is achieved through diffusion from the wide channel through a porous membrane. Hoechst was used on a living monolayer of cells and the intensity profile resulting in the monolayer matched that of Hoechst gradient generated in the wide channel.

We started to experiment with this gradient-generating device at the very end of the thesis project, and several experimental challenges need to be faced to try and have a working experiment. In Fig. 4.11, we present one example of an experiment we conducted on a SOX2-GFP reporter cell line. In this experiment, cells were cultivated for 2 days on Petri dishes and seeded on day 2 in a gradient-generating chip. From day 4 to day 7, BMP (10ng/mL) and SHH (200ng/mL) were provided in the input of the device to generate antiparallel gradients. We had to fix and stain cells on day 7 and not day 9 because of leaks and difficulties in maintaining pressure. Cells in the wide channel were $SOX2^+$, and cells on the upper part of the image

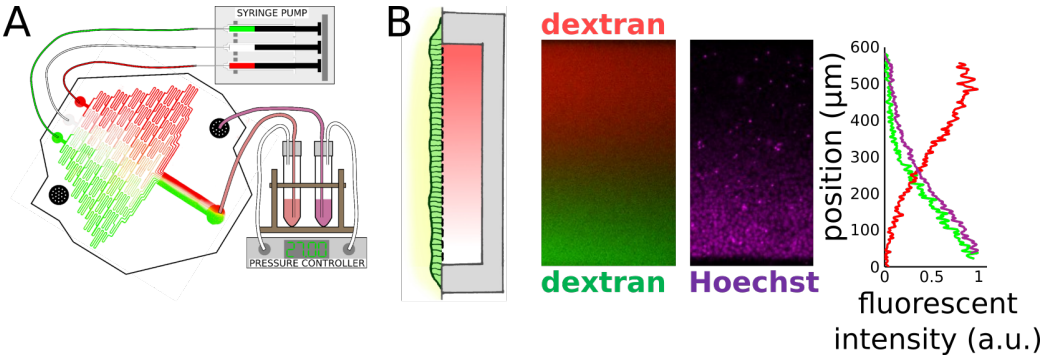


Figure 4.10: **The microfluidic chip device to generate basal antiparallel gradients. A** Scheme of the generation of gradients in the microfluidic chip. **B** Cells in the wide channel sense the gradient from their basal side through a porous membrane. Dextran was used to monitor the establishment of gradients in the wide channel and Hoechst to assess how a gradient in the wide channel resulted in an intensity gradient in the monolayer of cells.

– corresponding to high doses of BMP and low doses of SHH – had higher pSMAD1/5 signals. On the contrary, cells in the lower part of the image – corresponding to high doses of SHH and low doses of BMP – did not express the ventral neural marker NKX6.1. We are confident that reproducing this experiment, staining on day 9 and making sure SHH is not lost in the tubing, might lead to dorso-ventral patterning of neural identities on the chip.

We hope that this device will eventually be able to generate stripes of neural identities along the gradient. The question we would like to address is whether, by applying antiparallel gradients of BMP and SHH, we can reproduce the entirety of the neural tube. Indeed, in other experimental setups, we could only get either dorsal or ventral patterns of identities. Having both in the same experiment and in a rigorously organized manner would make it possible to study how both signals can be integrated simultaneously and test models that currently lack experimental data [Zagorski et al., 2017].

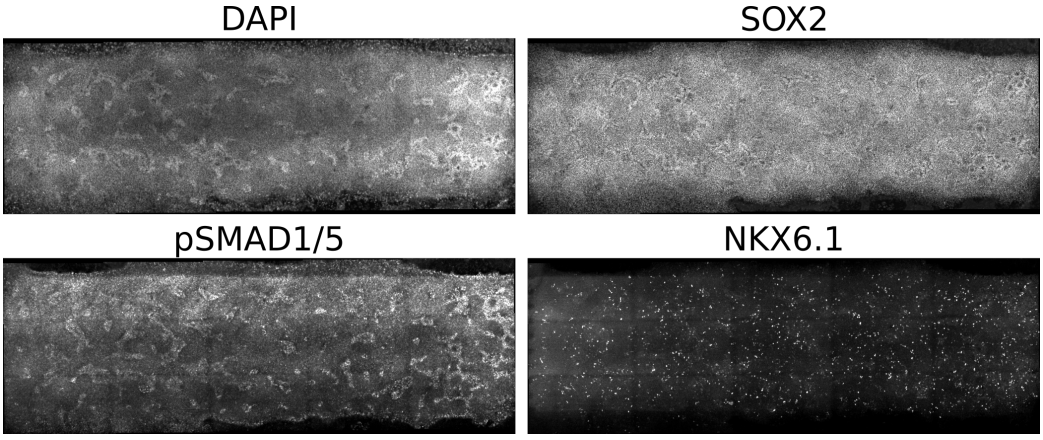


Figure 4.11: **Neural progenitors on the microfluidic chip.** DAPI, pSMAD1/5 and NKX6.1 stainings of the wide channel of the microfluidic chip on a SOX2-GFP reporter cell line. BMP was provided in the upper part of the wide channel and SHH in the lower part.

## 4.3 Timetracking with reporter cell lines

Most of the experiments presented in the former chapter consisted in immunostainings and statistical averaging. While these are easier to perform since they only require adequate antibodies, they do not get full advantage of the 2D setup that allows real-time microscopy. In this section, we will describe how we try to generate reporter cell lines. Because of the COVID pandemic, we could not advance on this topic as much as we would have liked to, but we still firmly believe generating reporter cell lines would allow more efficient generation of data and analysis of experiments, be they on micropatterned substrates, on micro-transwells or in a microfluidic chip.

### 4.3.1 Design of DNA constructs

We used the PiggyBac system [Lacoste et al., 2009] to integrate genetic constructs of transposable elements in the genome of hESCs. We first designed different DNA constructs that we integrated into the PiggyBac plasmid. Ex-

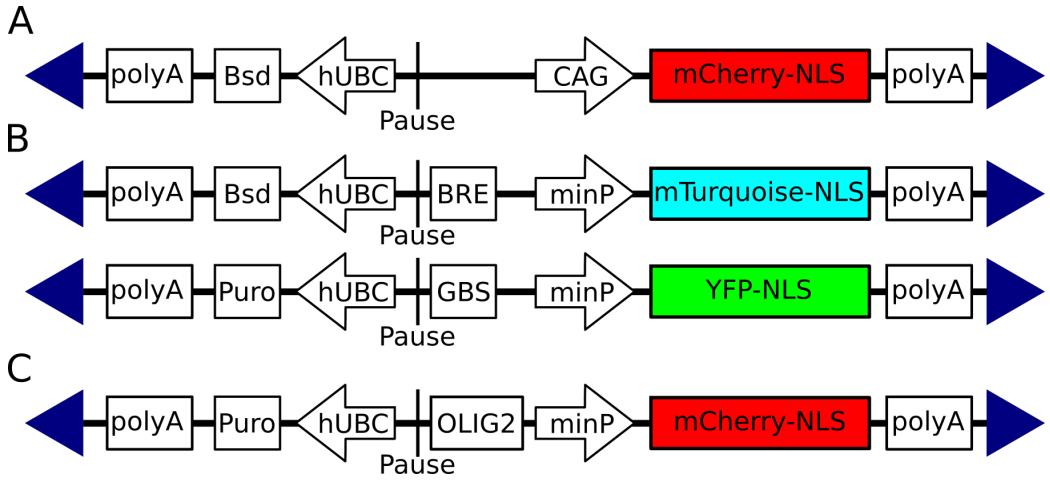


Figure 4.12: **DNA constructs.** Examples of DNA constructs designed to monitor gene expression. To be integrated into the genome, these constructs are co-transfected with the ePiggyBac transposase plasmid. **A** Bsd-CAG-mCherry-NLS DNA construct that used to evaluate the transfection protocol and as a nuclear marker. **B** Bsd-BRE-minP-mTurquoise-NLS and Puro-GBS-minP-YFP-NLS DNA constructs used to generate reporter cell lines for BMP and SHH signaling pathways. **C** Puro-OLIG2-minP-mCherry-NLS DNA construct used to generate a reporter cell line for live imaging of OLIG2 expression

amples of such constructs are presented in Fig. 4.12:

- The blue arrows correspond to 5'- and 3'-terminal repeats that will be recognized by the transposase and favor integration of the sequence in the genome.

- The left part of the construct confers resistance of the transfected hESC line to an antibiotic. We tried three different antibiotics: Blasticidin (Bsd), Puromycin (Puro) and Zeocin. We had good results in terms of selection with the first two antibiotics (10µg/mL for Bsd and 0.5µg/mL for Puro).

- The right part corresponds to the conditional expression of a fluores-

cent protein under the control of cis-regulatory elements. We used the expression of NLS-mCherry under the control of a universal CAG promoter to evaluate our transfection protocols, and as a nuclear marker (Fig. 4.12A). We used a weak promoter minP – which has a low basal signal – and added cis-regulatory elements specific to signaling pathways, such as BMP Responsive Element (BRE) for BMP or Gli Binding Site (GBS) for SHH (Fig. 4.12B), or specific to transcription factors expressed in neural progenitors (OLIG2 in MNs) (Fig. 4.12C)

It is interesting to have the same construct with different antibiotics and fluorescent proteins if we want to transfect hESCs with more than one construct. For instance, integrating both constructs presented in Fig. 4.12B would allow for simultaneous monitoring of BMP and SHH signaling. That would be useful in the microfluidic chip setup that we presented in the former section.

### 4.3.2 Generation of stable reporter cell lines

Genetic engineering of the DNA constructs was performed with Carine Vias. Some of the constructs were harder to build and sequence because of repeating units and GC-enriched sequences.

We transfected cells using a lipofection protocol that was further optimized during the master internship of Geoffray Marie:

1. Wells from a 24 well-plate were coated with Matrigel and left at 4°C overnight.

2. WT hESCs from a confluent 35mm Petri Dish were harvested in 1mL Accutase+RI. Harvested cells were added to a solution of DMEM-F12+RI at a 1:10 ratio to prevent further action from the Accutase and counted using a Malassez counting chamber, then centrifugated at 300g for 4 min and resuspended in mTESR+RI at a concentration

of 1M cells/mL. A well from the 24 well-plate was filled with 400µL mTESR+RI and 100µL of the media containing resuspended cells was added into the well, amounting to a total of 100k cells/well.

3. 24 hours after seeding, cells were lipofected with 1.5µL Lipofectamine Stem and 0.5µg DNA (at a ratio 2:3 PiggyBac plasmid / 1:3 transposase plasmid).

4. 48 hours later, selection with Blasticidin (10µg/mL) or Puromycin (0.5µg/mL) was started and maintained for at least 7 days.

At this point, we obtain a stable polyclonal population that can be frozen. We tried to generate monoclonal reporter cell lines by plating $\sim$ 500-1000 single cells detached with Accutase in a 24 well-plate, and by manually picking, transferring and expanding individual colonies.

### 4.3.3 Evaluation of reporter cell lines

We used the CAG-mCherry-NLS cell lines as a control that transfection and monoclonal selection protocols worked properly (Fig. 4.13). Before monoclonal selection, we could see that cells express different levels of fluorescence. Signals emitted by cells from the same progeny appeared rather homogeneous.

To show an example of what this technique can achieve, we transfected hESCs with Bsd-CAG-mCherry-NLS and Puro-BRE-minP-mTurquoise-NLS plasmids in a single transfection. After selection and monoclonal expansion, we managed to get five monoclonal cell lines that we labeled with the number of the 24-well plate they originated from (Line 5, 6, 7, 9 and 11).

At that point, we could not probe the intensity of the BRE signal, because stimulating hESCs with BMP would induce differentiation. For each expanded cell line, we seeded cells on Laminin-coated PDMS in 2 wells of a Chamlide. One of the wells was kept in pluripotency mTESR media. In the

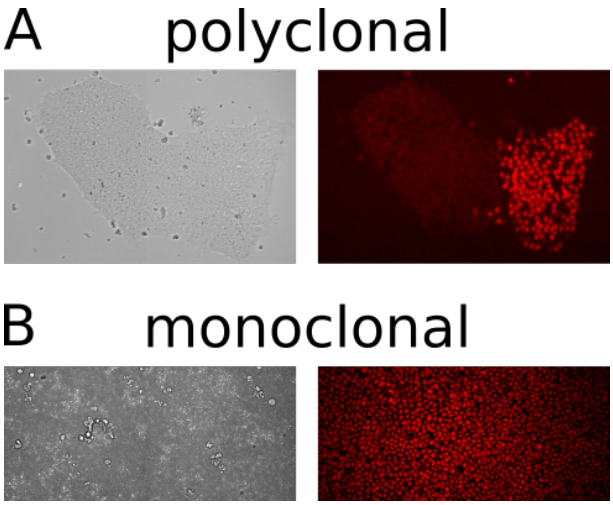


Figure 4.13: **Evaluating polyclonal and monoclonal selection. A** BF and RFP channel fluorescent image in a polyclonal Bsd-CAG-mCherry-NLS cell line 7 days after Blasticidin selection. **B** BF and RFP channel fluorescent image in a Bsd-CAG-mCherry-NLS Puro-BRE-minP-mTurquoise-NLS cell line after monoclonal selection.

other one, we added BMP at a concentration of 50ng/mL for 6 hours, then fixed the cells. Four stacks were taken for each condition.

We were able to segment monolayers of cells using a Python code available on `https://github.com/GabrielThon/Thesis-code`. For each Z-stack, we used OpenCV built-in functions to perform watershed segmentation of nuclei on the CAG-mCherry-NLS signal. We extracted mean nuclear intensities in the BRE-minP-mTurquoise-NLS channel for nuclei whose area was between 100 and 300 pixels. We then compared Z-stacks to identify the plane of maximal intensity for each cell. Finally, for each condition, we plotted the mean, first and third quartiles of intensities. Results for the five different monoclonal cell lines are presented in Fig.4.14.

The five cell lines displayed mTurquoise nuclear signal in the presence of BMP. Differences in levels and homogeneity of the signal were observed. We show an example of a signal that we recorded on cell line 11 in Fig. 4.15.

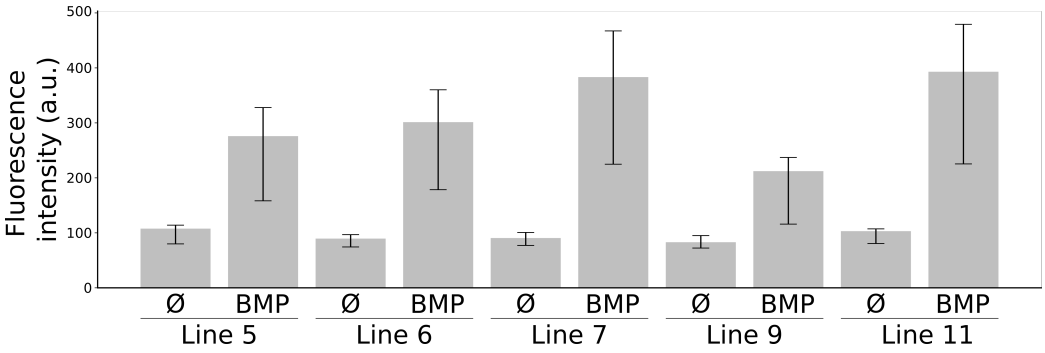


Figure 4.14: **Fluorescence of BRE reporter cell lines.** Mean fluorescent signals in the mTurquoise channel for five different monoclonal Bsd-CAG-mCherry-NLS Puro-BRE-minP-mTurquoise-NLS cell lines in the absence and in the presence of BMP (50ng/mL for 6 hours). Error bars represent the first and third quartiles.

### 4.3.4 Issues with reporter cell lines

We would like to point out a few issues that we were faced with in our attempt to generate stable reporter cell lines and discuss how these issues could be solved.

- We witnessed heterogeneity in cell response in monoclonal colonies. The experimental procedure for monoclonal selection might need to be improved. Manual picking of colonies was hard to perform – we scratched colonies and aspirated them.

- The intensities of recorded fluorescent signals were very low. Switching to a stronger promoter than minP could improve the signal. hSP68 promoter is currently being tested. While a stronger promoter might produce higher signals, we need to check carefully that potential promoter leakage does not lead to high signals in the absence of stimulation.

- We were not able to detect any signal in monoclonal reporter cell lines for the ventral neural transcription factors NKX6.1 or OLIG2. To

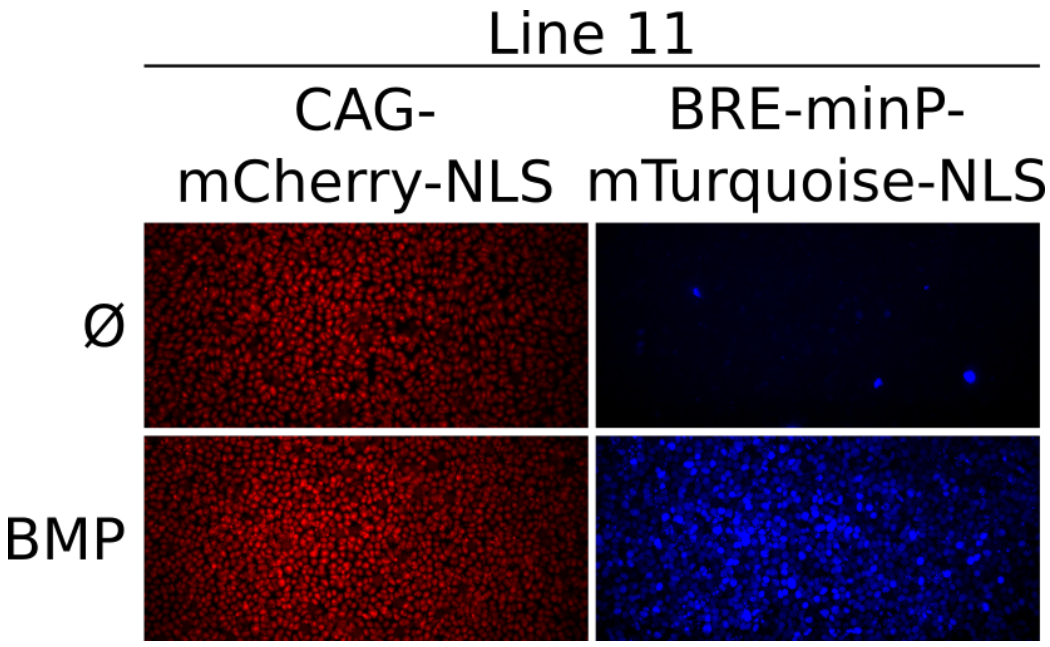


Figure 4.15: **Heterogeneity in BRE reporter cell lines.** mCherry and mTurquoise signals on the Bsd-CAG-mCherry-NLS Puro-BRE-minP-mTurquoise-NLS monoclonal cell Line 11. mCherry is used as a nuclear marker. In the presence of BMP (50ng/mL for 6 hours), mTurquoise expression is induced heterogeneously across the colony.

monitor the signal, we followed the protocols that yielded positive cells on micropatterns. Even after 9 days of differentiation, no fluorescence signal was observed. Once again, the minP promoter might be too weak, and switching to a stronger promoter could improve our results. It is also possible that the transposon was inserted in the genome of hESCs in a location that is not transcribed in neural progenitors due to chromatin remodeling. We are currently considering inserting the DNA construct at a universally expressed locus, such as AAVS1, using CRISPR genome-editing rather than the PiggyBac transposase system.

## 4.4 Conclusion

Micropatterned substrates are a great tool to induce self-organization of tissues and extract quantitative data about the patterning process. Dorsoventral specification of neural progenitors can be transposed to micropatterns and spatial organization occurs as a result of dorsal and ventral exogenous and endogenous signals. There remains a lot to be understood as to how signaling pathways interact and build the diversity of neural progenitors, and micropatterns can be an interesting setup to capture these interactions.

A better understanding of neural specification would definitely rely on improving our control of stimulation and building reporter cell lines that enable us to track the activity of signaling pathways and identities of neural progenitors.

# Chapitre 5

# Résumé substantiel en français

Nous proposons dans ce chapitre un résumé en français de nos travaux de thèse conforme aux règles de l'Ecole Doctorale Physique en Ile-de-France et de l'Université de Paris.

L'idée directrice de cette thèse a été de s'inspirer des protocoles de différenciation de cellules souches embryonnaires humaines (hESC) en progéniteurs neuraux (NP) et de les transposer à plusieurs dispositifs expérimentaux qui génèrent de l'organisation spatiale entre différents destins cellulaires, avec pour but l'étude contrôlée de l'organisation dorso-ventrale dans la moëlle épinière. Nous nous sommes principalement intéressés aux substrats micropatternés – sur lesquels l'adhérence des cellules est restreinte à un motif géométrique 2D contrôlé – mais nous discutons également d'autres dispositifs expérimentaux pour améliorer notre contrôle de l'organisation spatiale des destins cellulaires.

## 5.1 Introduction

### 5.1.1 Le tube neural est patterné par des gradients de morphogènes

Le tube neural est induit au cours du développement embryonnaire par la notochorde sous-jacente et donnera notamment naissance aux cellules neurales dans le cerveau et la moëlle épinière. Selon leur position le long de l'axe antéro-postérieur (ou rostro-caudal) et de l'axe dorso-ventral, les progéniteurs neuraux acquièrent des identités cellulaires distinctes qui se traduiront en des fonctions anatomiques variées.

L'acquisition par les cellules de cette information de position au sein du tissu semble remplir les critères du modèle historique du « drapeau français »[Wolpert, 1969]. En effet, le long de l'axe dorso-ventral, des structures situées de part et d'autre du tissu (notochorde puis plaque du plancher du côté ventral, ectoderme adjacent puis plaque du toit du côté dorsal) sécrètent des signaux diffusibles, appelés morphogènes (Shh du côté ventral, BMP et Wnt du côté dorsal). En diffusant dans le tissu, ces morphogènes établissent des profils de concentration qui sont interprétés par la cellule en information de position.

Dans le cas du tube neural, le modèle du « drapeau français »ne permet pas d'expliquer entièrement la dynamique de la réponse cellulaire aux morphogènes telle qu'elle est observée expérimentalement. Un modèle plus détaillé, le « Gene Regulatory Network », prenant en considération des répressions mutuelles entre facteurs de transcription dont l'expression est régulée en aval des voies de signalisation, a permis d'intégrer une dimension temporelle à la spécification des cellules neurales le long de l'axe dorso-ventral [Sagner and Briscoe, 2019].

### 5.1.2 Reproduire la différentiation neurale de cellules souches

Avec la découverte des cellules souches et l'identification de conditions en permettant la culture et l'induction [Martin, 1981; Thomson et al., 1998; Takahashi and Yamanaka, 2006], de nouvelles perspectives d'étude développementale ont émergé. Peut-on reproduire *in vitro* la diversité cellulaire observée *in vivo* et ainsi tester des modèles théoriques ?

Trois étapes majeures ont été identifiées pour générer des neurones à partir d'ESCs :

- Les ESCs acquièrent d'abord une identité de NP. Ce processus se déroule de manière dynamique le long de l'axe antéro-postérieur et concomitante à l'élongation du tube neural. Deux protocoles distincts permettent de générer des structures antérieures ou postérieures. Pour les progéniteurs les plus antérieurs (cerveau et moëlle épinière cervicale), l'induction de NP passe par l'inhibition des voies BMP et Activin/Nodal. Les progéniteurs plus postérieurs passent par un stade intermédiaire de progéniteurs neuromésodermaux (NMP) – caractérisé par la coexpression de marqueurs neuraux (Sox2) et mésodermaux (Brachyuri) – sous l'action des voies Wnt, FGF et GDF. Les NMP acquièrent ensuite une identité de NP sous l'action de l'acide rétinoïque (RA). Les NP obtenus à ce stade conservent une pluripotence dans la mesure où ils ne sont pas contraints à une identité dorso-ventrale définie.

- Dans un deuxième temps, les NP acquièrent une identité dorso-ventrale sous l'action de gradients antiparallèles de BMP/Wnt et Shh.

- Finalement, les progéniteurs se différencient en neurones matures sous l'action de Notch et Activin/Nodal.

### 5.1.3 Les substrats micropatternés génèrent de l'organisation spatiale

La culture de cellules sur des motifs 2D d'adhérence cellulaire avait initialement pour objectif de contrôler la forme, la taille et la densité des colonies pour améliorer la reproductibilité des résultats. De manière intéressante, les substrats micropatternés se sont avérés être particulièrement efficaces pour induire de l'organisation spatiale au sein des colonies. Grâce à des mécanismes de localisation différentielle des récepteurs membranaires – moins accessibles au centre de la colonie qu'à la périphérie – et de diffusion d'inhibiteurs sécrétés – davantage concentrés au centre de la colonie qu'à la périphérie –, une concentration homogène d'un morphogène dans le milieu de culture peut aboutir à une stimulation en gradient de la voie de signalisation en aval du morphogène.

Ce dispositif expérimental de substrats micropatternés a été utilisé pour étudier comment les voies de signalisation BMP, Wnt et Activin/Nodal sont interprétés conjointement par les cellules dans leur différenciation en ectoderme, mésoderme et endoderme [Warmflash et al., 2014; Etoc et al., 2016; Martyn et al., 2019; Simon et al., 2021]. Le patterning du neuroectoderme sous l'action de BMP et Wnt a aussi fait l'objet d'études récentes permettant de mettre en évidence que chacune des voies avaient des cibles distinctes [Xue et al., 2018; Britton et al., 2019].

### 5.1.4 Projet de thèse

Au cours de cette thèse, nous avions pour objectif d'utiliser les substrats micropatternés pour étudier l'action de plusieurs voies de signalisation impliquées dans l'établissement de la diversité dorso-ventrale lors de la formation du tube neural. L'essentiel de la thèse a donc consisté à transposer des protocoles de différenciation neurale à la culture sur micropatterns et à observer les identités dorso-ventrales des progéniteurs obtenus.

## 5.2 Résultats

### 5.2.1 Génération d'une population homogène de progéniteurs spinaux sur micropatterns

Nous avons identifié des conditions permettant de différencier des hESCs en une population homogène de NP sur micropatterns. Avant d'obtenir ce résultat, nous avons constaté qu'ensemencer les cellules dès jour 0 (J0) dans un milieu de culture de différenciation neurale (N2B27+CHIR+LDN+SB+RA) conduisait à une hétérogénéité au sein de la colonie à J4. En effet, si les cellules au centre de la colonie expriment les marqueurs neuraux PAX6 et SOX1, ce n'est pas le cas des cellules au bord de la colonie.

Un ensemencement plus tardif à J2 a permis de résoudre cette hétérogénéité non désirée. A J4, tous les progéniteurs obtenus expriment de manière homogène PAX6 et SOX1, indépendamment de leur position dans la colonie.

Nous avons également caractérisé l'identité rostro-caudale des progéniteurs neuraux obtenus, qui expriment les marqueurs GBX2 et CDX2 ainsi que les ARNm *HOXA2*, *HOXA4* et *HOXA5*, ce qui indique une identité spinale des progéniteurs générés. En l'absence de stimulation de la voie Wnt avec CHIR, il est possible d'obtenir des progéniteurs neuraux $OTX2^{+}$, $GBX2^{-}$, $CDX2^{-}$, ce qui correspond à un état plus antérieur.

### 5.2.2 Deux phénotypes distincts émergent en l'absence de stimulation dorso-ventrale exogène

Nous avons ensuite poussé la différenciation jusqu'à J9 pour que les progéniteurs neuraux acquièrent une identité dorso-ventrale. Avant d'essayer de modifier cette identité au moyen d'une stimulation exogène des voies BMP ou SHH, nous avons cherché à connaître l'identité « par défaut »en l'absence de stimulation exogène.

La présence du marqueur PAX7 dans toutes les colonies « par défaut »a

permis d'affirmer que les progéniteurs neuraux s'orientaient vers des destins dp1-dp6 du côté dorsal du tube neural. En cherchant à obtenir une information plus précise sur l'identité dorso-ventrale des progéniteurs neuraux, nous avons identifié deux phénotypes principaux au sein des colonies étudiées. Dans près de la moitié des colonies, toutes les cellules expriment le marqueur OLIG3, ce qui est caractéristique de destins dp1-dp3 dorsaux. Dans les autres colonies, OLIG3 n'est exprimé qu'à la périphérie de la colonie, formant un anneau de 2 à 3 cellules de largeur, donc les cellules au centre sont dp4-dp6 et celles à la périphérie sont dp1-dp3.

Ce résultat est surprenant si on le compare aux destins « par défaut »dans des cultures 3D d'organoïdes dans lesquelles l'obtention des destins cellulaires dorsaux dp1-dp3 nécessite un signal dorsalisant de BMP ou de WNT. Nous avons complété nos observations précédentes par des expériences d'inhibition ciblant BMP, WNT et ACTIVIN/NODAL et constaté que seul le phénotype où OLIG3 était restreint à la périphérie persistait en présence d'inhibiteurs. Ceci suggère l'existence d'une signalisation endogène dorsalisante dans les colonies « par défaut ». Nous avons confirmé une activité des voies de signalisation BMP et WNT en observant respectivement la phosphorylation des protéines SMAD1/5 et SMAD2/3 qui intervient en aval de chacune de ces voies.

### 5.2.3 Des destins cellulaires plus dorsaux et organisés spatialement sous l'action de BMP4

Nous avons exposé les colonies à des signaux dorsalisants de BMP4 en modulant la concentration en BMP4 ainsi que la période d'exposition au morphogène.

A faible concentration (1 ou 2ng/mL de J4 à J9) comme à exposition de courte durée (10ng/mL de J6 à J9 ou de J8 à J9), toutes les colonies arborent une identité dp1-dp3 de manière homogène. Ce phénotype correspond à l'un des deux observés en l'absence de BMP, sauf qu'ici, l'intégralité des colonies

exhibe le même phénotype dorsalisé.

A plus haute concentration (5 ou 10ng/mL de J4 à J9) ainsi que pour une exposition de plus longue durée (10ng/mL de J3 à J9 ou de J4 à J9), nous avons décrit l'émergence d'un anneau externe de cellules OLIG3$^{-}$ ; PAX7$^{+}$ ; TFAP2$\alpha^{+}$, que nous attribuons à un destin encore plus dorsal de crête neurale. Au centre de ces colonies, des patchs de cellules dp1-dp3 subsistent, et nous suggérons que les cellules non marquées par PAX7 ou OLIG3 puissent être des cellules de la plaque du toit.

### 5.2.4 Ventralisation des progéniteurs neuraux sous l'action d'un agoniste de SHH (SAG), une stimulation régulée par ACTIVIN/NODAL ?

Finalement, nous avons exposé les colonies de J4 à J9 à un agoniste de SHH (SAG) dans l'objectif de ventraliser les identités cellulaires obtenus.

Si, à une concentration de 500nM, le SAG permet de ventraliser tous les progéniteurs, comme en atteste l'expression homogène du marqueur NKX6.1, nous avons constaté avec surprise que seules les cellules à la périphérie exprimaient le marqueur de progéniteurs de motoneurones (pMN) OLIG2. Dans les organoïdes 3D, cette concentration de SAG permet de générer une population homogène de pMN.

Nous avons monitoré plus précisément la temporalité de l'expression d'OLIG2 au cours de la différenciation. Nos résultats indiquent qu'OLIG2 est d'abord exprimé de manière relativement homogène au sein de la colonie, et est restreint au bord de la colonie entre J7 et J9. Nous avons pensé que ceci pouvait être une interprétation graduelle de la voie de signalisation en aval de SHH. Pour tester cette hypothèse, nous proposons un début de réponse grâce à une lignée rapportrice polyclonale dans laquelle l'expression d'une protéine fluorescente (YFP) est sous contrôle d'un marqueur transcriptionnel en aval de SHH (GBS pour Gli Binding Site). La dynamique d'expression de GBS

semble cohérente avec la dynamique d'expression d'OLIG2, avec une restriction à la périphérie entre J7 et J9.

Nous avons également inhibés les signaux dorsalisants BMP, WNT et ACTIVIN/NODAL au sein de colonies stimulées par SAG pour voir si des signaux endogènes dorsalisants pourraient également expliquer le pattern d'OLIG2 observé à J9. Seul l'inhibition d'ACTIVIN/NODAL par SB parvient à modifier le phénotype des colonies, et génèrent des colonies dans lesquelles l'expression d'OLIG2 ainsi que GBS est plus homogène.

Comme la voie ACTIVIN/NODAL est également impliquée dans la maturation des progéniteurs neuraux, nous avons regardé si dès ce stade, des neurones matures étaient présents dans les colonies, et si l'homogénéisation du pattern d'OLIG2 pourrait s'expliquer par une modification de la balance entre progéniteurs et neurones matures. Les colonies stimulées par SAG possèdent $\sim 10$ % de motoneurones matures ISL1$^+$ alors qu'aucun motoneurone mature n'est observé lorsqu'ACTIVIN/NODAL est inhibé. Ceci confirme l'implication d'ACTIVIN/NODAL dans la maturation des progéniteurs. Cependant, il ne semble pas évident de formuler une hypothèse qui explique le pattern d'OLIG2 uniquement par une activité endogène d'ACTIVIN/NODAL, d'autant que certains résultats expérimentaux, comme l'expression homogène de NKX6.1 au sein des colonies stimulées par SAG, semblent constituer un argument contre cette hypothèse.

## 5.3 Discussion et perspectives

### 5.3.1 Des marquages supplémentaires nécessaires dans les différents conditions étudiées

Nous proposons des pistes pour poursuivre l'étude de la spécification dorsoventrale de progéniteurs neuraux sur micropatterns.

- Etudier la dynamique des marqueurs neuraux PAX6, SOX1 et CDX2

pourrait permettre de préciser l'identité des NP que nous avons utilisés au cours de nos expériences.

- Caractériser davantage les voies endogènes impliquées dans l'établissement du destin « par défaut »et regarder si les contraintes mécaniques imposées aux cellules sur micropatterns ne peuvent pas également expliquer certains résultats expérimentaux comme la persistance d'un anneau d'OLIG3 de 2-3 cellules même en présence d'inhibiteurs.

- Compléter les expériences de dorsalisation par des marquages supplémentaires semble nécessaire pour affirmer avec certitude les identités dorsales observées (SOX10, ATOH1, MSX1 par exemple).

- Etudier la dynamique en aval de SHH (PTCH1, GLI1) et d'ACTIVIN/NODAL (pSMAD2/3) permettrait de formuler un mécanisme expliquant l'émergence d'un patterning ventral lors d'une stimulation par SAG.

### 5.3.2 Mieux contrôler la stimulation des progéniteurs neuraux

Si les micropatterns génèrent de l'organisation spatiale, celle-ci est difficilement contrôlable par l'expérimentateur, qui ne peut pas imposer un profil d'activité d'une voie de signalisation au sein de la colonie. Nous proposons deux dispositifs expérimentaux alternatifs sur lesquels nous avons commencé à réaliser des expériences de différenciation dorso-ventrale de progéniteurs neuraux.

Le premier consiste en des micropuits qui permettent une stimulation basale et localisée d'une monocouche de progéniteurs neuraux. Ceci permet de s'affranchir des effets de bords inhérents aux micropatterns. Des expériences préliminaires de stimulation dorsale par BMP ou ventrale par

SHH de progéniteurs neuraux suggèrent une bonne correspondance entre les concentrations de morphogène et les destins cellulaires observés.

Le deuxième permet toujours de stimuler de manière basale et localisée, mais cette fois-ci en imposant un gradient, voire des gradients antiparallèles, dont le profil est contrôlé par l'expérimentateur, au moyen d'une puce à gradient microfluidique élaborée au sein de l'équipe. Nous pensons que ce dispositif pourrait permettre de générer des bandes d'identités dorso-ventrales distinctes et reproduire l'intégralité du tube neural.

### 5.3.3 Mieux comprendre la dynamique des signaux grâce à des lignées rapportrices

L'un des avantages de la culture 2D contrôlée de progéniteurs neuraux consiste en la facilité avec laquelle elle peut se coupler à une observation en temps réel. Si nous n'avons pas pu profiter de cet avantage autant que nous l'aurions souhaité, nous pensons que la génération de lignées rapportrices adaptées permettrait un suivi dynamique des destins cellulaires et des mouvements au sein de la colonie.

Nous avons commencé à réaliser certaines lignées rapportrices par le système transposable PiggyBac. Dans des cas simples où la lignée peut être testée par stimulation dès l'état pluripotent, nous avons évalué l'homogénéité et l'intensité du signal. Dans des cas plus complexes où l'expression de la protéine fluorescente est sous contrôle d'un facteur de transcription neural qui n'est pas exprimé à l'état pluripotent, nous n'avons malheureusement pas pu observer de signal. Il faudrait recourir à d'autres constructions génétiques plus élaborées, qui permettent par exemple de s'assurer que l'insertion dans le génome s'est bien déroulée et à un site accessible à l'état de NP.

# Bibliography

Ashe, H. L. and Briscoe, J. (2006). The interpretation of morphogen gradients.

Balaskas, N., Ribeiro, A., Panovska, J., Dessaud, E., Sasai, N., Page, K. M., Briscoe, J., and Ribes, V. (2012). Gene regulatory logic for reading the sonic hedgehog signaling gradient in the vertebrate neural tube. *Cell*, 148(1-2):273–284.

Bardot, E. S. and Hadjantonakis, A.-K. (2020). Mouse gastrulation: coordination of tissue patterning, specification and diversification of cell fate. *Mechanisms of development*, 163:103617.

Ben-Zvi, D., Shilo, B.-Z., and Barkai, N. (2011). Scaling of morphogen gradients. *Current opinion in genetics & development*, 21(6):704–710.

Bertrand, N., Castro, D. S., and Guillemot, F. (2002). Proneural genes and the specification of neural cell types. *Nature Reviews Neuroscience*, 3(7):517–530.

Bier, E. and De Robertis, E. M. (2015). Bmp gradients: A paradigm for morphogen-mediated developmental patterning. *Science*, 348(6242).

Boergermann, J., Kopf, J., Yu, P., and Knaus, P. (2010). Dorsomorphin and ldn-193189 inhibit bmp-mediated smad, p38 and akt signalling in c2c12 cells. *The international journal of biochemistry & cell biology*, 42(11):1802–1807.

Briscoe, J., Pierani, A., Jessell, T. M., and Ericson, J. (2000). A homeodomain protein code specifies progenitor cell identity and neuronal fate in the ventral neural tube. *Cell*, 101(4):435–445.

Briscoe, J. and Small, S. (2015). Morphogen rules: design principles of gradient-mediated embryo patterning. *Development*, 142(23):3996–4009.

Britton, G., Heemskerk, I., Hodge, R., Qutub, A. A., and Warmflash, A. (2019). A novel self-organizing embryonic stem cell system reveals signaling logic underlying the patterning of human ectoderm. *Development*, 146(20):dev179093.

Byfield, S. D., Major, C., Laping, N. J., and Roberts, A. B. (2004). Sb-505124 is a selective inhibitor of transforming growth factor-$\beta$ type i receptors alk4, alk5, and alk7. *Molecular pharmacology*, 65(3):744–752.

Cambray, N. and Wilson, V. (2007). Two distinct sources for a population of maturing axial progenitors.

Chamberlain, C. E., Jeong, J., Guo, C., Allen, B. L., and McMahon, A. P. (2008). Notochord-derived shh concentrates in close association with the apically positioned basal body in neural target cells and forms a dynamic gradient during neural patterning. *Development*, 135(6):1097–1106.

Chambers, S. M., Fasano, C. A., Papapetrou, E. P., Tomishima, M., Sadelain, M., and Studer, L. (2009). Highly efficient neural conversion of human es and ips cells by dual inhibition of smad signaling. *Nature biotechnology*, 27(3):275–280.

Chen, B., Dodge, M. E., Tang, W., Lu, J., Ma, Z., Fan, C.-W., Wei, S., Hao, W., Kilgore, J., Williams, N. S., et al. (2009). Small molecule–mediated disruption of wnt-dependent signaling in tissue regeneration and cancer. *Nature chemical biology*, 5(2):100–107.

Chesnutt, C., Burrus, L. W., Brown, A. M., and Niswander, L. (2004). Coordinate regulation of neural tube patterning and proliferation by tgf$\beta$ and wnt activity. *Developmental biology*, 274(2):334–347.

Cox, W. G. and Hemmati-Brivanlou, A. (1995). Caudalization of neural fate by tissue recombination and bfgf. *Development*, 121(12):4349–4358.

Crawford, T. Q. and Roelink, H. (2007). The notch response inhibitor dapt enhances neuronal differentiation in embryonic stem cell-derived embryoid bodies independently of sonic hedgehog signaling. *Developmental dynamics: an official publication of the American Association of Anatomists*, 236(3):886–892.

D'Arcangelo, E. and McGuigan, A. P. (2015). Micropatterning strategies to engineer controlled cell and tissue architecture in vitro. *Biotechniques*, 58(1):13–23.

del Corral, R. D. and Storey, K. G. (2004). Opposing fgf and retinoid pathways: a signalling switch that controls differentiation and patterning onset in the extending vertebrate body axis. *Bioessays*, 26(8):857–869.

Dertinger, S. K., Chiu, D. T., Jeon, N. L., and Whitesides, G. M. (2001). Generation of gradients having complex shapes using microfluidic networks. *Analytical Chemistry*, 73(6):1240–1246.

Dessaud, E., McMahon, A. P., and Briscoe, J. (2008). Pattern formation in the vertebrate neural tube: a sonic hedgehog morphogen-regulated transcriptional network.

Dessaud, E., Ribes, V., Balaskas, N., Yang, L. L., Pierani, A., Kicheva, A., Novitch, B. G., Briscoe, J., and Sasai, N. (2010). Dynamic assignment and maintenance of positional identity in the ventral neural tube by the morphogen sonic hedgehog. *PLoS biology*, 8(6):e1000382.

Dias, J. M., Alekseenko, Z., Applequist, J. M., and Ericson, J. (2014). Tgf$\beta$ signaling regulates temporal neurogenesis and potency of neural stem cells in the cns. *Neuron*, 84(5):927–939.

Driever, W. and Nüsslein-Volhard, C. (1988). A gradient of bicoid protein in drosophila embryos. *Cell*, 54(1):83–93.

Dupin, E., Calloni, G. W., Coelho-Aguiar, J. M., and Le Douarin, N. M. (2018). The issue of the multipotency of the neural crest cells. *Developmental biology*, 444:S47–S59.

Duval, N., Vaslin, C., Barata, T. C., Frarma, Y., Contremoulins, V., Baudin, X., Nedelec, S., and Ribes, V. C. (2019). Bmp4 patterns smad activity and generates stereotyped cell fate organization in spinal organoids. *Development*, 146(14):dev175430.

Ericson, J., Rashbass, P., Schedl, A., Brenner-Morton, S., Kawakami, A., Van Heyningen, V., Jessell, T., and Briscoe, J. (1997). Pax6 controls progenitor cell identity and neuronal fate in response to graded shh signaling. *Cell*, 90(1):169–180.

Etoc, F., Metzger, J., Ruzo, A., Kirst, C., Yoney, A., Ozair, M. Z., Brivanlou, A. H., and Siggia, E. D. (2016). A balance between secreted inhibitors and edge sensing controls gastruloid self-organization. *Developmental cell*, 39(3):302–315.

Fasano, C. A., Chambers, S. M., Lee, G., Tomishima, M. J., and Studer, L. (2010). Efficient derivation of functional floor plate tissue from human embryonic stem cells. *Cell stem cell*, 6(4):336–347.

Frith, T. J., Granata, I., Wind, M., Stout, E., Thompson, O., Neumann, K., Stavish, D., Heath, P. R., Ortmann, D., Hackland, J. O., et al. (2018). Human axial progenitors generate trunk neural crest cells in vitro. *Elife*, 7:e35786.

Gajović, S., St-Onge, L., Yokota, Y., and Gruss, P. (1998). Retinoic acid mediates pax6 expression during in vitro differentiation of embryonic stem cells. *Differentiation*, 62(4):187–192.

Garcia-Castro, M. I., Marcelle, C., and Bronner-Fraser, M. (2002). Ectodermal wnt function as a neural crest inducer. *Science*, 297(5582):848–851.

Gard, C., Curto, G. G., Frarma, Y. E.-M., Chollet, E., Duval, N., Auzié, V., Auradé, F., Vigier, L., Relaix, F., Pierani, A., et al. (2017). Pax3-and pax7-mediated dbx1 regulation orchestrates the patterning of intermediate spinal interneurons. *Developmental biology*, 432(1):24–33.

Gilbert, S. F. (2000). *Developmental Biology, 6th edition*. Sunderland (MA): Sinauer Associates.

Gonzalez-Gobartt, E., Blanco-Ameijeiras, J., Usieto, S., Allio, G., Benazeraf, B., and Martí, E. (2021). Cell intercalation driven by smad3 underlies secondary neural tube formation. *Developmental Cell*, 56(8):1147–1163.

Goulding, M. and Pfaff, S. L. (2005). Development of circuits that generate simple rhythmic behaviors in vertebrates. *Current opinion in neurobiology*, 15(1):14–20.

Gouti, M., Tsakiridis, A., Wymeersch, F. J., Huang, Y., Kleinjung, J., Wilson, V., and Briscoe, J. (2014). In vitro generation of neuromesodermal progenitors reveals distinct roles for wnt signalling in the specification of spinal cord and paraxial mesoderm identity. *PLoS biology*, 12(8):e1001937.

Henrique, D., Abranches, E., Verrier, L., and Storey, K. G. (2015). Neuromesodermal progenitors and the making of the spinal cord. *Development*, 142(17):2864–2875.

Jeng, K.-S., Jeng, C.-J., Jeng, W.-J., Sheen, I., Li, S.-Y., Leu, C.-M., Tsay, Y.-G., Chang, C.-F., et al. (2019). Sonic hedgehog signaling pathway as

a potential target to inhibit the progression of hepatocellular carcinoma. *Oncology letters*, 18(5):4377–4384.

Jessell, T. M. (2000). Neuronal specification in the spinal cord: inductive signals and transcriptional codes. *Nature Reviews Genetics*, 1(1):20–29.

Kiecker, C. and Niehrs, C. (2001). A morphogen gradient of wnt/$\beta$-catenin signalling regulates anteroposterior neural patterning in xenopus.

Kosodo, Y. and Huttner, W. B. (2009). Basal process and cell divisions of neural progenitors in the developing brain. *Development, growth & differentiation*, 51(3):251–261.

Lacoste, A., Berenshteyn, F., and Brivanlou, A. H. (2009). An efficient and reversible transposable system for gene delivery and lineage-specific differentiation in human embryonic stem cells. *Cell stem cell*, 5(3):332–342.

Lai, H. C., Seal, R. P., and Johnson, J. E. (2016). Making sense out of spinal cord somatosensory development. *Development*, 143(19):3434–3448.

Lanford, P. J., Lan, Y., Jiang, R., Lindsell, C., Weinmaster, G., Gridley, T., and Kelley, M. W. (1999). Notch signalling pathway mediates hair cell development in mammalian cochlea. *Nature genetics*, 21(3):289–292.

Le Dréau, G., Garcia-Campmany, L., Rabadán, M. A., Ferronha, T., Tozer, S., Briscoe, J., and Martí, E. (2012). Canonical bmp7 activity is required for the generation of discrete neuronal populations in the dorsal spinal cord. *Development*, 139(2):259–268.

Le Dréau, G. and Martí, E. (2012). Dorsal–ventral patterning of the neural tube: a tale of three signals. *Developmental neurobiology*, 72(12):1471–1481.

Lee, K. J., Dietrich, P., and Jessell, T. M. (2000). Genetic ablation reveals that the roof plate is essential for dorsal interneuron specification. *Nature*, 403(6771):734–740.

Lee, K. J. and Jessell, T. M. (1999). The specification of dorsal cell fates in the vertebrate central nervous system. *Annual review of neuroscience*, 22(1):261–294.

Lehmann, R. and Nusslein-Volhard, C. (1991). The maternal gene nanos has a central role in posterior pattern formation of the drosophila embryo. *Development*, 112(3):679–691.

Li, P. and Elowitz, M. B. (2019). Communication codes in developmental signaling pathways. *Development*, 146(12):dev170977.

Liem Jr, K. F., Tremml, G., and Jessell, T. M. (1997). A role for the roof plate and its resident tgf$\beta$-related proteins in neuronal patterning in the dorsal spinal cord. *Cell*, 91(1):127–138.

Lippmann, E. S., Williams, C. E., Ruhl, D. A., Estevez-Silva, M. C., Chapman, E. R., Coon, J. J., and Ashton, R. S. (2015). Deterministic hox patterning in human pluripotent stem cell-derived neuroectoderm. *Stem cell reports*, 4(4):632–644.

Liu, J.-P. (2006). The function of growth/differentiation factor 11 (gdf11) in rostrocaudal patterning of the developing spinal cord.

Louvi, A. and Artavanis-Tsakonas, S. (2006). Notch signalling in vertebrate neural development. *Nature Reviews Neuroscience*, 7(2):93–102.

Maden, M. (2006). Retinoids and spinal cord development. *Journal of neurobiology*, 66(7):726–738.

Magown, P., Rafuse, V. F., and Brownstone, R. M. (2017). Microcircuit formation following transplantation of mouse embryonic stem cell-derived neurons in peripheral nerve. *Journal of neurophysiology*, 117(4):1683–1689.

Mansour, A. A., Khazanov-Zisman, S., Netser, Y., Klar, A., and Ben-Arie, N. (2014). Nato3 plays an integral role in dorsoventral patterning of the spinal cord by segregating floor plate/p3 fates via nkx2. 2 suppression and foxa2 maintenance. *Development*, 141(3):574–584.

Marcon, L. and Sharpe, J. (2012). Turing patterns in development: what about the horse part? *Current opinion in genetics & development*, 22(6):578–584.

Marti, E., Bumcrot, D. A., Takada, R., and McMahon, A. P. (1995). Requirement of 19k form of sonic hedgehog for induction of distinct ventral cell types in cns explants. *Nature*, 375(6529):322–325.

Martin, G. R. (1981). Isolation of a pluripotent cell line from early mouse embryos cultured in medium conditioned by teratocarcinoma stem cells. *Proceedings of the National Academy of Sciences*, 78(12):7634–7638.

Martyn, I., Brivanlou, A. H., and Siggia, E. D. (2019). A wave of wnt signaling balanced by secreted inhibitors controls primitive streak formation in micropattern colonies of human embryonic stem cells. *Development*, 146(6):dev172791.

Maury, Y., Côme, J., Piskorowski, R. A., Salah-Mohellibi, N., Chevaleyre, V., Peschanski, M., Martinat, C., and Nedelec, S. (2015). Combinatorial analysis of developmental cues efficiently converts human pluripotent stem cells into multiple neuronal subtypes. *Nature biotechnology*, 33(1):89–96.

Meinhardt, A., Eberle, D., Tazaki, A., Ranga, A., Niesche, M., Wilsch-Bräuninger, M., Stec, A., Schackert, G., Lutolf, M., and Tanaka, E. M.

(2014). 3d reconstitution of the patterned neural tube from embryonic stem cells. *Stem cell reports*, 3(6):987–999.

Mitchell, P. J., Timmons, P. M., Hébert, J. M., Rigby, P., and Tjian, R. (1991). Transcription factor ap-2 is expressed in neural crest cell lineages during mouse embryogenesis. *Genes & development*, 5(1):105–119.

Mouilleau, V., Vaslin, C., Robert, R., Gribaudo, S., Nicolas, N., Jarrige, M., Terray, A., Lesueur, L., Mathis, M. W., Croft, G., et al. (2021). Dynamic extrinsic pacing of the hox clock in human axial progenitors controls motor neuron subtype specification. *Development*, 148(6):dev194514.

Multerer, M. D., Wittwer, L. D., Stopka, A., Barac, D., Lang, C., and Iber, D. (2018). Simulation of morphogen and tissue dynamics. In *Morphogen Gradients*, pages 223–250. Springer.

Muñoz-Sanjuán, I. and Brivanlou, A. H. (2002). Neural induction, the default model and embryonic stem cells. *Nature Reviews Neuroscience*, 3(4):271–280.

Niewiadomski, P., Niedziółka, S. M., Markiewicz, Ł., Uśpieński, T., Baran, B., and Chojnowska, K. (2019). Gli proteins: regulation in development and cancer. *Cells*, 8(2):147.

Peng, T., Thorn, K., Schroeder, T., Wang, L., Theis, F. J., Marr, C., and Navab, N. (2017). A basic tool for background and shading correction of optical microscopy images. *Nature communications*, 8(1):1–7.

Placzek, M., Tessier-Lavigne, M., Yamada, T., Jessell, T., and Dodd, J. (1990). Mesodermal control of neural cell identity: floor plate induction by the notochord. *Science*, 250(4983):985–988.

Plouhinec, J.-L., Vieira, M., Simon, G., Collignon, J., and Sorre, B. (2020). Dissecting signalling hierarchies in the patterning of the mouse primitive streak using micro-patterned epilc colonies. *bioRxiv*.

Qu, Q., Li, D., Louis, K. R., Li, X., Yang, H., Sun, Q., Crandall, S. R., Tsang, S., Zhou, J., Cox, C. L., et al. (2014). High-efficiency motor neuron differentiation from human pluripotent stem cells and the function of islet-1. *Nature communications*, 5(1):1–13.

Romanos, M., Allio, G., Roussigné, M., Combres, L., Escalas, N., Soula, C., Médevielle, F., Steventon, B., Trescases, A., and Bénazéraf, B. (2021). Cell-to-cell heterogeneity in sox2 and bra expression guides progenitor motility and destiny. *Elife*, 10.

Sagner, A. and Briscoe, J. (2019). Establishing neuronal diversity in the spinal cord: a time and a place. *Development*, 146(22):dev182154.

Sagner, A., Zhang, I., Watson, T., Lazaro, J., Melchionda, M., and Briscoe, J. (2020). Temporal patterning of the central nervous system by a shared transcription factor code. *BioRxiv*.

Saka, Y. and Smith, J. C. (2007). A mechanism for the sharp transition of morphogen gradient interpretation in xenopus. *BMC developmental biology*, 7(1):1–9.

Sanchez-Ferras, O., Coutaud, B., Samani, T. D., Tremblay, I., Souchkova, O., and Pilon, N. (2012). Caudal-related homeobox (cdx) protein-dependent integration of canonical wnt signaling on paired-box 3 (pax3) neural crest enhancer. *Journal of Biological Chemistry*, 287(20):16623–16635.

Shaker, M. R., Lee, J.-H., Kim, K. H., Ban, S., Kim, V. J., Kim, J. Y., Lee, J. Y., and Sun, W. (2021). Spatiotemporal contribution of neuromesodermal progenitor-derived neural cells in the elongation of developing mouse spinal cord. *Life Sciences*, page 119393.

Shakhova, O., Sommer, L., et al. (2010). Neural crest-derived stem cells.

Simon, G., Plouhinec, J.-L., and Sorre, B. (2021). Differentiation of epilcs on micro-patterned substrates generated by micro-contact printing. *Methods in Molecular Biology*.

Sorre, B., Warmflash, A., Brivanlou, A. H., and Siggia, E. D. (2014). Encoding of temporal signals by the tgf-$\beta$ pathway and implications for embryonic patterning. *Developmental cell*, 30(3):334–342.

Takahashi, K. and Yamanaka, S. (2006). Induction of pluripotent stem cells from mouse embryonic and adult fibroblast cultures by defined factors. *cell*, 126(4):663–676.

Thomson, J. A., Itskovitz-Eldor, J., Shapiro, S. S., Waknitz, M. A., Swiergiel, J. J., Marshall, V. S., and Jones, J. M. (1998). Embryonic stem cell lines derived from human blastocysts. *science*, 282(5391):1145–1147.

Tozer, S., Le Dréau, G., Marti, E., and Briscoe, J. (2013). Temporal control of bmp signalling determines neuronal subtype identity in the dorsal neural tube. *Development*, 140(7):1467–1474.

Turing, A. M. (1952). The chemical basis of morphogenesis. *Phil. Trans. R. Soc. Lond. B*, 237:37–72.

Tuson, M., He, M., and Anderson, K. V. (2011). Protein kinase a acts at the basal body of the primary cilium to prevent gli2 activation and ventralization of the mouse neural tube. *Development*, 138(22):4921–4930.

Van Straaten, H., Hekking, J., Thors, F., Wiertz-Hoessels, E., and Drukker, J. (1985). Induction of an additional floor plate in the neural tube. *Acta morphologica Neerlando-Scandinavica*, 23(2):91–97.

Waddington, C. (1957). The strategy of the genes. allen.

Wang, R. N., Green, J., Wang, Z., Deng, Y., Qiao, M., Peabody, M., Zhang, Q., Ye, J., Yan, Z., Denduluri, S., et al. (2014). Bone morphogenetic

protein (bmp) signaling in development and human diseases. *Genes & diseases*, 1(1):87–105.

Warmflash, A., Sorre, B., Etoc, F., Siggia, E. D., and Brivanlou, A. H. (2014). A method to recapitulate early embryonic spatial patterning in human embryonic stem cells. *Nature methods*, 11(8):847–854.

Watterson, R. L., Goodheart, C. R., and Lindberg, G. (1955). The influence of adjacent structures upon the shape of the neural tube and neural plate of chick embryos. *The Anatomical Record*, 122(4):539–559.

Wichterle, H., Lieberam, I., Porter, J. A., and Jessell, T. M. (2002). Directed differentiation of embryonic stem cells into motor neurons. *Cell*, 110(3):385–397.

Wind, M., Gogolou, A., Manipur, I., Granata, I., Butler, L., Andrews, P. W., Barbaric, I., Ning, K., Guarracino, M. R., Placzek, M., et al. (2021). Defining the signalling determinants of a posterior ventral spinal cord identity in human neuromesodermal progenitor derivatives. *Development*, 148(6):dev194415.

Wolpert, L. (1969). Positional information and the spatial pattern of cellular differentiation. *Journal of theoretical biology*, 25(1):1–47.

Wymeersch, F. J., Huang, Y., Blin, G., Cambray, N., Wilkie, R., Wong, F. C., and Wilson, V. (2016). Position-dependent plasticity of distinct progenitor types in the primitive streak. *Elife*, 5:e10042.

Xiong, F., Tentner, A. R., Huang, P., Gelas, A., Mosaliganti, K. R., Souhait, L., Rannou, N., Swinburne, I. A., Obholzer, N. D., Cowgill, P. D., et al. (2013). Specified neural progenitors sort to form sharp domains after noisy shh signaling. *Cell*, 153(3):550–561.

Xue, X., Sun, Y., Resto-Irizarry, A. M., Yuan, Y., Yong, K. M. A., Zheng, Y., Weng, S., Shao, Y., Chai, Y., Studer, L., et al. (2018). Mechanics-guided embryonic patterning of neuroectoderm tissue from human pluripotent stem cells. *Nature materials*, 17(7):633–641.

Yamada, T., Pfaff, S. L., Edlund, T., and Jessell, T. M. (1993). Control of cell pattern in the neural tube: motor neuron induction by diffusible factors from notochord and floor plate. *Cell*, 73(4):673–686.

Zagorski, M., Tabata, Y., Brandenberg, N., Lutolf, M. P., Tkačik, G., Bollenbach, T., Briscoe, J., and Kicheva, A. (2017). Decoding of position in the developing neural tube from antiparallel morphogen gradients. *Science*, 356(6345):1379–1383.

Zechner, D., Müller, T., Wende, H., Walther, I., Taketo, M. M., Crenshaw III, E. B., Treier, M., Birchmeier, W., and Birchmeier, C. (2007). Bmp and wnt/$\beta$-catenin signals control expression of the transcription factor olig3 and the specification of spinal cord neurons. *Developmental biology*, 303(1):181–190.

Zheng, Y., Xue, X., Resto-Irizarry, A., Li, Z., Shao, Y., Zheng, Y., Zhao, G., and Fu, J. (2019). Dorsal-ventral patterned neural cyst from human pluripotent stem cells in a neurogenic niche. *Science advances*, 5(12):eaax5933.